P: 3-17-80

E80-10124
NASA CR-
160564

(E80-10124) A METHODOLOGY FOR DETERMINING OPTIMUM MICROWAVE REMOTE SENSOR PARAMETERS (Kansas Univ. Center for Research, Inc.) 200 p HC A09/MF A01 CSCL 14B

N80-26714

Unclas
G3/43 00124

THE UNIVERSITY OF KANSAS CENTER FOR RESEARCH, INC.
2291 Irving Hill Drive—Campus W
Lawrence, Kansas 66045

THE UNIVERSITY OF KANSAS CENTER FOR RESEARCH, INC.

2291 Irving Hill Drive—Campus West
Lawrence, Kansas 66045

Telephone: 864-4832

A METHODOLOGY FOR DETERMINING OPTIMUM MICROWAVE REMOTE SENSOR PARAMETERS

RSL TR 380-1

by

V. H. Kaupp

Principal Investigator
J.C. Holtzman

February 1980

Contract No. NAS 9-~~15062~~ 15602

ABSTRACT

A methodology is proposed for determining the operating characteristics and parameters of both active and passive microwave remote sensors which are both optimum for certain earth resources applications and cost-effective to implement. This methodology involves designing a program for collecting the experimental data required, collecting these data, mathematical analyses, and statistical inference or an "optimum" solution. Both simulated microwave data and measured microwave data can be used as experimental data. General microwave sensor data simulation methodologies are also presented.

PURPOSE

The objectives of this work were to perform tradeoff analyses and to determine cost-effective microwave sensor configurations satisfying a range of earth resources applications. This could not be accomplished because there is no general agreement as to what values of critical sensor parameters are optimum for the various earth resources applications. A methodology was developed instead whereby an optimum configuration could be determined rigorously after a minimum amount of data, both real and simulated were collected.

This work was performed under Contract No. NAS 9-15602 for NASA Johnson Space Center.

SCOPE

The work reported here has resulted in a general methodology for determining the optimum operating characteristics and parameter values for microwave remote sensors. This methodology can use either (or both) actual or simulated sensor data for determining the optimum sensor configuration. The work performed was limited to developing and reporting both the general microwave sensor configuration methodology as well as the general microwave sensor data simulation techniques. Results of simulations are included in an Appendix.

SUMMARY

This report documents an effort which developed a technique for the selection of optimum microwave sensor parameters for specific applications. This method is an empirical exploration of the unknown function which relates sensor parameters, such as, resolution, bandwidth, or polarization, to the utility of the sensor data for specific applications, e.g. soil moisture detection, crop classification, or sea state estimation. A configuration of sensor parameters which optimize this function is selected as the best for each specific application. Because this technique is based upon empirical observation, data must be collected and the parameter/utility function estimated. The data in this case is both sensor products representing various system configurations and the utility of those products for specific applications. Unfortunately there does not exist a data base of sensor products extensive enough to supply the needed data. Therefore a large portion of this report was devoted to illustrating how image simulation for both passive and active microwave sensors can be used to provide the required data.

There are many sensor parameters which affect the utility of the output products. An efficient technique for specifying the specific combinations of sensor parameter to be evaluated is required. This report thus reviews linear statistical models and the estimation of the model parameter. A linear statistical model is used to describe the unknown parameter/utility relationship.

The combination of sensor image simulation and statistical modeling is a powerful approach for determining an optimum set of microwave sensor parameters for a wide variety of applications.

TABLE OF CONTENTS

TABLE OF CONTENTS (cont.)

1.0 INTRODUCTION

We propose a methodology for determining the operating characteristics and parameters of microwave remote sensors which are both optimum for a range of earth resources applications and cost effective to implement. This methodology is developed from the Response Surface Methodology (RSM) which is essentially a collection of procedures involving experimental strategy, mathematical methods, and statistical inference which, when combined, enable the experimenter to make an efficient, empirical exploration of the system in which he is interested [Myer, 1971]. The methodology proposed will aid in this design of both active (i.e., radars) and passive (i.e., radiometers) microwave systems which are optimum remote sensors for specific applications, as well as those which complement and supplement existing optical (e.g., LANDSAT) and thermal infrared remote sensors.

The methodology involves designing a program for collecting the experimental data required, collecting these data, mathematical analyses, and statistical inference of an "optimum" solution. Both simulated microwave data and measured microwave data can be, and are recommended to be, used as experimental data.

In this report, the general methodology is presented and discussed in Chapter 2, and specific techniques for simulation of microwave sensor data (i.e., radar and radiometer data) are reported in Chapter 3. The simulation techniques are included as simulation is a viable alternative for acquiring experimental data. The general simulation models are presented and their implementation on a general purpose digital computer are discussed and results are included in Appendix B.

1.1 Optimum Sensor Configuration Defined

Microwave systems are sensitive to different target characteristics than the ones to which optical and thermal infrared systems are sensitive. Active systems, radars, are sensitive to the roughness of a target and its dielectric properties. Passive systems, radiometers, are sensitive to the thermal emissions from this target, itself, as well as this thermal emission from the sky. So are thermal infrared systems, but at microwave frequencies, it is this change in emissivity that produces most of the significant differences between the various targets, whereas at thermal infrared frequencies, it is the change in temperature that is significant.

The choice of a "best" set of parameters from which to design and construct a microwave system is very difficult. First, the specific earth resources applications which the resultant instrument is to satisfy must be identified. Then, the common parameter values must be determined and tradeoff analyses conducted for establishing the rest of them. While this is being done, the existing "state-of-the-art" in microwave sensor technology and data processing capabilities must be assessed so that each parameter value determined can be weighted relative to the state-of-the-art. An optimum sensor configuration for a microwave sensor would be the one which struck the best weighted balance between the percentage of satisfaction of each application, versus the cost, the time to design, build and test, this risk and feasibility of success, versus alternative configurations.

1.2 Earth Resources Applications (Literature Review)

Early in this study, we tried to group together significant sets of the earth resources applications by major microwave system parameters such as frequency, polarization, resolution, look angle, etc. The thought

was that such groupings would constitute a large enough set that specific microwave systems could be postulated that would optimize satisfaction of the applications versus cost and versus sensor technology. Accordingly, an extensive review of the literature was conducted in serach of proven earth resources applications involving microwave sensors. Many papers were identified, obtained, and reviewed for quantitative statements concerning which sensor parameters should be used for satisfying a specific application. For the most part, it could only be conjectured as to which sensor parameters should be used. Thus, this approach was abandoned and the methodology for determining an optimum sensor configuration was developed, and is reported here.

The results of the literature search conducted are summarized and presented in Appendix A. For the purposes of this report, proven earth resources applications via microwave sensors and those deemed as high on the priority list for future systems are the following seven main categories:

1) Mineral resources;
2) Water resources;
3) Land use resources and geographic applications;
4) Natural vegetation;
5) Cultivated vegetation;
6) Damage assessment and hazard surveys;
7) Oceanography.

As can be seen in Appendix A, this listing of applications is by user categories and originates primarily from the NASA (National Aeronautics and Space Administration) active microwave workshops (1975, 1976).

1.3 Background

Since the LANDSAT satellites are, for all practical purposes, providing continuing coverage of the earth and its resources in the optical, near infrared, and to a lesser degree in the thermal infrared frequency bands, microwave sensor configurations are less likely to be approved as primary sources for general earth resources data. This is especially true when the proposed sensor configuration is speculative and is based on an inadequate data base.

Radar has been used by the civilian scientific community since the early 1960's for various earth observations. Radiometers have been employed as a sensor of both geophysical and meteorological phenomena since the late 1960's. Both radars and radiometers are listed as candidate earth resources systems in the post-LANDSAT D era (e.g., AW & ST, 1979).

A recurrent theme has called for development of a multi-frequency, multi-polarization, imaging radar [e.g., the active microwave workshop reports (1975, 1976) and the applications review (1976)]. This theme arises from continuing investigations, some of which have been quantitative and analytical (e.g., Bush, 1977), and some of which have not. As noted by the National Academy of Science upon reviewing the proposed NASA microwave remote sensing five year plan - 1977 to 1982 - (1977), "In the committee's view the experimental data base, as presented, is too limited to support this development (ed - a dual-frequency, dual-polarization, imaging radar for vegetation classification and soil moisture measurement)". The NAS committee went on to recommend that extensive and repeated experiments with multi-frequency and multi-polarization sensors be conducted, and that for general earth resources surveys, microwave techniques from space should be considered an adjunct to the LANDSAT surveys rather than a primary source.

Thus, a methodology is needed for determining an optimum set of sensor parameters for specific earth resources applications from diverse, but viable, microwave data. A way is needed to predict the optimum sensor from data collected via existing sensors. Such a methodology is proposed here.

2.0 OPTIMIZATION METHODOLOGY

In designing microwave sensors for earth resources surveys, a balance is normally desired between cost and technology on the one hand, and selecting values of system variables which will satisfy the survey application on the other hand. As noted previously, earth resources survey applications span the gamut from searching for mineral resources, to monitoring and classifying vegetation, and even extend to the science of oceanography (cf, 1.2). A microwave sensor which has been designed for surveying the earth's surface in search of signs of mineral resources probably is not well-suited for monitoring the growth and health of vegetation, or for classifying vegetation. The question arises of whether or not there is a different sensor design which will satisfy the combination of applications, even though to a lesser degree.

A quantitative, general linear statistical model is proposed here to resolve that question. The techniques to be employed here are patterned after the Response Surface Methodology (RSM) which has been developed previously [Meyers, 1971; Box and Hunter, 1957; and Williges and Simon, 1971]. This approach presents a complete methodology for designing the operating parameters of a microwave system which will satisfy specific earth resources applications to a desired level with attainment of this, weighted against cost and technology considerations. The complete methodology works in the following way. First, identify the earth resources applications for which a microwave sensor is desired (e.g., measuring soil moisture and classifying cultivated vegetation). Second, decide whether the system is to produce unique data about the target's characteristics, or whether the data produced will complement or supplement another system's

data such as that produced by LANDSAT. Third, determine which microwave system parameters are of primary importance for each application the resultant system is to serve (note: determination of parameter values will be the final result of this technique and are not specified here, or at any other stage). Table 1 offers a candidate listing of the kinds of parameters which might be deemed important and, as such, is not an exhaustive listing.

Fourth, design an experimental procedure for acquiring experimental data having the desired variability in structure (i.e., data representing different levels of each parameter). Fifth, collect the data. These data can be acquired from existing systems by flying them over the desired targets, or they can be generated from sensor simulations via digital computer techniques.

Sixth, analyze the data and apply utility measures, U_a, (e.g., probability of correct classification) having functional relationships between the data or derivatives of the data and the desired parameters for the various applications, $x_1, x_2, \ldots, x_k$, as

$$U_{a\ell} = f_{a\ell}(x_1, x_2, \ldots, x_k) \tag{2-1}$$

where $U_{a\ell}$ is the ℓ^{th} utility measure and $f_{a\ell}(x_1, x_2, \ldots x_k)$ is the functional relationship between the sensor parameters, $x_1, x_2, \ldots x_k$, for application a. seventh, assume a low-order polynomial for modeling the functional interaction between parameter values expressed in (1). For example, a first-order polynomial model would be

$$U_{a\ell} = f_{a\ell}(x_1, x_2, \ldots x_k) = \beta_o + \sum_{i=1}^{k} \beta_i x_i \tag{2-2}$$

and a second-order polynomial model would be

TABLE 1

CANDIDATE MICROWAVE SENSOR PARAMETERS

ACTIVE SYSTEM	PASSIVE SYSTEM
Frequency	Frequency
Polarization	Polarization
Final Spatial Resolution	Final Spatial Resolution
Number of Looks	Integration Time
Bandwidth	Bandwidth
Peak Radiated Power	System Noise Temperature
Depression Angle	Scanning Period

$$U_{a\ell} = f_{a\ell}(x_1, x_2, \ldots x_k) = \beta_o + \sum_{i=1}^{k} \beta_i x_i + \sum_{j=1}^{k} \beta_j x_j^2 + \sum_{\substack{j=1 \\ i \neq j}}^{k} \sum_{i=1}^{k} \beta_{ij} x_i x_j \quad (2\text{-}3)$$

Higher-order models can be assumed, but the lowest-order ones are generally sufficient as they account for interaction between parameters a pair at a time.

Eighth, perform a regression analysis on the data. That is, estimate the coefficients, the β's, for the model assumed (i.e., for (2), or (3), or other model). Ninth, optimize the solutions for the U_a.

The mathematical model is described in 2.1. Coefficient estimation is recounted in 2.2. Collecting data in reviewed in 2.3. Predicting optimum sensor parameters in related in 2.4. Collecting data via sensor simulation is presented in Chapter 3.

2.1 Mathematical Basis

Because there are no specific physical laws governing the relationship between the utility of a microwave image and the sensor parameters a probabilistic model will be used to describe this relationship. Specifically, the general linear statistical model will be used. This model is written as

$$y = \beta_o + \sum_{i=1}^{k} \beta_i z_i + \varepsilon \quad (2\text{-}4)$$

where the z_i's represent in this case known sensor parameters (or functions of parameters) and the β_i's are unknown model parameters which define the desired relationship. This model is called "linear" because it is linear in the unknown model parameters. Both the β_i's and z_i's are deterministic values; the random component, ε, characterizes the stochastic

nature of the observation y. The usual assumption for this model is that $E[\varepsilon] = 0$ and the Var $[\varepsilon] = \sigma^2$ and the ε is normally distributed.

To reduce the number of observations required to estimate the β_i's we will use the following specific form of the general linear model:

$$y = \gamma_0 + \sum_{i=1}^{k} \gamma_i x_i + \sum_{i=1}^{k} \gamma_{ii} x_i^2 + \sum_{j=1}^{k} \sum_{i=1}^{k} \gamma_{ij} x_i x_j \qquad (2\text{-}5)$$

This model assumes that all three way interactions (e.g., $x_i \; x_j \; x_k$ terms) do not significantly contribute to the response y and are thus neglected. This model can also be viewed as a quadradic fit to the true higher order surface which defines the relationships between the sensor parameters and the response y.

2.2 Model Parameter Estimation

The model parameters are found by collecting observations and performing a minimum mean square estimation. This procedure is well known but will be reviewed here in the context of determining optimum microwave sensor parameters.

Consider the following experiment. N observations (the utility of sensor data) given M different sensor configurations. Using the model presented in Section 2.1 the experiment can be mathematically written as

$$\underline{Y} = Z\beta + \varepsilon \qquad (2\text{-}6)$$

where

$$\underline{Y} = \begin{pmatrix} y_1 \\ \vdots \\ y_N \end{pmatrix}, \quad \varepsilon = \begin{pmatrix} \varepsilon_1 \\ \vdots \\ \varepsilon_N \end{pmatrix}$$

$$Z = \begin{pmatrix} Z_{11} & \cdots & Z_{\ell 1} \\ \vdots & & \vdots \\ Z_{1N} & \cdots & Z_{\ell N} \end{pmatrix}, \quad \beta = \begin{pmatrix} \beta_0 \\ \vdots \\ \beta_\ell \end{pmatrix}$$

and

$$\ell = k^2 + k + 1$$

for the second order model described by equation (2-5). Each ε_i is assumed to be zero mean Gaussian with identical variance σ^2, further ε_i is independent of ε_j for all i,j, i≠j. The matrix z defines the experimental conditions under which the observations were made and note that

$$\beta_i = \gamma_i \qquad \text{for } i = 0 \ldots k$$

$$\beta_i = \gamma_{ii} \qquad \text{for } i = k + 1 \ldots 2k + 1$$

$$\beta_i = \gamma_{ij} \qquad \text{for } i = 2k + 2 \ldots k^2 + k + 1$$

and

$$Z_i = x_i \qquad \text{for } i = 1 \ldots k$$

$$Z_i = x_i^2 \qquad \text{for } i = k + 1 \ldots 2k + 1$$

$$Z_i = x_i x_j \qquad \text{for } i = 2k + 1 \ldots k^2 + k + 1.$$

The minimum mean square estimate for the model parameters, $\hat{\beta}$, is defined by the vector which minimizes

$$L = (\underline{Y} - Z\hat{\beta})^T (\underline{Y} - Z\hat{\beta}) \tag{2-7}$$

Following [Meyers, 1977)

$$\begin{aligned} L &= (\underline{Y} - Z\hat{\beta})^T\underline{Y} - (\underline{Y} - Z\hat{\beta})^T Z\hat{\beta} \\ &= \underline{Y}^T\underline{Y} - (Z\hat{\beta})^T\underline{Y} - \underline{Y}^T Z\hat{\beta} + (Z\hat{\beta})^T Z\hat{\beta} \\ &= \underline{Y}^T\underline{Y} - \hat{\beta}^T Z^T\underline{Y} - \underline{Y}^T Z\hat{\beta} - \hat{\beta}^T Z^T Z\hat{\beta} \\ &= \underline{Y}^T\underline{Y} - 2\hat{\beta}^T Z^T Y + \hat{\beta} Z^T Z\hat{\beta} \end{aligned} \tag{2-8}$$

Setting $\frac{2L}{2\hat{\beta}} = 0$ the best fit is found as

$$\frac{2L}{2\hat{\beta}} = -2Z^T\underline{Y} + 2Z^TZ\hat{\beta} = 0 \tag{2-9}$$

solving for $\hat{\beta}$

$$\hat{\beta} = (Z^TZ)^{-1}Z^T\underline{Y} \tag{2-10}$$

The expected value of $\hat{\beta}$ is simply found by

$$\begin{aligned} E[\hat{\beta}] &= E[(Z^TZ)^{-1}Z^T\underline{Y}] \\ &= E[(Z^TZ)^{-1}Z^T(Z\beta + \varepsilon)] \\ &= E[(Z^TZ)^{-1}(Z^TZ\beta - Z^T\varepsilon)] \\ &= E[(Z^TZ)^{-1}(Z^TZ)\beta + (Z^TZ)^{-1}Z^T\varepsilon] \\ &= I\beta + E[(Z^TZ)^{-1}\underline{Y}^T\varepsilon] \\ &= \beta \end{aligned} \tag{2-11}$$

And the covariance matrix of $\hat{\beta}$ is found as [Meyers, 1977]

$$\begin{aligned} Cov[\hat{\beta}] &= E[(\hat{\beta} - \beta)(\hat{\beta} - \beta)^T] \\ &= Cov[(Z^TZ)^{-1}Z^T\underline{Y}] \\ &= (Z^TZ)^{-1}Z^TCov(\underline{Y}) \\ &= (Z^TZ)^{-1}Z^T\sigma^2I(Z^TZ)^{-1}Z^T \\ &= \sigma^2(Z^TZ)^{-1} \end{aligned} \tag{2-12}$$

The minimum mean square estimate (MMSE) for the model parameters has been defined by the observation vector $\underline{Y}$ and the design matrix Z. Further the MMSE was found to be unbiased and have a covariance $\sigma^2(Z^TZ)^{-1}$. The covariance matrix can be used to establish confidence intervals for each of the model parameters and allows the establishment of a prediction interval around any observation especially the optimum sensor utility.

There are many ways for which an experiment can be designed (i.e., selection of the design matrix Z) to allow efficient estimation of the model parameters. Entire text books are devoted to presenting these

techniques (Cox, 1958; Myers, 1977) for a wide variety of conditions. Therefore, a review of experimental design in general is not appropriate here. We only point out that these techniques are available and a specific design is required for each situation to minimize the number of observations while maintaining reasonable estimates for the model parameters. The importance of the design matrix will become evident in the following section.

2.3 Data Collection

To apply the general linear model to this problem it is necessary to collect information relating to the utility of a particular sensor system configuration with respect to a specific application. There are two major problems associated with this task. First, quantitative definitions of data utility for the applications listed in Section 1.2 are not available. Second, a wide variety of operational sensor systems do not exist to collect the needed data and it is not reasonable to expect that such a data base of sensor information will ever exist because of the cost involved.

The second problem is easily solved by applying recently developed digital sensor simulation. Sensor simulations are flexible enough to produce the desired image data simulating any desired sensor configuration. Using current array processor technology the cost of applying simulation to this problem would be reasonable. Two such techniques for sensor simulation, one for active and the other for passive microwave sensors, are presented later in this report.

The first problem, that of assessing the utility of sensor data is more difficult to define. One approach is to subject the data to its

intended applications in a controlled environment and develop a ranking procedure to evaluate the results. For example, if the data were to be used for geologic mapping a controlled experiment would be designed which would present several simulated images from different simulated systems to radar geologists. These interpreters would then rank the utility images using some standard criteria. The obvious disadvantage of this approach is wide variability in interpretive responses. The human factors aspect of this method would have to be addressed.

A better approach would be to subject the data to machine analysis. For example, if the data were to be used for agricultural mapping then automatic classification algorithm would be applied and the percent correct classification would provide an excellent utility response. In either case care must be taken not to violate the assumption of the model.

2.4 Optimization of Sensor Parameters: Analysis of the Prediction Equation

The result of applying the technique described in the previous sections is a prediction equation which relates the sensor parameters to data utility for specific application. The goal of this research is to determine the optimum set of sensor parameters for each application. The optimum set of sensor parameters will yield the largest data utility. Thus the obvious approach is to apply multivariable calculus to find the maximum response given the prediction equation, an excellent discussion of this problem is found in Myers (1971).

The data gathered in this experiment would also directly provide information concerning the magnitude of importance of individual or groups of sensor parameters. The analysis of variance techniques would be applied to obtain this information. For example, suppose we wish to test

the hypothesis that sensor parameter x_1 does not significantly affect the utility of the sensor data. The first step to answer this question would be to calculate the sum of squares for error (SSE) for the original model equation 2-6. The SSE is defined as

$$SSE = \sum_{i=1}^{N} (y_i - \hat{y}_i)^2 \tag{2-13}$$

where y_i = observed response for the experimental conditions defined by the i^{th} row in the design matrix Z.

$\hat{y}_i$ = estimated (using eq 2-10) response for the experimental conditions defined by the i^{th} row in the design matrix Z.

Note that SSE/N-(k+1) is a estimate for σ^2. Next a reduced model would be defined by deleting all x_1 terms in the original model. A SSE would then be calculated using the reduced model, SSE_1. The test statistic for the given hypothesis is given by

$$F = \frac{\dfrac{SSE_1 - SSE}{k - g}}{\dfrac{SSE}{N - (k + 1)}} \tag{2-14}$$

where N = number of observations

$k + 1$ = number of parameters (β_i) in the original model

$g + 1$ = number of parameters in the reduced model.

This test statistic has a F-distribution (probability density function) with $(k - g)$, $N - (k + 1)$ degrees of freedom. Therefore if $F > F_{(k-g),(N-(k+1),\alpha}$ we reject the hypothesis that the sensor parameter x_1 does not significantly effect the utility of the sensor data with the probability of a TYPE I error equal to α. Remember that a TYPE I error is rejecting the hypothesis when it should be accepted. So if we reject, then the data has provided strong evidence that the sensor parameter x_i is important. Similar techniques can be applied to any term or group of terms in the original model. For example, we might wish to see if all quadratic terms, X_i^2, do not

significantly effect the response. The motivation would be to simplify the model and thus supply more degrees of freedom for estimating the remaining parameters.

Using these techniques we finally arrive at a simplified model and a set of optimum sensor parameters for specific applications. It would now be important to establish a prediction interval (Mendenhall, 1968) around the optimum response. This interval would define a range where some future response would lie given this set of parameters and thus provide an indication of the operational utility of the sensor.
To develop the prediction interval we will first define the optimum set of parameters as the vector O, i.e.

$$O^T = (1\ x_{o_1} \ldots x_{o_k}) \tag{2-15}$$

The expected value of the response given O is

$$E[\hat{Y}] = O^T\beta \tag{2-16}$$

and its variance can be shown to be

$$Var[\hat{Y}] = [O^T(Z^TZ)^{-1}O]\sigma^2 \tag{2-17}$$

The error, E, between a future response, Y_F, and the estimated response, $\hat{y}$, as defined by the estimated model parameters is

$$E = Y_F - \hat{Y} \tag{2-18}$$

so clearly

$$E[E] = 0 \tag{2-19}$$

$$Var\ [E] = Var\ [Y_F] + Var\ [\hat{Y}] - 2\ Cov(Y_F, \hat{Y}) \tag{2-20}$$

but the future and the estimated response would be uncorrelated yielding

$$Var[E] = Var[Y] + Var[Y_F] \tag{2-21}$$

The variance of the future utility of the sensor data, Y_F, is assumed to be σ^2 thus

$$\text{Var}[E] = \sigma^2[1 + 0^T(Z^TZ)^{-1}0] \tag{2-22}$$

A prediction interval, $(1 - \alpha)\%$, can now be defined (remember Y and Y_F are both normal so E is also normal) as

$$\hat{y} \pm t_{N-(k+1),\alpha/2}\, s\sqrt{1+0^T(Z^TZ)^{-1}0} \tag{2-23}$$

where s^2 = estimate of σ^2 = SSE/N-(k+1)

$t_{N-(k+1),\alpha/2}$ = the t value for N-(k+1) degrees of freedom at $\alpha/2$.

The interpretation of this interval is simple; there is an $(1-\alpha)\%$ probability that a future measurement of the sensor's data utility will lie inside this interval. This interval would be used, for example, to predict the range of percent correct classification of agriculture areas using a specific microwave sensor configuration. Analysis of the estimated prediction equation i.e. estimation of the β's, would provide the final results of this study which would be 1) the optimum set of sensor parameters for specific applications, 2) indications of the relative importance of the various sensor parameters for the selected applications and 3) a prediction interval which would be used to establish performance bounds of the optimum sensor configurations.

3.0 MICROWAVE SENSOR DATA SIMULATION

Simulation of microwave sensor data is a viable alternative to collecting actual mission data. Simulation provides both an inexpensive alternative and, to the extent that supporting data requirements are met (i.e., to the extent that backscatter data and a suitable digital map are available), it provides a way for varying experimental conditions while retaining cortrol of the resultant data. However, simulation results are only as good as the computer programs, the digital maps, and the backscatter data used to make them. For these reasons, it is generally advisable to validate the simulation system by producing simulation results for one or more of the system configurations from which actual mission data were acquired. This is recommended in addition to generating all the experimental simulation results.

A methodology for the simulation of the data produced by active microwave systems has been developed and reported previously [Kaupp, 1979; Holtzman, et al., 1977a and 1977b; Holtzman, et al., 1978]. This methodology has been extended and modified for the simulation of passive microwave systems in the work performed here. Since simulation is recommended to form an integral part of the optimizing methodology proposed in this report, the simulation approach is summarized in the following sections. An overview of the simulation approach is presented in 3.1. The simulation of active systems via the Point Scattering Model (PSM) is summarized in 3.2. The simulation of passive systems is reviewed in 3.3.

3.1 Microwave Sensor Data Simulation: An Overview

Figure 1 presents a conceptual view of microwave sensor data simulation as developed and implemented at the University of Kansas. In the figure,

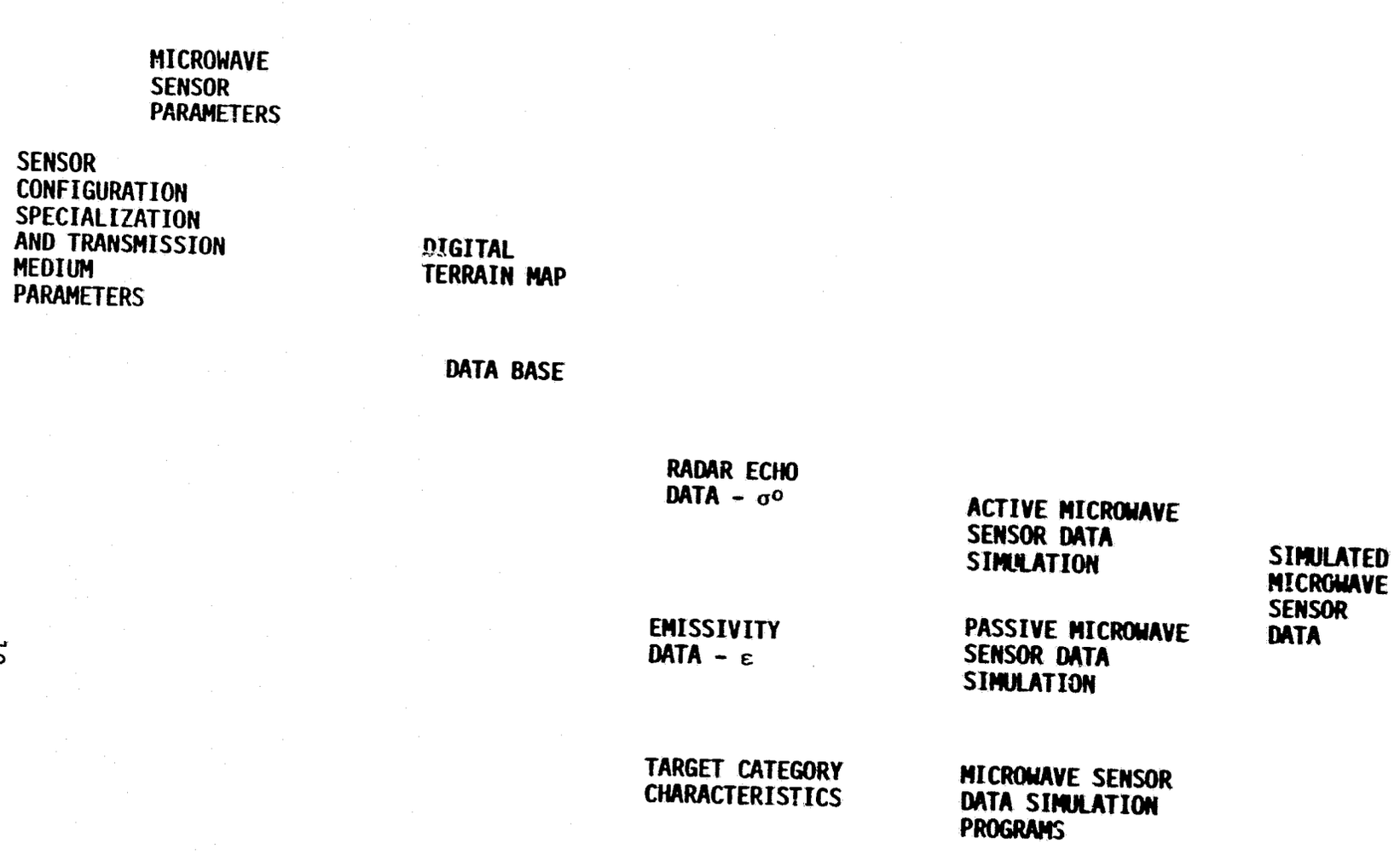

FIGURE 1: CONCEPTUAL VIEW OF MICROWAVE SENSOR DATA SIMULATION

the microwave sensor data simulation programs are shown to require input of three (3) kinds of information: (1) microwave sensor parameters, (2) digital terrain map, and (3) target category characteristics. The first of these, sensor parameters, is required so that the programs can be specialized for each unique simulation configuration, so that a suitable terrain map can either be acquired or produced, and so that data can be obtained which is descriptive of the microwave characteristics of the targets to be simulated. The second input data base which provides the spatial information regarding the relative topography of the area to be simulated and which specifies the types of categories present at each sample point. The third input data, target category characteristics, is the mechanism required for modeling the electromagnetic characteristics of the target categories within a region to be simulated, and is the interaction relation utilized for predicting how much energy is received by the sensor for each target type.

As is shown in Figure 1, these three (3) kinds of data are appropriately utilized at the input and the simulation programs produce simulated microwave sensor data at the output. This approach treats all aspects of the simulation problem as a closed system with all three (3) major components of the system being modelled: the ground, the sensor, and the final data medium.

When specialized for simulating active microwave systems, the computer programs and general simulation philosophy are referred to as the Point Scattering Model (PSM). When specialized for simulating passive microwave sensors, the programs and philosophy are referred to as the Point Radiation Model (PRM). Each specialization is discussed in one of the following two sections.

3.2 Active Microwave Sensor Simulation

The Point Scattering Model (PSM) for simulating radar data has been developed and implemented on a digital computer. By simulating radar data is meant synthesis, via digital computer, of the data which would have been recorded by a radar flying the same ground track over the prescribed ground sites. The radar senses the reradiated flux from the ground and its cover in the microwave portion of the electromagnetic spectrum and stores the results. The radar produces an output proportional to the reflectivity characteristics at a fixed wavelength of the terrain and when recorded in an image, displays the terrain in fine detail and with spectacular relief. So does the simulated radar image produced via the PSM. The PSM is not limited to simulating images, it is viable with suitable alterations for most recording formats.

The PSM represents the radar, the ground and its microwave response, and the stored data by a closed-system model. The model rests on firm, theoretical foundations and is mathematically rigorous. It incorporates all aspects of the radar problem starting with the transmitter, including such aspects as the antenna during transmission, the propagation path to the ground, the ground response, the return data, the antenna during reception, and the receiver; and concluding with data storage and presentation. The PSM has been tested and validated for a specific class of radar targets; distributed targets.*

---

*As used throughout, distributed targets are areas of natural terrain or ground cover such as wheat or corn fields, grassy expanses, forests, plowed ground, paved areas, etc., which are approximately homogeneous and large relative to a radar resolution element.

Just as all mathematical models are abstractions of reality, so is the PSM. It attempts to describe in closed form the processes of the system consisting of radar, ground, and data storage. The PSM is completely general and capable of synthesizing data having a desired accuracy if the cost is paid in time, complexity, and resources expended. But the true value of the PSM arises from the ease with which a specific implementation can be tailored or specialized, to take advantage of simplifications and approximations valid for a specific application, thereby making it efficient and cost-effective to use.

An approach has been developed regarding simulation that insures all the requisite data and information needed to simulate the response of a specific radar from a desired ground site (target) are obtained. This approach is illustrated conceptually in Figure 2 as the PSM simulation implementation philosophy. Figure 2 can be considered to represent an expansion of the implementation blocks of Figure 1.

The PSM implementation philosophy is the framework which identifies the various simulation requirements and relates these to one another. As can be seen from Figure 2, three (3) basic kinds of data and information interact with one another and serve as inputs to the simulation computer programs. These are: (1) data base; (2) reflectivity data; and (3) simulation parameters. Upon complete specification of these, the simulation computer programs can be run and radar data can be simulated for the system being modeled as if it, the radar, were flown over the data base (i.e., the ground site).

As the PSM has been implemented on a digital computer, its required input data must be in digital form. The first of these input data is a data base, a digital replica of the ground in the target area. This digital representation of the ground, called data base hereafter, models

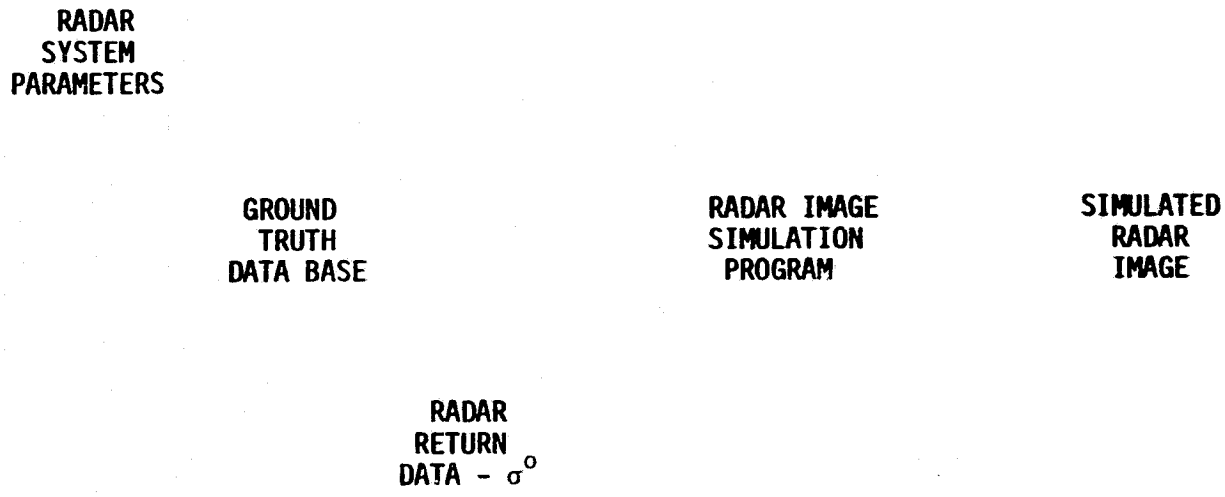

FIGURE 2: PSM SIMULATION IMPLEMENTATION PHILOSOPHY

the ground and its cover in the desired site and contains a facsimile of both the dielectric categories present, called backscatter categories, as well as the geometric variations, called elevation data. The data base is, thus, a sampled replica of the backscatter categories present in a target simulation scene (both distributed and cultural* targets, or categories) and the elevation surface. A data base typically consists of a digital matrix having at least four (4) dimensions: two (2) for the spatial location of each point, one (1) for its elevation, and at least one (1) for its backscatter category. The resolution built into a data base is determined by the sampling frequency and is highly dependent upon such factors as the resolution of the radar system being simulated, the application for which a particular data base is required, and available time and resources.

Within a target site numerous different types of vegetation and terrain cover exist. Some of these are distributed targets such as forests, wheat fields, grasslands, highways, runways, water bodies, etc., and some are cultural targets such as buildings and vehicles. Each different type of target is modeled as a different backscatter category in a data base. Backscatter category is, thus, the smallest spatial unit, or 'field' into which regions having homogeneous dielectric properties can be divided commensurate with the data base resolution, radar system, and application.

---

*As used here, cultural targets are targets, such as buildings, vehicles, etc., which are smooth relative to radar wavelengths and whose backscatter properties are essentially specular.

Also within a target site, the surface of the ground varies in relative height from point to point above a datum surface. This height variation from point to point creates unique patterns in radar data which must be modeled for simulation purposes. Elevation data are, as the name suggests, the value of the relative height of each point in a data base. The resolution of elevation data is described by the sampling frequency of the data base and the accuracy of the data from which obtained.

A ground response model is the second type of input data required by the PSM. The ground response model normally utilized in the PSM to reflect the properties of each of the different types of ground cover identified in the target site and included in the data base is backscatter, the differential scattering cross-section (σ^0). The PSM uses σ^0 to simulate the interaction between the ground and the electromagnetic energy incident from the radar, and to predict the percentage of reradiation back to the radar. For each different ground cover type specified in a data base (called backscatter category), the PSM requires a set of σ^0 data, either experimental or theoretical, to be provided.

Third, the PSM requires input of system parameters, storage parameters, and ground track information. These data are required to modify the computational algorithms of the PSM so they reflect the desired system and storage parameters and, in addition, are required so that the computational algorithms can be simplified to increase efficiency and cost effectiveness. They are also used to specify key parameters pertinent to this data base and its construction, such as resolution, orientation, etc. Finally, these data are used to specify the flight-

line parameters which allow determination of altitude, angles of incidence, and thus the geometrical aspects of the simulation problem.

Upon satisfaction of all input data requirements shown in Figure 2, the computational algorithms of the PSM are invoked to simulate the response of a desired radar flying a particular flight line over a specified portion of ground. The geometrical relationships between the location and orientation of the simulated radar and its platform and each point in the data base are solved with such effects as foreshortening, layover, shadow, look-direction, etc., being treated. Upon solution of this geometry, the PSM predicts the amount of power reradiated from each point in the data base back to the receiving antenna by finding the backscatter category of each point and solving the functional form of the appropriate backscatter data for the conditions at each point. The resulting calculations are further refined to account for reception, detection, and storage of the power from each point, and the data output from the PSM are stored on computer-compatible digital magnetic tapes.

3.2.1 Theoretical Foundation of the PSM

An appropriate starting point for this development of the PSM would be a description of the principles of imaging radars. However, as these principles have been well documented in the literature [*Skolnik*, 1970; *Moore*, 1975], they will not be repeated here. The starting point for this discussion of the PSM is the block diagram shown in Figure 3.

Figure 3 is being used to illustrate representative signal paths and processing systems which it might be necessary to model for simulation

purposes. As can be seen from Figure 3, P_R represents the instantaneous power impinging on the antenna from all sources within the "view" of the antenna. After being collected by the antenna, P_R is routed via appropriate "plumbing" to the receiver. The receiver is a complex electronic system which filters, demodulates, detects, and adjusts the incoming signal into an intensity (I) exiting it. In the general case, the receiver transfer function can be viewed as an operator (M) transforming the incoming Power (P_r) into an intensity exiting the receiver

$$I = M(P_R; B, \tau, \ldots) \tag{3-1}$$

In this notation, the functional dependence is shown of the receiver output intensity (I) upon both the input signal level (P_R) as well as various system parameters such as the receiver bandwidth (B), the integration time (τ), etc. In the specific case where the receiver transfer function is linear and time independent then this expression reduces to multiplication [i.e., for a receiver having a linear input to output relationship, $I = P_R[M(B, \tau, \ldots)]$.

Depending upon the function for which a radar is designed, the intensity exiting the receiver can be processed and stored in numerous ways; several are shown in Figure 3. As two extremes, it can be seen that the intensity voltage can be used to produce an image directly, or it can be converted into digital data, stored, processed, and then used to produce an image. Many alternative ways between these two exist. For modeling purposes, assume first the intensity exiting the receiver is input to an analog-to-digital converter having an input/output quantization transfer function specified as Q. The digital intensity exiting this converter can be specified as

$$I_D = Q(I; B_s, \tau_s, \ldots) = Q[M(P_R, B, \tau, \ldots); B_s, \tau_s, \ldots] \tag{3-2}$$

In this notation, the functional dependence of the digitized

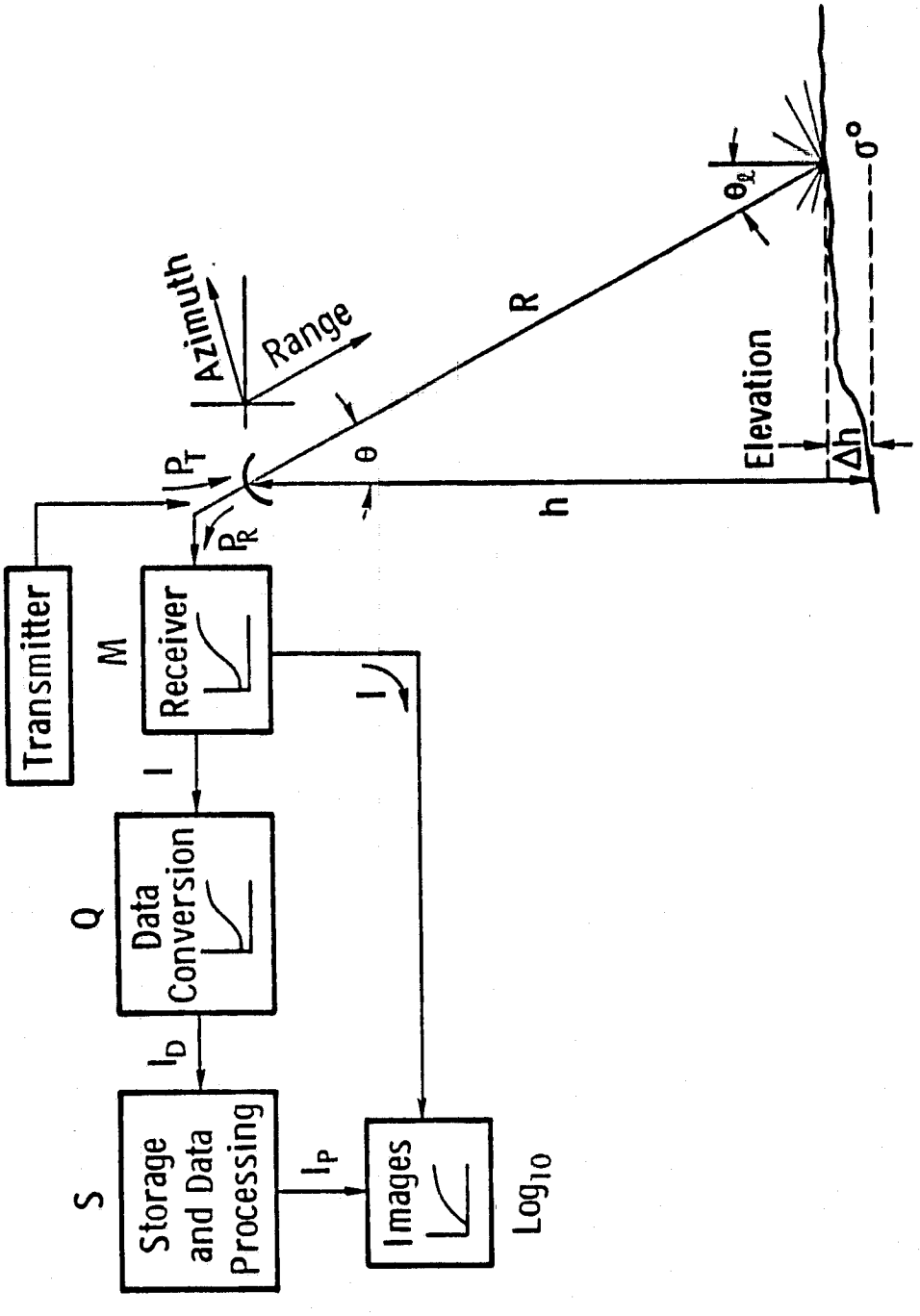

Figure 3. Block Diagram of PSM

intensity (I_D) upon both the input signal level (I) and various sampling parameters such as the sampling bandwidth (B_s) and integration time (τ_s), etc. is shown, as well as upon the system parameters and input power level as indicated in (3-1). Again, if the quantizing transfer function is linear and time independent then this expression reduces to multiplication $\left[\text{i.e., } I_D = I[Q(B_s,\tau_s,\ldots)]\right]$.

This output of the converter can be input to a data processing station for calibration and data reduction. If the effects of such data processing and calibrations (S) are to convert the input digital intensity (I_D) into a processed intensity (I_p) output from the processing software

$$I_p = S(I_D;\, c_i, \ldots) = S[Q(I;\, B_s,\, \tau_s, \ldots);\, c_i, \ldots] \qquad (3\text{-}3)$$

where the processed intensity is shown to be determined from various calibrations and conversions (c_i, $i = 1, 2, \ldots$), etc., operating upon the digital data described by (3-2) and (3-1).

If this intensity is utilized to expose a sheet of ordinary photographic film, then after exposure and development of this film the density (D) of silver grains present at each pixel (picture element) has been shown to be

$$D = \gamma[\log_{10} I_p] + \log_{10} K = \gamma\{\log_{10}[S(I_D;\, c_i, \ldots)]\} + \log_{10} K \qquad (3\text{-}4)$$

where γ is a positive constant representing the slope of the linear portion of the film curve of density (D) versus logarithm of exposure (The Hurter-Driffield curve), and where K is a constant depending upon the exposure time and the film development time and is the extrapolated intercept value of the Hurter-Driffield curve [*Goodman*, 1968].

Rewriting the expression for density (3-4) to show explicitly the various effects gives

$$D = \gamma\left\{\log_{10}\left\{S\left[Q(M(P_R;\, B,\, \tau, \ldots));\, B_s,\, \tau_s, \ldots\right];\, c_i, \ldots\right\}\right\} + \log_{10} K \qquad (3\text{-}5a)$$

which for a linear system can be rewritten

$$D = \gamma \left\{ \log_{10} P_R + \log_{10} M(B, \tau, \ldots) + \log_{10} Q(B_s, \tau_s, \ldots) + \log_{10} S(c_i, \ldots) \right\} + \log_{10} K \qquad (3\text{-}5b)$$

Alternatively, the intensity exiting the receiver (I) may be recorded directly on film as shown in Figure 3. In this case, the density expression is written as

$$D = \gamma \left[\log_{10} M(P_R; B, \tau, \ldots) \right] + \log_{10} K \qquad (3\text{-}6a)$$

which for a linear system becomes

$$D = \gamma \left[\log_{10} P_R + \log_{10} M(B, \tau, \ldots) \right] + \log_{10} K \qquad (3\text{-}6b)$$

Expressions (3-5) and (3-6) represent final data storage as an image on photographic film. Other ways of storage may be utilized. For instance, the output of the data processing software (I_p) may be stored as intensity data on a computer-compatible magnetic tape, rather than as density data as is the case for film. In this case, the final result can be expressed as (Equation 3-3).

$$I_p = \left\{ S \left\{ Q \left[M(P_R; B, \tau, \ldots) \right]; B_s, \tau_s, \ldots ; \right\} c_i, \ldots \right\} \qquad (3\text{-}7a)$$

or, rewriting for a linear system

$$I_p = P_R \left[S(c_i, \ldots) Q(B_s, \tau_s, \ldots) M(B, \tau, \ldots) \right] \qquad (3\text{-}7b)$$

This has not been an exhaustive listing of alternative ways to process the power received (P_R). It has been presented to illustrate that when simulating radar images for faithful reproduction of system operation, specialization for each unique system transfer function is required.

In all the foregoing no assumptions were made about the transfer function of any electronic system through which the radar signal is processed. Each transfer function depends entirely upon the system design and hardware implementation chosen. These transfer functions may vary from extremely complex, highly non-linear ones to very simple, linear ones, with all cases in between possible. For instance, predetection filters, square-law detection, automatic gain control, and large signal saturation, or small signal compression may combine as a linear, or non-linear transfer function.

The exact form for each transfer function must be decided when an implementation of the PSM is developed to model a specific radar system and application. First, it must be decided whether equations (3-5), (3-6), or (3-7), or another variant is valid and then what form of transfer function is appropriate for each subsystem. Unless there is an overpowering reason to specify the transfer function of each subsystem as exactly as possible, much can be gained in time and resources saved by making the loosest permissible approximations.

Up to now little has been said about P_R. P_R is the power reradiated from all the scattering centers located within the instantaneous field of view of the antenna. P_R is the collection of all this reradiated power impinging upon the antenna at each instant. In reality, the return power, P_R, is not a deterministic process as the foregoing discussion might imply. The magnitude of the return power received by an antenna mounted on a moving vehicle fluctuates widely from instant to instant because of variations in the phase of the reradiation from different scatterers in the illuminated area. This phenomenon accounts for the speckled nature ("grainy" appearance) of radar images and is called "fading". The statistics of a "fading" signal have been well documented for many homogeneous targets found in typical terrestrial scenes, and it has been shown that the signal amplitude can be described by a Rayleigh probability distribution* and the signal phase by a uniform probability distribution [*Skolnik*, 1970; *Moore*, 1975; *Bush and Ulaby*, 1976].

---

*The Rayleigh probability distribution is one feasible probability model which can be used to describe the signal amplitude variation [*Zelenka*, 1976; *Porcello et al.*, 1976]. Use of a different probability model is justified for some targets and appropriate modifications to the development reported here need to be made.

If square-law detection is assumed for the receiver, then the post-detection signal is a random variable having a χ-square probability density function with 2N degrees of freedom [*Nash and Ulaby*, 1976] where N specifies the number of "independent samples" averaged. The number of "independent samples" can be determined from [*Moore*, 1975]

$$N = N_a N_r = \left(\frac{2R\lambda}{L^2}\right)\left(\frac{B_c}{B}\right) \tag{3-8}$$

where N_a and N_r are number of "independent samples" in the azimuth and range directions, respectively. Figure 3 shows the azimuth and range directions. The number of independent samples in azimuth is given by

$$N_a = \frac{r_a}{r} = \frac{R\beta}{L/2} = \frac{2R\lambda}{L^2} \tag{3-9}$$

This arises naturally by defining the azimuth resolution as $r_a = R\beta$ which is appropriate for a real-aperture radar having a diffraction-limited beamwidth β given by λ/L (the illuminating wavelength divided by the real antenna length) and where R specifies the range from antenna to target. The maximum resolution possible for this case is $r = L/2$. Thus, the number or samples in the azimuth direction is $N_a = r_a/r$.

The number of "independent samples" in range is given by

$$N_r = \frac{B_c}{B} \tag{3-10}$$

This result is appropriate for a radar employing frequency averaging where the total bandwidth, B_c, is not utilized in improving resolution, and represents the total bandwidth, B_c, divided by the resolution bandwidth, B.

This results from defining the resolution in the range direction as $r_r = C\tau/2 = C/2B$ which is a conventional estimate of range resolution for a pulsed radar having a pulse duration τ, resolution bandwidth $B = 1/\tau$, and where C is the speed of light. The finest resolution possible if all the bandwidth is used to improve resolution is $r = C\tau_C/2 = C/2B_C$ where B_C is the total system bandwidth. Thus, the number of independent samples in the range direction can be seen to be $N_r = r_r/r$.

Averaging a large number of "independent samples" reduces signal "fading" (i.e., it reduces the variance of the "fading" signal thereby smoothing the image appearance) [*Zelenka*, 1976; *Porcello, et al.*, 1976]. Because of the direct relationship between the number of "independent samples" averaged and resolution, the larger resolution is made relative to the best resolution possible with a system, the larger N is made. Thus, if N is increased, resolution is degraded (larger resolution is poorer resolution).

Following *Frost* [1978, 1977a], after square law detection, the signal which originated with Rayleigh amplitude and uniform phase probability densities has been transformed into a power signal having a χ-squared probability density after square-law detection:

$$P_R = \left(\frac{\overline{P}_R}{2N}\right)(Y) = \overline{P}_R(X_1) \qquad (3\text{-}11)$$

where $\overline{P}_R$ is the expected value of the return power P_R from a resolution cell (i.e., $\overline{P}_R = E[P_R]$), Y is a random variable with a standard χ-square distribution having 2N degrees of freedom, and N is the number of

"independent samples" averaged (i.e., equation (3-8)) and $x_1 = \frac{Y}{2N}$. When the number of independent samples being averaged is large, (3-11) becomes

$$P_R = \bar{P}_R\left(1 + \frac{Z}{\sqrt{N}}\right) = \bar{P}_R(X_2) \tag{3-12}$$

where Z is a standardized Gaussian random variable (i.e., one having zero mean and unit variance) and $x_2 = (1 + z/\sqrt{N})$.

Combining these last two results, (3-11) and (3-12), with the earlier expressions for the final record of the radar intensity from a linear system, (3-5b), (3-6b), and 3-7b); gives

$$D = \gamma[\log_{10}\bar{P}_R + \log_{10}(X_i) + \log_{10}M + \log_{10}Q + \log_{10}S] + \log_{10}K, \qquad i = 1,2 \tag{3-13}$$

or

$$D = \gamma[\log_{10}\bar{P}_R + \log_{10}(X_i) + \log_{10}M] + \log_{10}K, \qquad i = 1,2 \tag{3-14}$$

or

$$I_P = SQM\bar{P}_R(X_i), \qquad i = 1,2 \tag{3-15}$$

where $X_1 = Y/2N$ and $X_2 = (1 + Z/\sqrt{N})$.

The values from expressions (3-13), (3-14), and (3-15) represent the final result as far as a linear radar system is concerned, but these results must be quantizied for implementation on a digital computer. In the case of the expression for intensity (3-15) the data are to be quantizied into 2^n discrete levels (i.e., into a computer word having n-bits). If it is desired to quantize a specific m dB (decibels) of the intensity

signal dynamic range into these 2^n levels, this can be accomplished by specifying I_{MIN}, the intensity value which is to be set to zero and m, the range, as follows:

$$I_Q = \left[\left(\frac{2^n - 1}{10^{\frac{m}{10}} - 1}\right)\left(\frac{I_P}{I_{MIN}} - 1\right)\right] \tag{3-16}$$

where I_Q represents the quantized intensity data, I_{MIN} is the intensity level for which $I_Q = 0$, I_P are the intensity data available via equation (3-15), m is the number of decibels of radar data dynamic range which are to be quantized (e.g., $m = 10\log_{10}(I_{max}/I_{min})$, and n is the number of bits of computer word into which the m-dB are to be quantized.

If, instead, it is desired to specify the quantized value of a specific intensity level (I_C), the following can be used

$$I_Q = \left(\frac{2^n - 1}{10^{\frac{m}{10}} - 1}\right)\left[\left(\frac{I_P}{I_C}\right)\left(I_{QC}\left(\frac{10^{\frac{m}{10}} - 1}{2^n - 1}\right) + 1\right) - 1\right] \tag{3-17}$$

where I_C is the intensity level that is assigned the quantization level I_{QC}, and all other parameters are the same as in (3-16). Both (3-16) and (3-17) are linear mappings of intensity into quantized intensity. Alternatively, any desired nonlinear mappings can be implemented.

By way of example for equation (3-16), if it is desired to quantize 20 dB of radar data into 256 discrete levels then m = 20, n = 8 and (3-16) can be rewritten as $I_Q = \left(\frac{255}{99}\right)\left(\frac{I_P}{I_{MIN}} - 1\right)$. In this example, if

$I_P = I_{MIN}$, then $I_Q = 0$. If $I_P = 100\ I_{MIN}$ (i.e., I_P is 20 dB higher than I_{MIN}), then $I_Q = 255$, as was desired. If instead of specifying I_{MIN} it is desired to set a desired intensity, I_C, to a specific quantization level, I_{QC}, and if m = 20 dB and n = 8 as in the previous example, then equation (3-17) would be invoked and rewritten as $I_Q = \left(\frac{255}{99}\right)\left[\frac{I_P}{I_C} \cdot \left(I_{QC}\left(\frac{99}{255}\right) + 1\right) - 1\right]$. In this example, if $I_{QC} = 126$ and if $I_P = I_C/50$, then $I_Q = 0$. If instead, $I_P = I_C$, then $I_Q = I_{QC}$. Or if $I_P = 2I_C$, then $I_Q = 255$, as was desired. Thus, in one step, the radar intensity data have been quantized and the result has been calibrated via either equation (3-16) or (3-17) so that the desired portion of the intensity data has been linearly mapped into 2^n discrete levels.

Similary for the other two cases. If it is desired to quantize m dB into 2^n levels of the film density, this can be accomplished by

$$G_R = G_{R_C} + \frac{2^n - 1}{\frac{m}{10}} (D - D_C) \quad . \tag{3-18}$$

where G_R represents the greytone* of the quantized density data, D are the density data available via either equation (3-13) or (3-14), D_C is the density of the point in the image having the specified greytone G_{R_C}. Again, m represents the number of decibels of radar intensity data which are to be coded into the 2^n levels of grey. Here the subscript C refers to calibration and the two parameters D_C and G_{R_C} are employed as the mechanism for specifying which portion of the dynamic range of the

---

*Greytone here means the precise shade of grey between 0 (black) and $2^n - 1$ (white) of each pixel (picture element) in an image.

radar is to be coded into the 2^n levels. This represents picking a particular return power, P_{R_C}, and assigning it a desired greytone, G_{R_C}. This is better seen if (3-18) is rewritten as follows:

$$G_R = G_{R_C} + \frac{2^n - 1}{\frac{m}{10}} \left\{ \gamma \left[\log_{10} P_R - \log_{10} P_{R_C} + \log_{10} M - \log_{10} M_C + \log_{10} X_i \right] + \log_{10} \frac{K}{K_C} \right\} \quad (3\text{-}19)$$

where (3-14) was substituted for both D and D_C, appropriately subscripted. Thus, if P_{R_C} is assigned greytone G_{R_C}, then the image is calibrated relative to that return power. For example, if m = 20 dB, n = 8 bits, $M = M_C$ and $K = K_C$, then $G_R = G_{R_C} + \frac{255}{2} \left\{ \gamma \left[\log_{10} \frac{P_R}{P_{R_C}} \right] \right\}$. If $P_R = P_{R_C}$, then $G_R = G_{R_C}$. If $P_R = 100\ P_{R_C}$ and $G_{R_C} = 0$ (black), then $G_R = 255$ (white). If $P_R = P_{R_C}$, then $G_R = 0$ (black), and similarly for any other assignment of P_{R_C} and G_{R_C}. For example, if $G_{R_C} = \frac{255}{2}$, then $P_R = 10\ P_{R_C}$ will cause $G_R = 255$ and $P_R = P_{R_C}/10$ will cause $G_R = 0$, just as desired. Thus, (3-18) causes the radar density data of equations (3-13) and (3-14) to quantized and calibrated as discussed previously. Again, equation (3-18) represents a linear mapping of image density data into discrete greytone data. Any non-linear mapping could also be implemented.

In the development leading both to equations (3-17) and (3-18) - quantized intensity and density, respectively - the power available

at the receiving antenna was specified as P_R, the return power. This return arises as a result of the interaction between the ground and the illuminating electromagnetic energy and is a random process as previously noted in the discussion leading to equations (3-11) and (3-12). The form of $\overline{P}_R$ has not to this point been specified. Different models satisfy different conditions and applications. An excellent model for $\overline{P}_R$, the average return power, reradiated from distributed targets is given by the radar equation [*Skolnik*, 1970; *Moore*, 1975]:

$$\overline{P}_R = \left(\frac{P_T G^2 \lambda^2 \sigma^o A}{(4\pi)^3 R^4} \right) L_T L_R \qquad (3\text{-}20)$$

where the average transmitted power is represented by P_T. The two-way gain of the transmiting/receiving antenna (a function of the elevation and azimuth angles) is given by G^2. The transmitted wavelength is λ. The backscatter model (a function of the dielectric constant, local angle of incidence, wavelength, and polarization, among others) is σ^o. The element of area on the ground being sensed is A (a function of the ground slope, range resolution-pulse length, azimuth resolution-beamwidth, and altitude). The range from the antenna to the element of area being sensed is R. L_T and L_R represent the losses due to propagation of the electromagnetic energy through the atmosphere during transmission and reception, respectively.

Certain conditions must exist for this form of the radar equation to be a realistic and valid model for simulation. First, the area being sensed - resolution element - must be a distributed target,

a homogeneous region of a specific backscatter category. The resolution element must contain a large number of randomly located scattering centers. Second, it must be reasonable to assume that all the parameters of the radar system are constant across the resolution element. When these conditions are satisfied, then equation (3-20), a particularly tractable form of the radar equation for simulation via a digital computer, can be invoked to estimate the return power from each resolution element. Of course, any other appropriate model can be utilized to specify $\bar{P}_R$, equation (3-20) is just a particularly useful one. The details of the radar system, ground, and application will dictate what to use.

With specification of a model for calculation of $\bar{P}_R$, this development of the theoretical aspects of the Point Scattering Method is complete. Equations (3-17) and (3-18) are the final result for intensity and density, respectively. Implicit in these equations are all the normal radar effects such as layover, shadow, multipath, range compression, etc. Treatment of these and other effects occur as a result of explicit provisions designed into the software implementation of the PSM.

The theoretical aspects of the Point Scattering Model have been developed. Just as all mathematical models are abstractions of reality, so is the PSM. It describes the "real world" processes of the closed simulation system consisting of ground, radar, and storage medium. Implicit in the results obtained are certain assumptions upon which the PSM rests. These assumptions may be viewed both as the ones necessary to make the model work as well as the limitations and constraints of the model. Depending upon

the applications for which the model is intended to be used, these limitations and constraints may be of no significance or they may be of crucial importance. It is important that they be recognized and accounted for in order to insure that the model and a specific implementation of it are appropriate for a given task. For the general model, the more important of these assumptions can be succinctly listed as:

(1) Validity of using the radar equation for simulation;

(2) Validity of using the differential scattering cross-section (σ^0) to model the electromagnetic properties of the ground;

(3) Validity of modeling the ground via a digital replica (data base) in which the ground cover is reduced to a unique category per cell in the data base;

(4) Validity of whatever approximations are invoked for the transfer functions of various components of the system being simulated;

(5) Validity of a data storage model.

3.2.2 PSM Simulation Implementation Philosophy

A philosophy has been developed regarding simulation that insures all the requisite data and information needed to simulate the response of a specific radar from a desired ground site (target) are obtained. This philosophy is illustrated conceptually in a previous figure (2) as the PSM simulation implementation philosophy.

As can be seen from Figure 2, three (3) basic kinds of data and information interact and serve as inputs to the simulation computer programs. These are, starting with the one which should be specified first: (1) simulation parameters; (2) data base; and (3) reflectivity data. Important ramifications of each of these areas, interactions between them, and additional discussions explaining how some of the details can be solved are presented in succeeding sections. In Section

3.2.2.1 simulation parameters are discussed. In Section 3.2.2.2, simulation data base and the underlying philosophy are related. In Section 3.2.2.3 reflectivity data for simulation are presented.

After all three kinds of input data are specified, the simulation computer programs can be invoked and radar data can be simulated for the system being modeled. The computer programs solve the geometrical relationships between the position of the simulated radar and the ground (i.e., each point in the data base) for determining such parameters as resolution and local angle of incidence. These are discussed in Section 3.2.2.4. In addition, the computer programs are structured so as to model such propagation effects as layover, shadow, etc. These are discussed in Section 3.2.2.5.

3.2.2.1 Simulation Parameters

Simulation parameters are all those parameters of the imaging process required for specializing the PSM for one radar, desired ground sites, and pertinent flight paths over those sites. Table 1 is a sample listing only, and is provided for reference to suggest what is meant by "simulation parameters."

As can be seen by reference to the table, simulation parameters are listed according to three (3) headings. The first of these, "Radar Systems Parameters," lists the various radar parameters which must be obtained so that the data base, σ^0 data, and computer programs can be specialized for a particular radar system. The second listing of simulation parameters, "Flight Path Parameters," is required so that the desired data base can be constructed, so that σ^0 data for seasonally varying ground cover types can be obtained, and so that simulated data can be produced having the correct orientation, scale and radar effects such as layover and shadow. The third listing, "Application and Simu-

TABLE 2

SIMULATION PARAMETERS

SYMBOL	DESCRIPTION	POTENTIAL IMPACT
Radar System Parameters		
λ	Wavelength	1,2,3
-	Polarization	1,2
G	Antenna pattern factor in range direction	3
β	Antenna azimuth beamwidth	1,3
τ	Pulse length	1,3
-	Scan format (i.e., PPI or SLAR)	1,3
M	Receiver transfer function	3
Q	Analog-to-digital converter transfer function	3
S	Data processing effects	3
γ	Slope of the linear portion of film curve or density versus logarithm of exposure	3
K	Intercept point of line having slope, γ	3
N	Number of "independent samples"	3
L	Real antenna length	3
B_C	Total system bandwidth	3
B	Resolution bandwidth	3
θ_N	Near-range edge of swath angle-of-incidence	3
θ_F	Far-range edge of swath angle-of-incidence	3

1 Data base
2 Reflectivity data
3 Computer programs

TABLE 2

SIMULATION PARAMETERS (continued)

SYMBOL	DESCRIPTION	POTENTIAL IMPACT
Flight Path Parameters		
h	Altitude above a mean surface	1,3
-	Latitude and longitude of target area	1
-	Direction of flight	1,3
-	Season and meteorological conditions	1,2,3
$L_T L_R$	Atmospheric losses	3
Application and Simulation Parameters		
-	Intended use of simulations for determining degree of accuracy required in specification of various parameters and transfer functions	1,2,3
n	Number of bits in the output computer word	3
m	Signal dynamic range which is to be in the final simulated radar data	3
I_{MIN}, I_{QC}, I_C	Intensity calibration data	3
P_{RC}, G_{RC}	Density calibration data	3

1 Data base
2 Reflectivity data
3 Computer programs

lation Parameters," is required for maximum specialization of the PSM to the application.

From Figure 2 and Table 2, it can be seen that the simulation parameters interact with the simulation phases labeled data base, σ^0 data, and simulation computer programs. These data are normally specified first, and the other phases of simulation follow.

Upon specification of these parameters, construction can begin on the data base if a new one is required. The location on the Earth, orientation, and size of the data base will have been specified. The resolution for which the data base will be constructed will have been determined. Ground cover differentiation criteria will have been devised (i.e., criteria defining how to differentiate between important and unimportant ground cover types will have been developed which, for example, will allow constructing a data base having ground cover type boundaries appropriate for a 16 GHz, HH polarization, 50 meter radar). Thus, important conditions for the data base will have been established and work can begin for constructing it.

Specification of these simulation parameters is necessary, also, for the σ^0 data, the second phase of interaction shown in Figure 2. The specification of frequency, polarization, angular range, season, and meteorological conditions together with the ground cover types identified in the data base label which σ^0 data are needed.

The PSM simulation computer programs can be specialized and modified upon specification of the simulation parameters. Simplifying approximations can be made for various aspects of the model such as for the receiver transfer function (M), where appropriate. Appropriate transfer functions, the antenna pattern, system parameters, etc., can be written into the simulation computer programs. Data handling simplifications can be designed either to reduce the cost of simulation, or to make simulation feasible, as from very large data bases.

The uses to which the simulation parameters are put have just been sketched out. This has not been an exhaustive discussion of how they interact for the details of interaction are system and application special. The intent here was to suggest what kinds of information are needed, how these information interact with various phases of simulation, and how simplifications can result from prudent use of the information.

3.2.2.2 Data Base

A data base is a digital replica of the ground modeling its topography and cover. A specific data base will contain a symbolic representation of the dielectric categories present as different ground cover types, or backscatter categories, as well as the elevation surface of a specific site. The data base is, thus, a sampled replica of the backscatter categories present in a target simulation scene and the elevation surface.

A data base typically consists of a digital matrix having at least four (4) dimensions: two (2) for the spatial location of each point, one (1) for its elevation, and at least one (1) for its microwave reflectivity category. More than four dimensions will be required for a data base when seasonal and meteorological variations are to be simulated. The finest resolution which can be built into a data base is determined by the ground spot size each matrix element represents and is highly dependent upon such factors as the resolution of the radar system being simulated, the application for which a particular data base is required, and available time and resources.

Accurate construction of a data base is crucial to the overall simulation effort. The final, simulated radar data can be no better than the data base and, frequently, it is a degraded form of it. At one extreme there is a one-to-one mapping of data base elements into radar resolution cells and on the other extreme is a many-to-one mapping. Most cases of radar simulation fall between these extremes

with, perhaps, four (4) to twenty-five (25) data base elements mapping into a single radar resolution cell.

Regardless of how many data base elements map into a resolution cell, the crucial element is the inherent accuracy of the data base; the accuracy built into the data base. This question of accuracy extends both to modeling the spatial distribution of ground cover types, distributed targets, as well as to specifying the elevation surface, elevation data. Accuracy of modeling the spatial distribution of ground cover types is a dual problem. First, is deciding the smallest size of distributed target which will be uniquely identified as a homogeneous region in the data base. Second, is correctly interpreting the source intelligence data from which the data base is built for determination of what kind of ground cover exists within each distributed target. Accuracy of specifying the elevation surface is also a dual problem. First, is finding a Nyquist sampling interval from the maximum rate-of-change of elevation in the area of interest and then relating this sampling interval to that required by the radar and applications. Second, is finding the accuracy underlying the source elevation data which are to be used.

There are several sets of criteria which interact to establish the sampling frequency of the ground and topography and, thus, the ground spot size each data base element represents. First, are the matters of accuracy just discussed. Second, are questions of resolution from the standpoints of both the radar system and the application (these data are determined from Table 2). Third, are economic considerations raised by the amounts of resources available to construct a data base and to produce simulations from it. The intersection of these sets of criteria probably represents the best choice which can be made for sampling frequency and accuracy in a data base. If the sets are non-intersecting, then the decision must be made on another basis.

After determination of the sampling frequency and accuracy for which a data base is to be constructed of a specific site, work on building it can begin. Data bases are typically built by hand from various sources of intelligence data such as high resolution aerial photographs, etc. [*Holtzman et al.*, 1977a]. A radar/photo-interpreter (PI) acquires the necessary intelligence data and employs manual cartographic feature extraction techniques to interpret the source data and to develop the data base.

The PI draws a map by hand on a stable-base drawing media. This map consists of boundary lines separating different features and ground cover types. Boundaries of major features either can be traced or transferred from the source data, or both. Boundaries of minor features are difficult to locate and are, therefore, obtained via subjective interpretation criteria employed by the PI. These interpretation criteria are normally developed through experience and are established to meet the appropriate requirements levied in Table 2. The construction of this hand-drawn data base map is a major effort if the desired resolution and accuracy is modest or better (less than 50 meters) for a target site of minimal size (i.e., even for one of approximately 50 square kilometers). It depends upon the judgement of the PI, his knowledge of the target site, and his familiarity with ground cover and feature types found in a site.

When the hand-drawn data base map has been finished, it is a symbolic line drawing of the boundaries separating distributed targets (such as forests and fields) and the locations of cultural targets (such as buildings and roads). For use on a computer, this line drawing must be digitized and converted into a completely specified matrix.

A large table digitizer* has been used in the past to digitize the boundary lines in the data base map and store these digital data on computer-compatible magnetic tape [*McNeil et al.*, 1977a]. A human operator traces each boundary with the cursor, and the computer interfaced to the table periodically samples and records the position of the cursor. After digitization--a long, time-consuming task subject to countless errors--a computer-compatible magnetic tape (or multiple such tapes) contain the sampled points stored consecutively, serially, of each boundary in the original data base map. These serial digital boundary data next must be expanded into a completely specified matrix.

Special software have been developed to convert the serial digital boundary data into a completely specified matrix. The task is to sort the boundary data by their X- and Y-values and fill-in the matrix. If it would be possible to assume that the digitized boundary data are error-free this task would not be difficult. Unfortunately, the digitized boundary data are subject to many errors. Both the human operator and the table and computer interfaces are sources of errors. Human errors range from inaccuracy of following lines with the cursor to completely missing boundaries, from incorrectly identifying each boundary to failing to identify some boundaries, and from tracing boundaries in the wrong direction to incorrectly registering the map, setting-up the coordinate system, and specifying the scale. Computer-generated errors

*A large table digitizer is here meant to be a table having a top surface one (1) by one and one-half (1½) meters, or more and having an underlying fine grid of wires (i.e., 75 per centimeter). A cursor is used to trace drawings on the top surface with electric fields identifying the intersecting pair of wires the cursor passes over.

range the complete gamut from scrambling the data to failing to operate. The multitude, variety, and complexity of errors in the digitized boundary data means this task requires a lot of interaction between man and machine because it isn't feasible, normally, to develop software "smart" enough to check for every error and correct for them in a single pass through the data.

At the completion of this activity, the hand-drawn data base map has been converted into a digital matrix. The data stored in each cell of this matrix is the data base information concerning the backscatter category of each spot on the ground. Each cell implicitly represents the location (X- and Y-location) of a ground spot relative to the known corner points and represents the ground spot size via the sampling frequency by which the data base was built, and explicitly specifies the backscatter category of each point. If seasonal or meteorological data are to be included in the data base, they have been added in the past by drawing a separate seasonal data base map, digitizing it, and juxtaposing these data with the category data.

Last, digital elevation data of the target site must be obtained and merged with the category data base. To this point, digital elevation data have been provided by various sponsors, thus, development work on this task has not been undertaken. The elevation data provided to date have come from DMA (Defense Mapping Agency) and have been produced either from standard 7½' quadrangle USGS maps (United States Geologic Survey) via suitable digitizing and interpolation techniques

[*McNeil et al.*, 1976], or from stereoscopic photo-pairs and the UNAMACE [*Bertram*, 1965] system. In either case, the work performed at RSL has been limited to merging elevation data from different computer-compatible magnetic tapes with the category digital data base.

Merging of the elevation data with the category data on a single computer-compatible magnetic tape completes the task of constructing a data base of a specific site. Assuming that all problems encountered have been either solved or safely skirted, this tape contains a data base of a specific site at a desired scale, resolution, and accuracy, and this data base is ready for input to the simulation computer programs.

3.2.2.3 Reflectivity Data

After specification of key simulation parameters in Table 2 (e.g., frequency and polarization) and after identification of the different backscatter categories during data base construction, then reflectivity data (σ^0, or backscatter data) can be obtained. Reflectivity data are used in the PSM to model the radar and ground interaction. The reflectivity data normally used in the PSM are backscatter, the differential scattering cross-section (σ^0). The PSM uses either experimental [*Bush and Ulaby*, 1976; *Cosgriff et al.*, 1960; *Ulaby*, 1975; etc.] or theoretical [*Hevenor*, 1971; *Fung and Chan*, 1969; etc.] data to simulate the interaction between the ground and the electromagnetic energy incident from the radar, and to predict the percentage of reradition back to the radar. For each different ground cover of feature type specified in a data base the PSM requires a set of σ^0 versus angle-of-incidence (a function of frequency and polarization), either experimental

or theoretical to be input. The different ground cover, or categories specified in a data base can be classified into three sets: (1) distributed targets; (2) cultural targets; and (3) seasonal or meteorological targets.

Distributed targets are homogeneous regions, each with a single category of ground cover throughout its total extent, or at least it must be reasonable to model it this way if equation (3-20) is to be used for predicting the return power. Each homogeneous region must be of a size that will provide a large number of scattering centers which are randomly located within it. When these conditions are satisfied, an average value of the differential scattering cross-section (σ^0) can be used to model the radar return from distributed targets and equation (3-20) is valid (providing also that radar parameters can be modeled as being constant across the target-data base cell). Most ground cover types located in data bases made to date satisfy these criteria reasonably well, thus, σ^0 data were used in conjunction with equation (3-20) to model the radar and ground interaction.

Cultural targets are defined within the context of radar simulation to be man-made objects. Their radar returns are characterized by the high probability of specular reflection, which is obviously dependent upon the construction geometry, orientation with respect to the radar platform, antenna beamwidth, and system resolution. The fact that radar returns from cultural targets are so highly dependent upon orientation, and the fact that they do not ordinarily satisfy the criteria

listed in the previous paragraph illustrate why σ^0 data for cultural targets are not usually obtainable and why cultural targets are not readily applicable to digital simulation.

An alternate means of indicating the existence of a cultural target in simulated radar data via the PSM has been utilized in the past; symbolic representation. In this representation, the cultural target is modeled as an isotropic radiator of X decibels. Thus, for any flight path and data base orientation, the cultural target behaves the same.

If this symbolic representation is not good enough, directional dependence can be introduced by specifying one or more directions relative to true North in which the cultural target is specular. This can be accomplished with a minimal increase in simulation complexity and cost; minimal relative to complete, accurate specification of each building, its geometry, corners, etc.

Seasonal or meteorological targets are defined here to mean the changes introduced in a data base to account for the perturbations introduced by adding seasonal or weather effects. The normal category data base represents a snap-shot of the target site. The seasonal or meteorological data base is one way of allowing the target site to mature with time. Normally, complex models can be developed or possibly found in the literature which predict the functional dependence of the underlying category in a desired altered state; altered by season or weather. Some simulations have been produced from a single data base which represent different times of the year.

Upon obtaining the requisite reflectivity data, the work preliminary to simulating radar data is finished. The computer programs have been specialized, the data base produced, and the reflectivity data obtained. It remains only to enter these data into a computer and produce desired simulations.

3.2.2.4 Geometrical Considerations

After specification of the input data requirements shown in Figure 2, the simulation computer programs solve the geometrical relationships between the position of the simulated radar platform and each incremental spot on the ground. These relationships are used for determining the size of the ground spot for each radar resolution cell, and for determining the local angle of incidence between the normal to each ground spot and a vector pointing back to the radar from each spot. One approach is presented in this section for determining the resolution size and local angle of incidence.

For many applications of simulation it is desirable to construct data bases in a finer grid matrix than the resolution cell of the radar would require. This condition generally arises when the application requires fairly modest data base accuracy or when a one-to-one mapping of data base elements into radar resolution cells produces a result which is too "blocky". The following method can be used for determining which cells from the underlying data base will map into a radar resolution cell.

This approach assumes that the data base samples the ground reflectivity categories and elevation surface on a finer scale than the radar resolution cell. A good ratio for data base elements to resolution

cells is twenty-five (25); five (5) data base cells in both the range and azimuth directions for one radar resolution cell. When this is satisfied, then the following method can be invoked for determining which data base elements contribute to the return power from each radar resolution cell. That is, this method allows determining what backscatter categories are physically present within the resolution cell thereby allowing simulation of multiple categories per resolution cell, and for determining such geometrical parameters as range, size of the cell, area, local angle of incidence, etc., as well as such propagation phenomena as shadow layover, etc.

Figure 4 shows the typical geometry in the range-direction for a short-pulse SLAR system. In the coordinate system of the figure, the SLAR antenna illuminates the ground in the y-direction, the vehicle carrying the SLAR travels in the x-direction, and altitude is shown in the z-direction. Figure 4 shows a profile of the ground in the plane-of-incidence (i.e., in the plane formed for x = i where i = 0 in the figure). Also shown in the plane-of-incidence are radar resolution arcs of equal range increments specified by $C\tau/2$. Superimposed on the ground, orthogonal to the vehicle flight path, and shown at the datum surface from which elevation data are referenced, is a fine-scale grid matrix representing the underlying data base. As can be seen, the data base samples the ground at a faster rate than does the radar.

The first return signal it is desired to process is the power reradiated back from the point where R_0 intersects the terrain, and the last is from R_N. The arc R_0 then represents the near-range edge of a SLAR image and R_N the far-range edge. Each succeeding arc between R_0

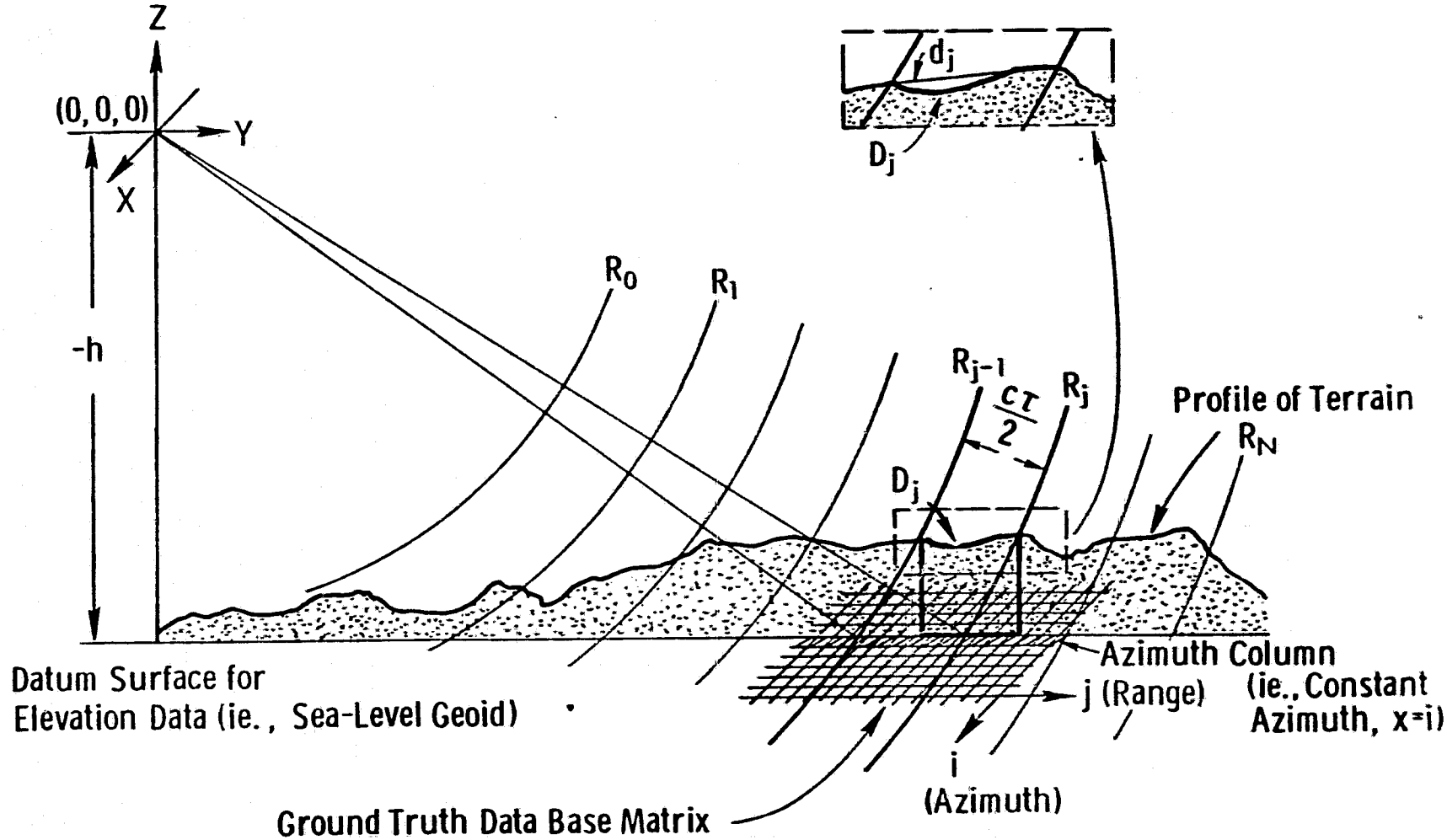

Figure 4. Range Resolution

and R_N is farther from the origin by $c\tau/2$ than the preceding one [i.e., $R_j = R_{j-1} + c\tau/2$].

The portion of terrain lying between successive arcs (e.g., R_{j-1} and R_j) is the portion of ground lying in one resolution cell (e.g., the one called A_j). If the intersection points of arcs R_{j-1} and R_j are projected down to the datum surface, the data base elements from the azimuth column of the plane-of-incidence and belonging to resolution cell A_j are identified. Arcs R_{j-1} and R_j can be expressed as

$$Y_{ij-1}^2 + Z_{ij-1}^2 = R_{j-1}^2 \tag{3-21}$$

$$Y_{ij}^2 + Z_{ij}^2 = R_j^2 \tag{3-22}$$

$$R_j = R_{j-1} + \frac{c\tau}{2} \tag{3-23}$$

where no functional dependence of the X-direction is shown because these relationships occur in a plane formed by holding X constant (i.e., X = i). A value for $c\tau/2$ and, thus, the R_j via (3-23) can be obtained from radar system parameters. The data pairs--(Y_{ij-1}, Z_{ij-1}) and (Y_{ij}, Z_{ij})--represent the range-coordinates (Y's) and elevation-coordinates (Z's) of the intersection points of arcs R_{j-1} and R_j, respectively.

In this scheme, the data base is oriented orthogonal to the flight path so that the SLAR antenna bore-sights down a column of constant azimuth (x = i) thereby allowing variations in range (y) and elevation (z). Thus, it is easily determined via equations (3-21, 3-22, and 3-23) which elements of the data base from the column specified by x = i are

closest to the intersection points of R_{j-1} and R_j with the ground. Those data base elements plus the ones in between belong to resolution cell A_j.

Figure 5 illustrates the geometry for a radar employing a narrow beamwidth antenna. For such systems, the half-power (-3 dB) contour (commonly called beamwidth and specified by β_h) of the two-way antenna power pattern is used to specify the azimuth resolution. This figure shows the beamwidth and plots the half-power contours in the elevation datum surface plane (i.e., the y = -h plane). Azimuth geometry has been added in this figure to the range geometry shown in Figure 4. One-half of resolution cell A_j is shown in Figure 5; the half shown in the direction of increasing L on the left side of the plane-of-incidence (plane-of-incidence is the x = i plane). The half which would extend out the right side has been eliminated for clarity. Thus, half of resolution cell A_j is shown as a solid object extending from the elevation datum surface (z = -h plane) to the surface of the ground, from arc R_{j-1} to R_{jN} in range, and from the plane-of-incidence (x = i plane) to the half-power contour in azimuth.

The problem is to find the intersection of the antenna half-power contour with the ground on both the left and right sides of the plane of incidence. The approach is to fix the range-coordinate at the mid-point of resolution cell A_j and test the azimuth, elevation data pairs on both sides of the plane-of-incidence for intersection of the half-power beamwidth with the ground.

The intersection of the half-power contour with the ground will occur a distance d_{ij} from the plane-of-incidence given by

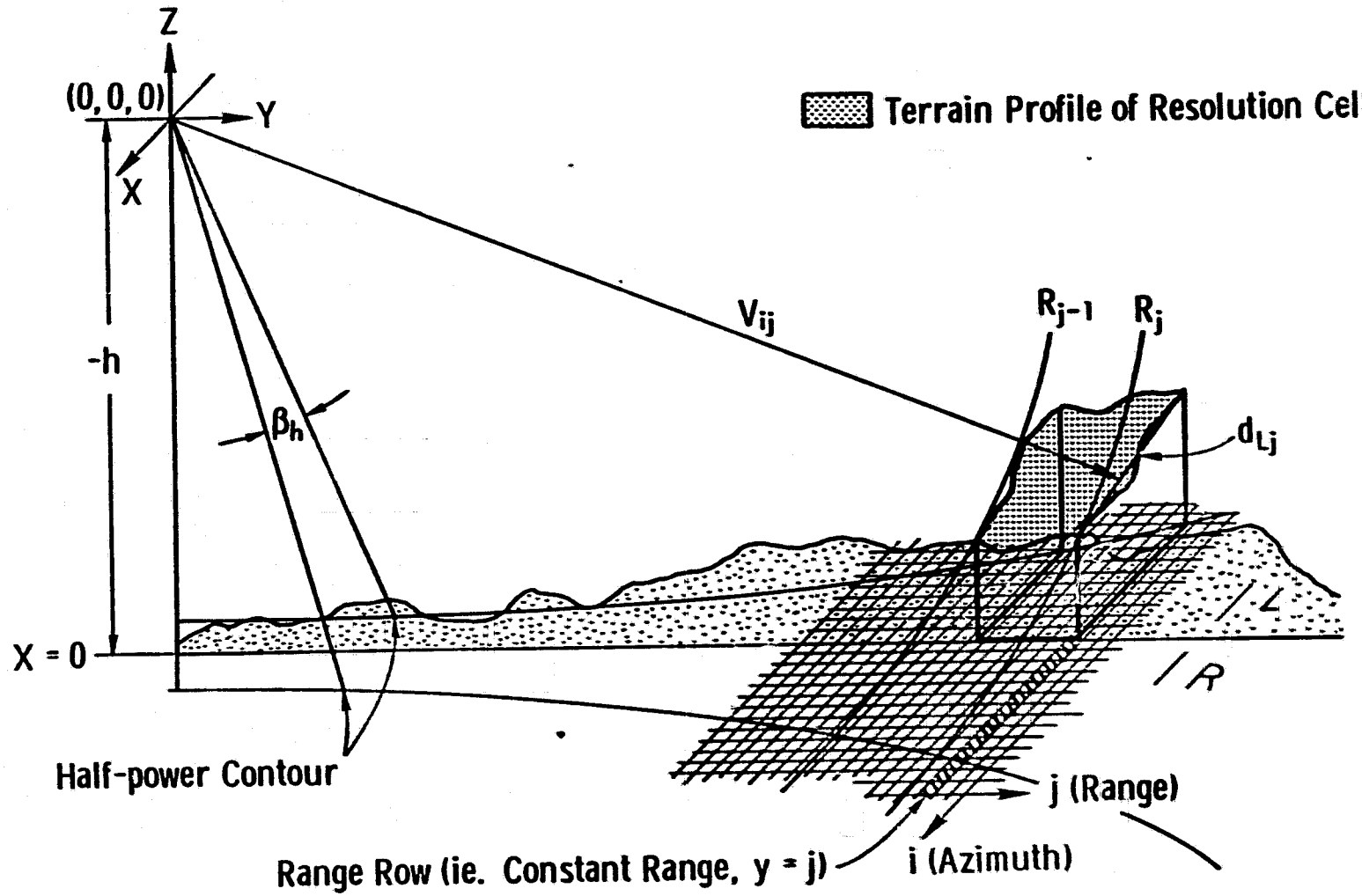

Figure 5. Azimuth Resolution

$$d_{ij} = \frac{R_{ij}\,\beta_h}{2} \qquad i = L,R \tag{3-24}$$

where R_{ij} is the range from the antenna to the ground cell of interest. If the range coordinate is fixed at the midpoint ($m = (j + j - 1)/2$) and data are evaluated on the left in azimuth ($i = L$), then

$$d_{Lm} = \frac{R_{Lm}\,\beta_h}{2} \tag{3-25}$$

Construct a vector $\vec{V}_{Lm}$ from radar antenna to each data base point on the row of range ($y = m$) being tested as shown in Figure 5. Since the coordinate system is set up so that the radar is at the origin (0,0,0), then it follows that

$$\vec{V}_{Lm} = (X_{Lm})\hat{x} + (Y_{Lm})\hat{y} + (Z_{Lm})\hat{z} \tag{3-26}$$

where (X_{Lm}, Y_{Lm}, Z_{Lm}) = coordinates of data base points being tested and $(\hat{x},\hat{y},\hat{z})$ are unit vectors in the x-, y-, z-directions, respectively. The magnitude of this vector is just the range from the radar to the ground at that point

$$R = |\vec{V}_{Lm}| = \sqrt{(X_{Lm})^2 + (Y_{Lm})^2 + (Z_{Lm})^2} \tag{3-27}$$

Set $R_{Lm} = R$ and solve equation (3-25) for an estimate of $\hat{d}_{Lm}$ and then test as follows:

$$\begin{aligned} &\text{If } \hat{d}_{Lm} - X_{Lm} > 0 \quad \text{test next point;} \\ &\text{If } \hat{d}_{Lm} - X_{Lm} = 0 \quad \text{half-power contour point;} \\ &\text{If } \hat{d}_{Lm} - X_{Lm} < 0 \quad \text{outside the half-power point;} \end{aligned} \tag{3-28}$$

where, as previously noted, the coordinate system is established so that the plane-of-incidence passes through the origin (i.e., the data base coordinate system is translated so that this occurs). The $\hat{d}_{Lm}$ are predictions from the data values of each point of how far away from the plane-of-incidence should be the half-power contour and the X_{Lm} are the exact distance. Thus, if the difference is positive as indicated in equation (3-28), then the point being tested lies between the plane-of-incidence and the half-power contour and another point should be tested. This test is made for each point until the test is satisfied on the left side and is then repeated on the right side.

If the left side and right side azimuth boundary points are found to be (X_{Lm},Y_{Lm},Z_{Lm}) and (X_{Rm},Y_{Rm},Z_{Rm}), respectively, then the data base points in the azimuth direction belonging to resolution cell A_j extend from X_{Lm} to X_{Rm}. From this point depending upon the data base resolution and application, modifications of the basic method can be adopted for finding the extent of a resolution cell. The sequence from equations (3-21) through (3-28) can be generalized and the data base elements belonging to resolution cell A_j can be specified exactly. Another approach would be to find only the end points of A_j and include only data base elements falling within those bounds. A simplification would be to use the two sets defined through the middle of A_j as just obtained and square-off the resolution cell.

The area of resolution cell A_j can be determined from:

$$A_j = d_j \, d_{LR}$$

$$d_j = \sqrt{(Y_{ij} - Y_{ij-1})^2 + (Z_{ij} - Z_{ij-1})^2} \qquad (3\text{-}29)$$

$$d_{LR} = \sqrt{(X_{Rm} - X_{Lm})^2 + (Y_{Rm} - Y_{Lm})^2 + (Z_{Rm} - Z_{Lm})^2}$$

where d_j comes from Figure 4 and d_{LR} comes from Figure 5. The area of a resolution cell would normally only be desired if simulating only single categories within a resolution cell. If simulating multiple categories within a resolution cell, then the area of each data base element would be used.

The next geometrical parameter of interest is the local angle of incidence.

Figure 6 shows an illustration of an idealized resolution cell. It can be seen that the cell is modeled as a plane facet having sides of length d_j and d_{LR} and, thus, area A_j. From the geometry of Figure 6 it can be shown that the local angle of incidence (θ_ℓ) is given by

$$\theta_\ell = \cos^{-1} [\hat{P} \cdot \hat{N}_{xyz}] \qquad \text{(Dot Product)} \qquad (3\text{-}30)$$

where

$\hat{P}$ = unit vector pointing from the center of the resolution cell through the antenna boresight;

$\hat{N}_{xyz}$ = unit vector normal to the resolution cell.

Also, it can be seen that the unit normal is given by

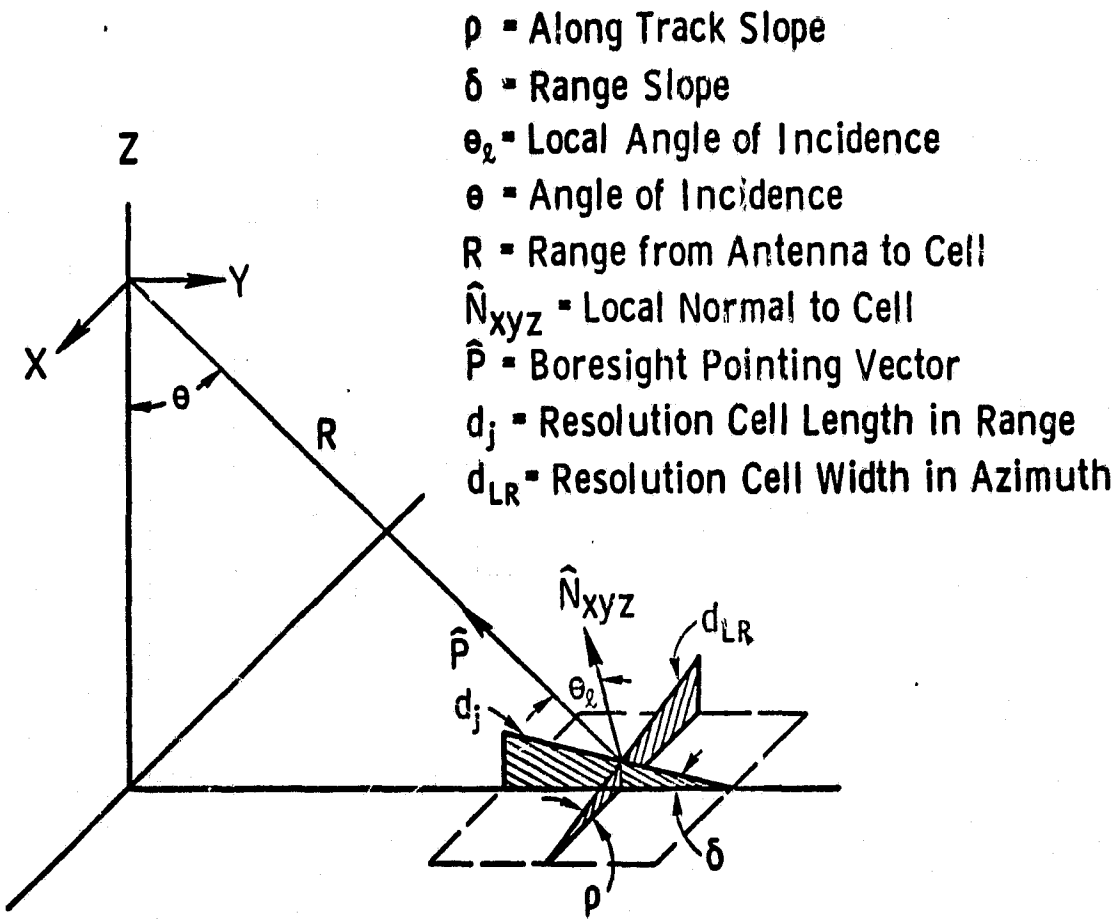

Figure 6. Geometrical Relationships for a Radar Resolution Cell with Arbitrary Slope (Plane Facet Model)

$$\hat{N}_{xyz} = \frac{\vec{d}_{LR} \times \vec{d}_j}{|\vec{d}_{LR} \times \vec{d}_j|} \qquad (3\text{-}31)$$

where

$\vec{d}_j = \hat{y} + (\tan\delta)\hat{z}$ = "tilt" in the range direction;

$\vec{d}_{LR} = \hat{x} + (\tan\rho)\hat{z}$ = "tilt" in the azimuth direction.

3.2.2.5 Propagation Phenomena

As alluded to earlier, the radar computer programs must incorporate provisions for certain special phenomena such as layover, shadow, etc. The following discussion summarizes the impact of these.

Radar is a ranging device and as such processes the signal returned versus the distance between the radar and features on the ground. Reradiation from nearer features is received, detected, and stored before that from more distant features. Also, radar provides its own source of illumination. These facts create what are here being called propagation phenomena: layover, shadow, local angle-of-incidence, range compression, etc. These phenomena must be treated if it is desired to produce the most accurate simulations which can be produced. The PSM simulation model incorporates all of these, and different applications will require different degrees of treatment. A brief discussion of these after [*Dellwig*, 1976] follows.

The condition called shadow, manifested as a black area on an image, is caused by obstructions on the ground, or by variations from point to point in the relative height and slope of the ground which mask illumination of certain areas. Masking illumination from certain

areas means that reradiation from the ground will not be received continuously, therefore, gaps are created in the return signal which are recorded as black areas on a radar image.

A point will be in shadow if a straight line from the source of illumination, the radar, to that point intercepts either an obstruction on the ground (e.g., a building, tree, etc.) or the ground, itself, at some intermediate point as illustrated in Figure 7. Shadow is incorporated in both specializations of the PSM presented in Section 3.4.

Layover is the condition where the return signal from objects, or the ground, itself, above a datum surface is received sooner and the signal from objects, or the ground below the datum is received later; also illustrated in Figure 7. Thus, the radar representation of the taller, or higher feature is displaced toward the radar such as is shown for the tower while that for the shorter, or lower feature is displaced away from the radar; precisely the opposite to that observed for optical systems. When a data processing scheme such as that discussed in Section 3.3.4 is used in identifying which data base cells belong in a particular radar resolution cell, layover is automatically treated. Layover is incorporated in both specializations of the PSM presented in Section 3.4.

Local angle of incidence is the angle formed between a beam of radar energy impinging the surface and a line drawn vertical to the surface at the point of incidence as shown in Figure 8. This angle is essential for calculating the value of σ^0 for each resolution cell. The local angle of incidence can be calculated via equation (3-30) and is calculated in both the PPI and SLAR software specializations discussed later.

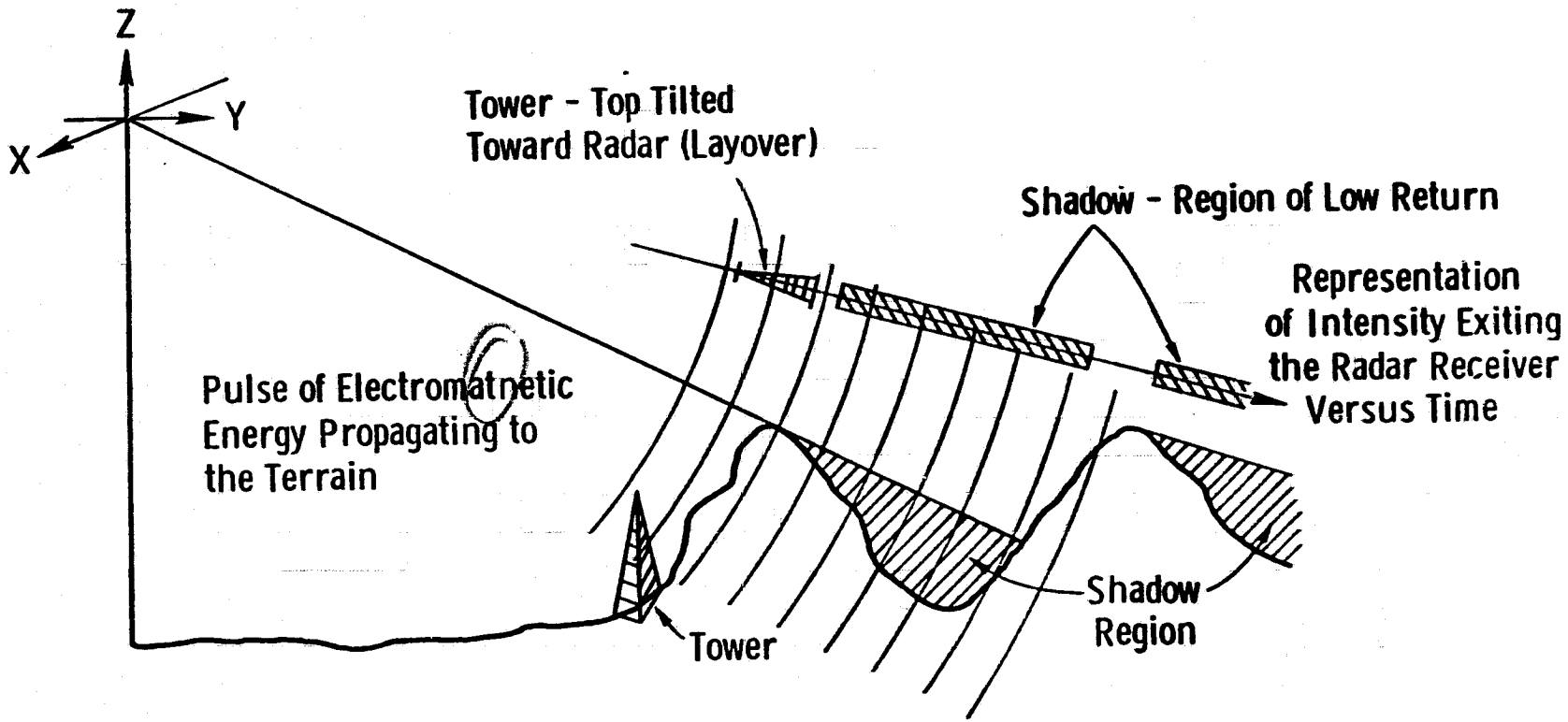

Figure 7. Shadow and Layover

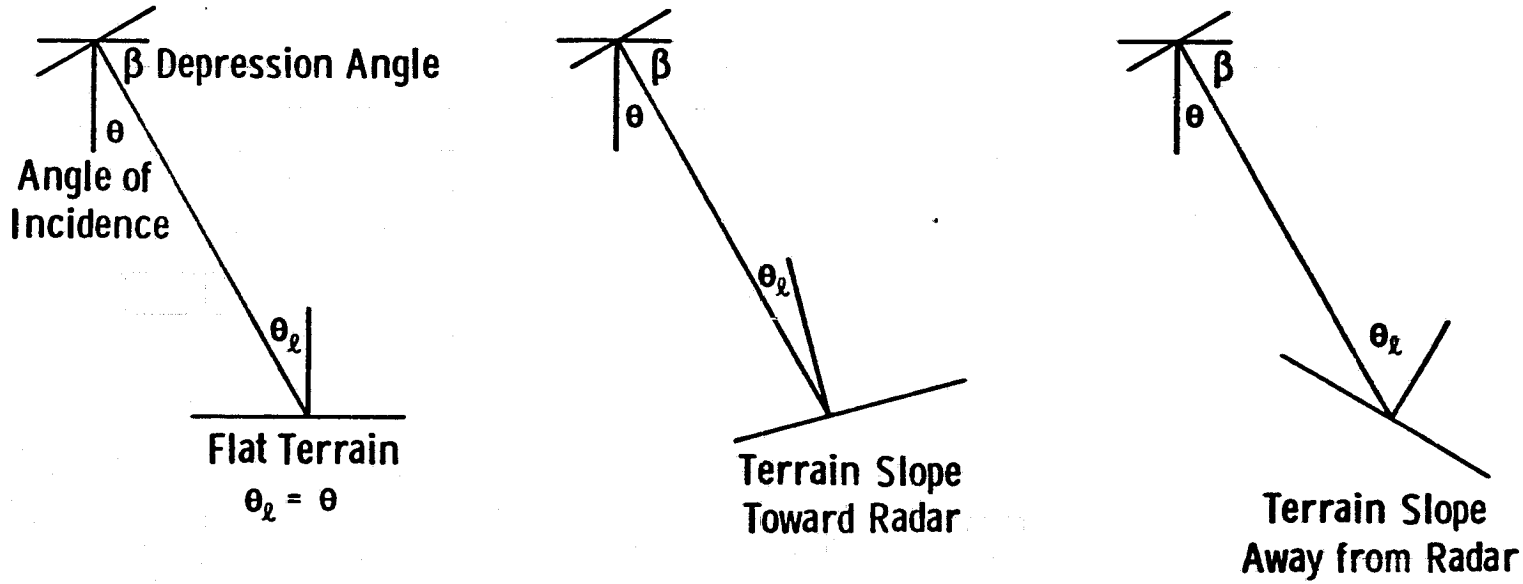

Figure 8. Local Angle of Incidence

Range compression is the condition created by recording radar data in the slant range mode. In the slant range format, data are recorded versus range (distance) rather than versus angular relationships and this produces a continuous scale change. The scale change is monotonic decreasing toward the near-range edge of an image as is illustrated in Figure 9. The distortion induced can be electronically corrected in the ground range format by applying a hyperbolic sweep to the CRT. The ground range format does not necessarily reproduce the true spatial relationships or features on the ground. Topographic relief, or elevation variations above or below a datum surface cause degradations which the ground range mode does not correct. As relief in a given area increases, distortion becomes more pronounced. The PSM specializations previously discussed are capable of simulating either the slant-range or the ground-range format.

3.2.3 PSM Simulation Computer Programs

3.2.3.1 Introduction to PSM Implementation

As shown conceptually in Figure 2, the PSM computer programs can be utilized to form simulated radar data only after satisfaction of the three input requirements for simulation parameters, data base, and reflectivity data. The results previously obtained for intensity -- (3-16) or (3-17) -- and density -- (3-18) -- are the final computational algorithms of the PSM. They do not represent the complete model. These algorithms, or modifications of them are invoked to produce final, desired results only after all the geometrical relationships between radar and ground spot (resolution element) have been solved and after all the propagational phenomena have been properly treated. These geometrical and propagational considerations are

$A = B = C$ - Ground
$A_1 < B_1 < C_1$ - Slant Range Presentation
$A_2 = B_2 = C_2$ - Ground Range Presentation

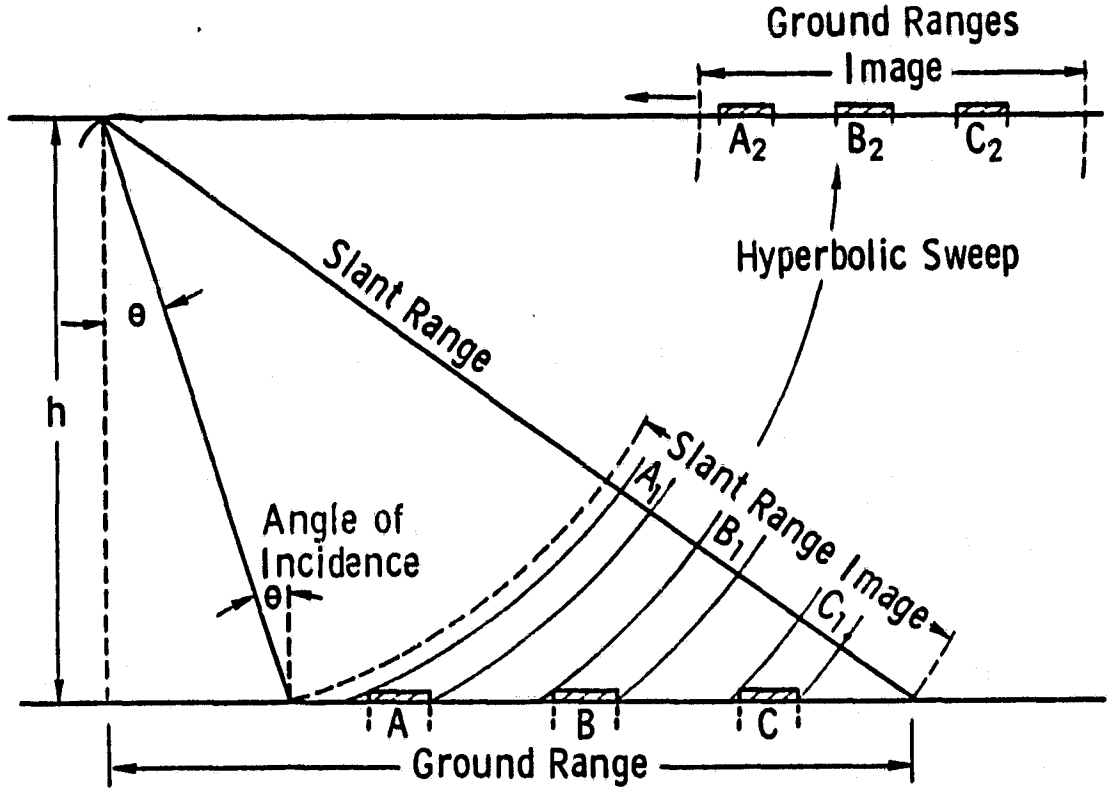

Figure 9. Range Compression

treated in the data handling and radar effects modeling which have been designed into a specific software realization of the PSM.

In general, geometrical effects such as radar resolution size, local angle of incidence, range, etc. and propagational phenomena such as shadow, layover, compression, etc. are treated explicitly by the software. They are developed from such considerations as the flight path parameters, and the ground topography modeled in the data base.

The general PSM computer software and all specializations incorporate the same data processing philosophy. This philosophy requires the data base to be stored on computer-compatible digital magnetic tape (CCT) as a matrix developed in a rectangular coordinate system. The first step for the PPI implementations is conversion of this data base from rectangular to polar coordinates (SLAR, of course, uses the rectangular coordinate system).

The simulation computer programs are structured into two separate phases. The first phase accepts the CCT containing the data base and calculates all the geometrical and propagational effects. This phase predicts the power for each point in the data base from the geometrical data and stores the power data on an interim CCT. The second phase incorporates the resolution aspects of the system being modeled and combines the predicted power for the appropriate number of data base points into each radar resolution cell. Finally, it converts the power predicted for each radar resolution element into the appropriate grey-tone value for each pixel (picture element) in the output image, and stores the results on a CCT.

If the application being simulated is a PPI radar, then the next function performed is conversion from polar coordinates back into rectangular coordinates. In either case, the final results are stored

on an output CCT in a raster scan format for evaluation on a visual system such as the VDI*.

This philosophy is developed in a little more detail in the following section for a SLAR implementation.

3.2.3.2 SLAR Software Realization of PSM

A SLAR is a radar mounted on an aircraft (or spacecraft) so as to be viewing the ground out to the side and employs either real or synthetic aperture techniques. SLAR's have historically been used as information gatherers. They have a proven history of value for remotely collecting information and presenting the data in image format. Some proven applications areas are those of geology [*MacDonald*, 1969], agriculture or vegetation monitoring [*Bush and Ulaby*, 1976], mapping in regions obscurred by clouds [*Wing*, 1971], military intelligence [*Frost et al.*, 1976], etc. The geometry of a SLAR is illustrated in Figure 10.

As shown in Figure 10, the SLAR is mounted so as to illuminate the ground perpendicular to the flight direction of the aircraft. Unlike the PPI, the SLAR antenna is rigidly attached to the vehicle and does not rotate. The radar transmits pulses of electromagnetic energy to the ground from the near range to the far range in a narrow swath as confined by the directional properties of the antenna. The return signal from each pulse is processed versus time and is input to a CRT (for example) where it is used to intensity modulate the electron

*VDI is a Video Digital Interface System manufactured by Interpretation Systems, Incorporated, Kansas.

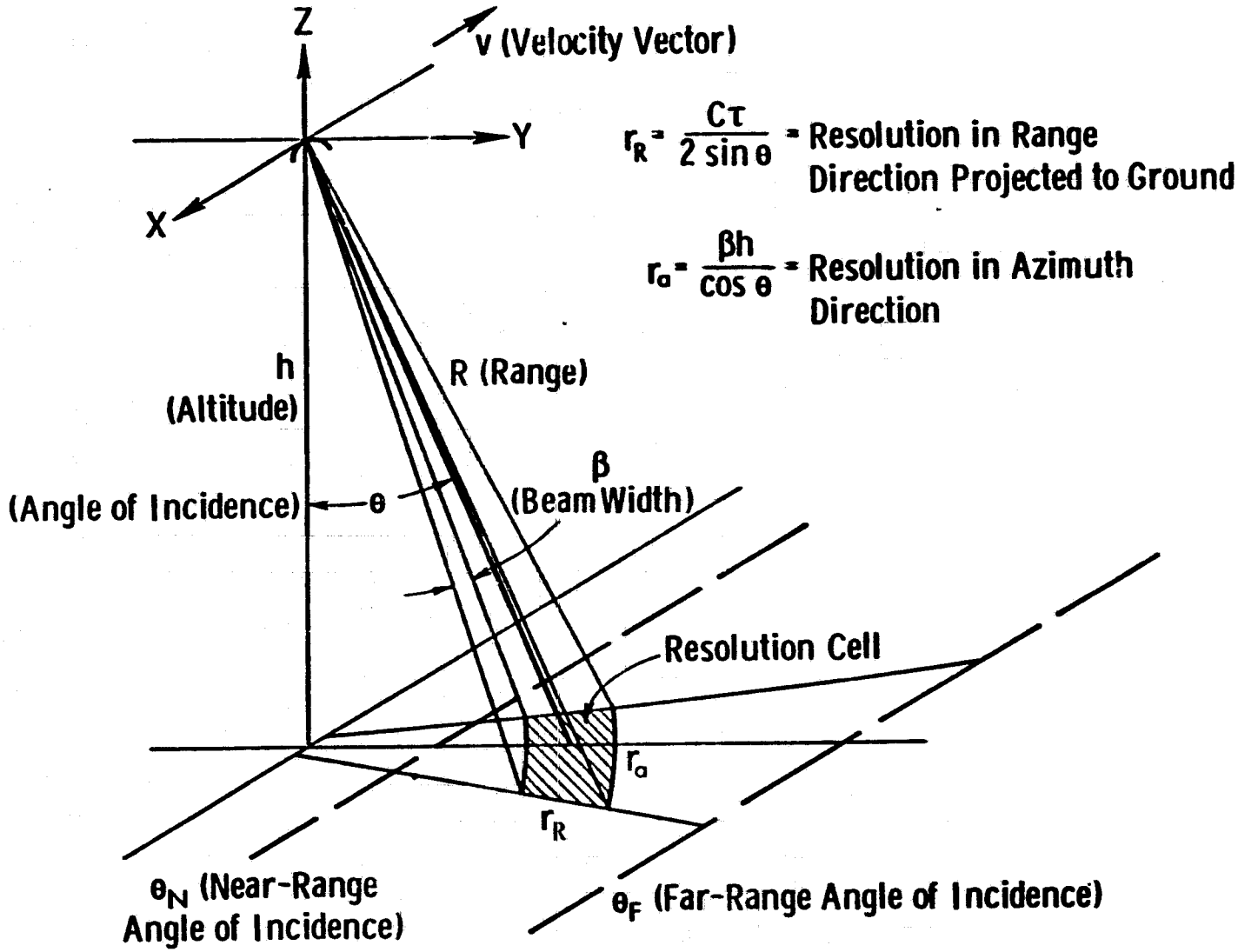

Figure 12. SLAR Scan Format and Geometry

beam as it sweeps across the face of the CRT. The sweep of the CRT is synchronized with the velocity of the vehicle. Each pulse transmitted illuminates a progressively different swath of ground and the sweep of the CRT is indexed accordingly (the sweep of the CRT might be used to expose film moving in synchronization with the vehicle velocity across the face of the CRT). In this way, a radar image is built up pulse-by-pulse and sweep-by-sweep. This summarizes the operation of a SLAR and describes the phenomena being modeled by a SLAR software realization of the PSM. Theoretical analyses of SLAR's are well-documented in the literature (e.g., [*Skolnik*, 1970; *Moore*, 1975].

One specific software realization of the PSM is described in this section. The software realization described is of a SLAR. The goal of this section is to describe the basic functions of the computer programs. In addition, the discussion is set in the context of the flow of data, from start to finish. Figure 11 illustrates, in block diagram form, how the separate pieces fit together and the interactions that occur between them when using these computer programs to simulate radar data.

Figure 11 shows the flow of data, from start to finish, when forming simulated SLAR data. The left side of Figure 11 illustrates where the data comes from, and the right side where it goes. The central portion of the figure shows the computer programs.

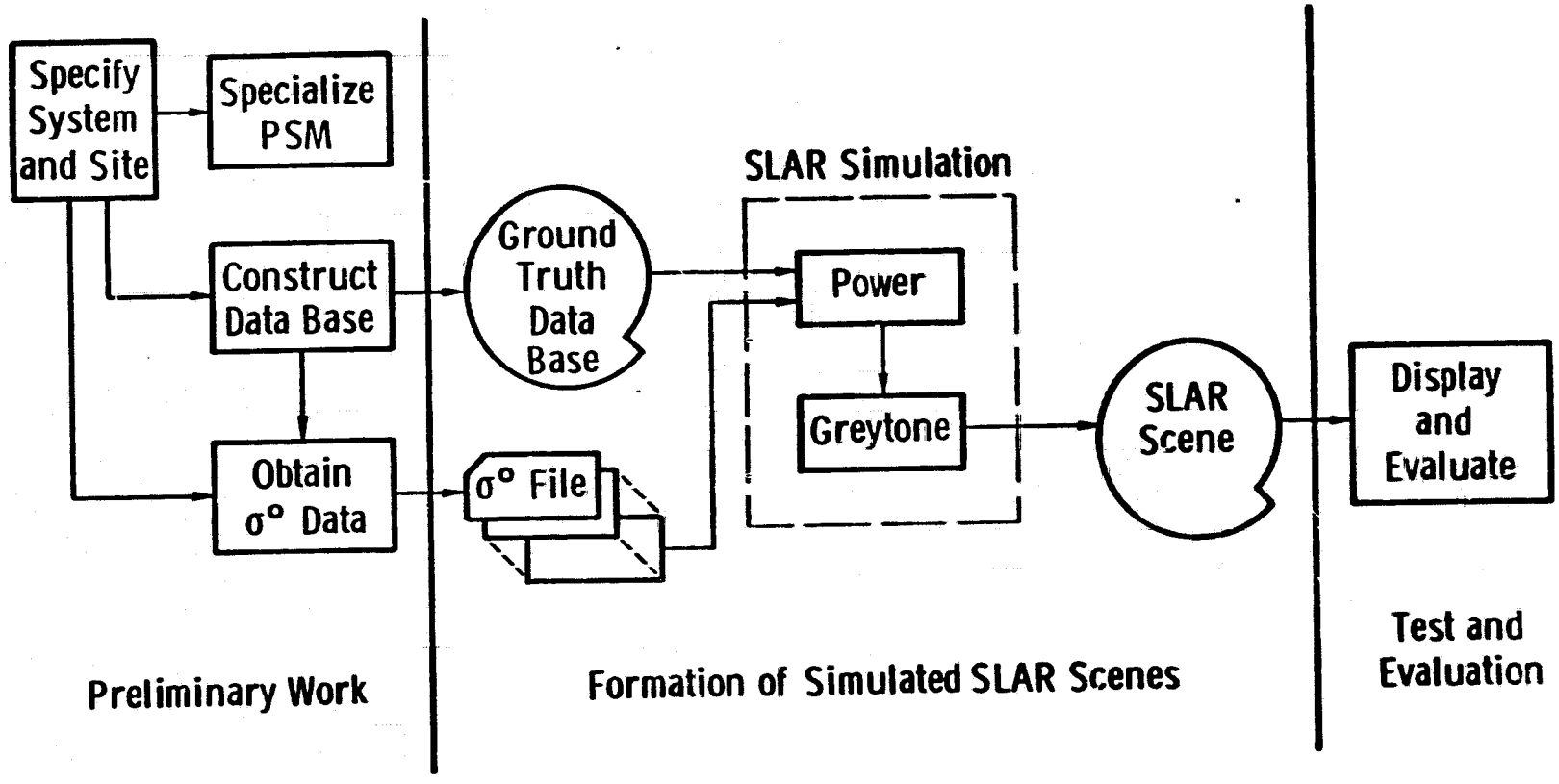

Figure 11. Flow of Data for Simulation of SLAR Data

As can be seen from Figure 11, the SLAR realization of the PSM is for a digital computer. Two separate computer programs (separate according to function) must be run sequentially in order to form simulated SLAR data. The first of these programs (POWER) accepts a data base in a rectangular coordinate system and solves all the complicated geometrical relationships between the SLAR and each ground element in the data base. It accepts, next, a file containing backscatter data (σ^0) and calculates the average return power for each data base ground point. The second program (GREYTONE) computes the SLAR resolution element, incorporates the appropriate antenna correlation function between resolution elements, and produces an output array of image density values (called greytones). Communication between programs is accomplished via computer-compatible magnetic tapes. The SLAR simulation programs are summarized and listed in the following sections.

Power

The first program, POWER, is a highly computational program requiring minimal core storage. This program accepts as input a data base stored on digital magnetic tape, the terrain backscatter data (σ^0 file) input via a data statement, and specification of the flight line and system parameters. POWER performs all of its computations for each element in the data base. It first determines whether or not each point will be in shadow. Then, for non-shadow points, it calculates various parameters (e.g., range, local angle of incidence, effective area, etc.) and uses these together with the σ^0 file to compute an average return

power for each element in the data base. POWER then performs a layover function and stores these data on an interim magnetic tape, its function completed.

For each point in the data base, POWER solves the geometry relating the position of the radar platform (three-dimensional position) to the point, calculates the slope of the terrain, the angle of incidence, and the range between platform and point. These calculations are made sequentially for each point of each record as the tape containing the data base is read into the computer. Upon determining these parameters for a point, POWER enters the main computational algorithm of the program which calculates the average power exiting the receiver from that point. This calculation of power uses the slope of the ground, the angle of incidence between radar and ground (both normal and local angles), the range from platform to the point on the ground being interrogated, the power pattern of the antenna, the category identification from the data base, backscatter data from the σ^0 file, and the transmitter/receiver/image model incorporated for the radar aystem whose response is being simulated. All of these variables and parameters are combined appropriately for calculating the estimate of power existing the radar receiver for each point on the ground. In this way POWER calculates the average power exiting the receiver on a point-by-point basis. The resultant data are stored on an interim magnetic tape for further processing in later stages. The data are ordered sequentially on this tape in the same form as the array in which the data base was input.

Greytone

The second program was developed to incorporate the spatial relations between adjacent resolution cells and to convert the resultant estimates of power into image greytones. This program, GREYTONE, combines data base cells into radar resolution cells via an autocorrelation. The shape and length of the autocorrelation are input parameters. In addition, GREYTONE produces pixels either to satisfy an input range-rate and PRF (pulse repetition frequency) or to produce a desired output image size. Upon completing this, GREYTONE converts the resultant power data into density values, greytones, quantizes them into the desired number of levels, computer word size, and biases the range of the resultant data to that desired for ultimate photographic storage.

The bias, G_{R_C}, required to display a desired power range in an image is an input parameter to GREYTONE. The desired mapping ratio of power exiting the receiver into density in the photograph is also an input parameter; the portion of the radar dynamic range (mdB) desired to be mapped into the dynamic range of the photograph (17 - 20 dB) is specified. Thus, upon specification of an autocorrelation function shape and length, range-rate and PRF, and quantizing parameters (bias and mapping ratio, or gain) GREYTONE operates on the power map input via digital magnetic tape from the previous program, POWER, producing the greytone map of the final image on a pixel-by-pixel basis. The greytone data are stored on a digital magnetic tape. The stored data order is still the same as the input data base.

At this point the simulated SLAR data are complete but the data are stored on digital magnetic tape. The "normal" data format is:

9 track digital magnetic tope;
1600 bpi;
N records;
M pixels per record;
0 corresponds to black;
255 corresponds to white.

This format is suitable for input to the display and evaluation device used, the VDI* located at RSL.

3.2.4 Results of the PSM

Results have been produced via the PSM for several different system configurations and several different geographic sites. These are included in Appendix B.

3.3 Passive Microwave Sensor Simulation

The Point Radiation Model for simulating radiometer data is developed following the general philosophical approach to microwave sensor simulation discussed in 3.2. It requires knowledge of the different target characteristics, transmission medium and receiver system parameters. The block diagram in Fig. (12) presents the basic flow of data for a radiometer simulation.

---

*VDI is an image processing system manufactured by Interpretation Systems, Inc., Kansas.

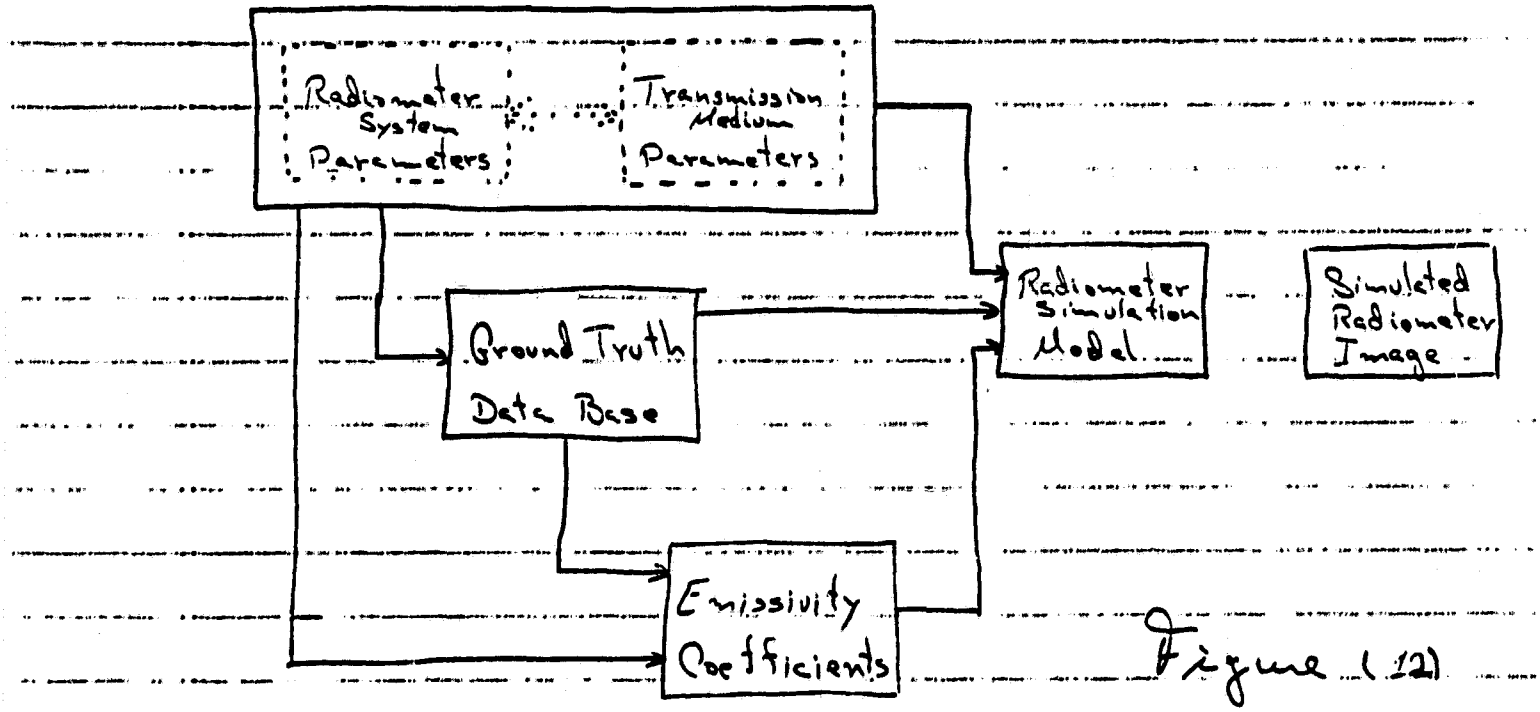

Figure (12)

Due to the signal-to-noise characteristics of a passive microwave system, transmission medium parameters are of fundamental importance and are treated with the same priority as the radiometer parameters themselves [Rainwater, 1978].

The general procedure for simulating a radiometer image consists of the following:

1) establishing the system and medium parameters and their interrelationships,
2) establishing a ground truth data base and its interrelationship to the sensor,
3) establishing the emissivity coefficients of the different targets and/or categories within the data base,
4) establishing a valid statistical model for the system
5) establishing the transfer function of the radiometer system which translates the ground truth data and geometrical relationship between sensor and target into radiometer output power, and
6) establishing a greytone equation which transforms the output power into greytones in an image.

It should also be remembered that this particular simulation was to illustrate a methodology and was therefore only a first-order approximation. Consequently, certain assumptions about the parameters have been made, such as the use of a calibrated system with antenna gain being equal to unity, linear filter and amplifier characteristics, and system fluctuations, and noise fluctuations which are negligible. The procedure developed is completely general such that any radiometer configuration and/or any ground truth data base can be used as the input, provided there is sufficient emissivity data for all the ground truth categories. Finally, it should be pointed out that the empirical assessment of emissivity values for different types of targets has been limited and to that end much of the data used here is extrapolated from a combination of theoretical and empirical studies and may not be entirely accurate. It is however, sufficient to illustrate the approach and methodology to radiometer simulation.

3.3.1 Theoretical Foundation of the PRM

A general block diagram of a radiometer system and surrounding medium is represented in figure (13) [Ref. 1,2,3,4]. With this schematic, we are attempting to answer two basic questions: What does a radiometer's antenna "see", and what does the radiometer's detector "see"? We deal with these questions separately. The question as to how the detected information is stored is treated in a later section.

A radiometer is a passive microwave system. It operates only as a receiver and detects whatever energy is already available from nature. This energy arises as a consequence of electromagnetic radiation emitted from targets of interest plus background contributions.

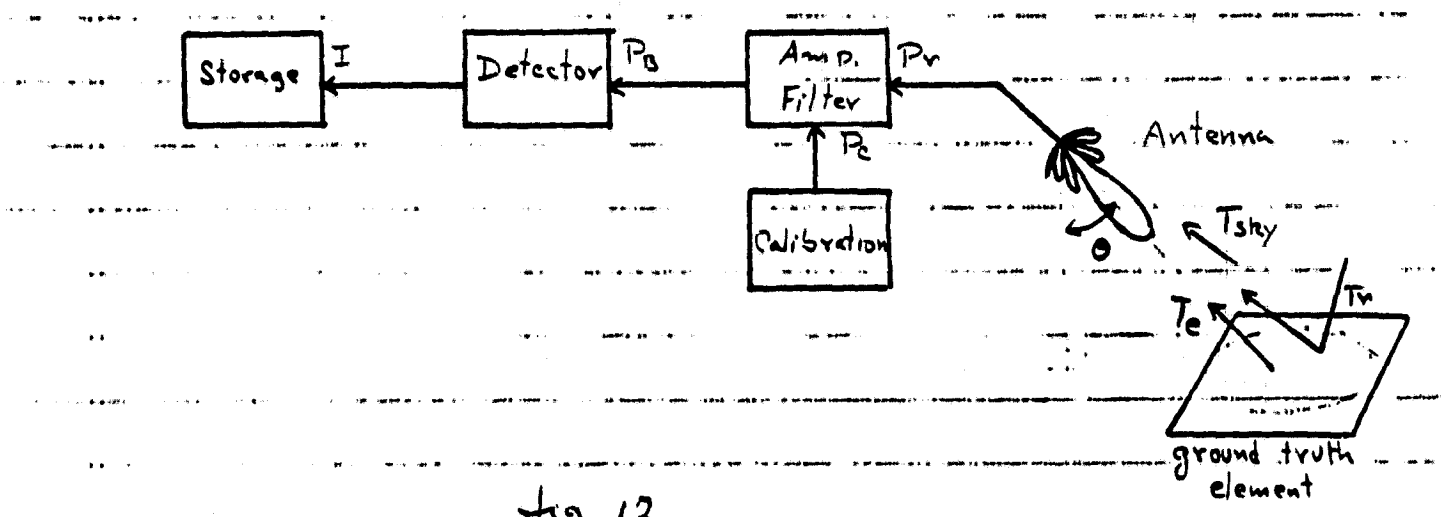

fig 13

The theory explaining the origins of this radiation level is very well-developed and documented in many sources [Refs. 1,2,3,4,5,6,7,8,9.10]. All objects with a temperature above absolute zero emit electromagnetic energy. The amount of energy a natural object radiates is a function not only of its physical temperature but also of its chemical composition, surface roughness and other such physical properties. The Rayleigh-Jeans approximation of Planks law predicts that for a perfect radiator, or so-called "black-body", there is a linear relationship between its physical temperature and its emitted radiation intensity [2,4] as given by the equation

$$\beta(\lambda,T) = \frac{2KT}{\lambda^2} \quad Wm^{-2}\ sr^{-1}\ Hz^{-1} \qquad (3\text{-}32)$$

where

$\beta(\lambda,T)$ = power radiated per unit frequency from $1m^2$ of a black body surface into a solid angle of 1 sr;

λ = wavelength (m);

T = physical temperature (°K);

K = Boltzmann's constant.

Natural objects which are less efficient, emit less radiation (1,4) according to the equation

$$\beta(\lambda,T) = \frac{2\varepsilon KT}{\lambda^2} \qquad (3\text{-}33)$$

where ε is the emissivity and is characteristic of the particular object at a particular angle of observation and is defined as the ratio between the radiation emitted by the object in relation to the energy which would be emitted by a perfect radiator at the same temperature. (4) If the term 'brightness temperature' T_β is then defined as the physical temperature of a black-body with the same emitted radiation as the physical object considered, it can be represented as the product of the bodies' physical temperature T, and its emissivity constant ε, according to the equation

$$T_\beta = \varepsilon T \qquad (3\text{-}34)$$

For an antenna pointing at the earth as seen in figure (13), the antenna brightness temperature 'observed' is the result of a sum of three basic sources:

1) The radiometric temperature of the target scene Te,
2) the radiometric temperature of the atmosphere Tsky, and
3) the brightness temperature due to electromagnetic energy coming from space (sun, stars, galaxie, 'big bang' and so forth) and reflecting off the earth (Tv).

Modifying these factors we have 'L', an atmospheric loss parameter, which is a function of the attenuation coefficient of the atmosphere (per unit thickness), the depth of the atmospheric strata, local weather conditions,

and the altitude of the antenna. Also, modifying the target scene temperature Te and the reflected sky temperature Tr we have the emissivity ε of the target scene. The antenna brightness temperature Ta' due to the three sources mentioned above is then defined in the equation

$$Ta' = \left(1 - \frac{1}{L}\right) T_{sky} + \frac{\varepsilon Te}{L} + \frac{(1 - \varepsilon)Tr}{L} \qquad (3\text{-}35)$$

for a smooth surface target assumption.

The total power Pr' radiated into the antenna is then equal to the antenna temperature, multiplied by Boltzmanns constant and by the bandwidth of the receiver, as shown by the equation

$$Pr' = Ta'K\Delta\nu \qquad (3\text{-}36)$$

where

Pr' = total power radiated into the antenna,

Ta' = antenna brightness temperature

K = Boltzmanns constant =

$\Delta\nu$ = Bandwidth of receiver

A general block diagram of a radiometer receiver ignoring noise considerations is shown in figure (14).

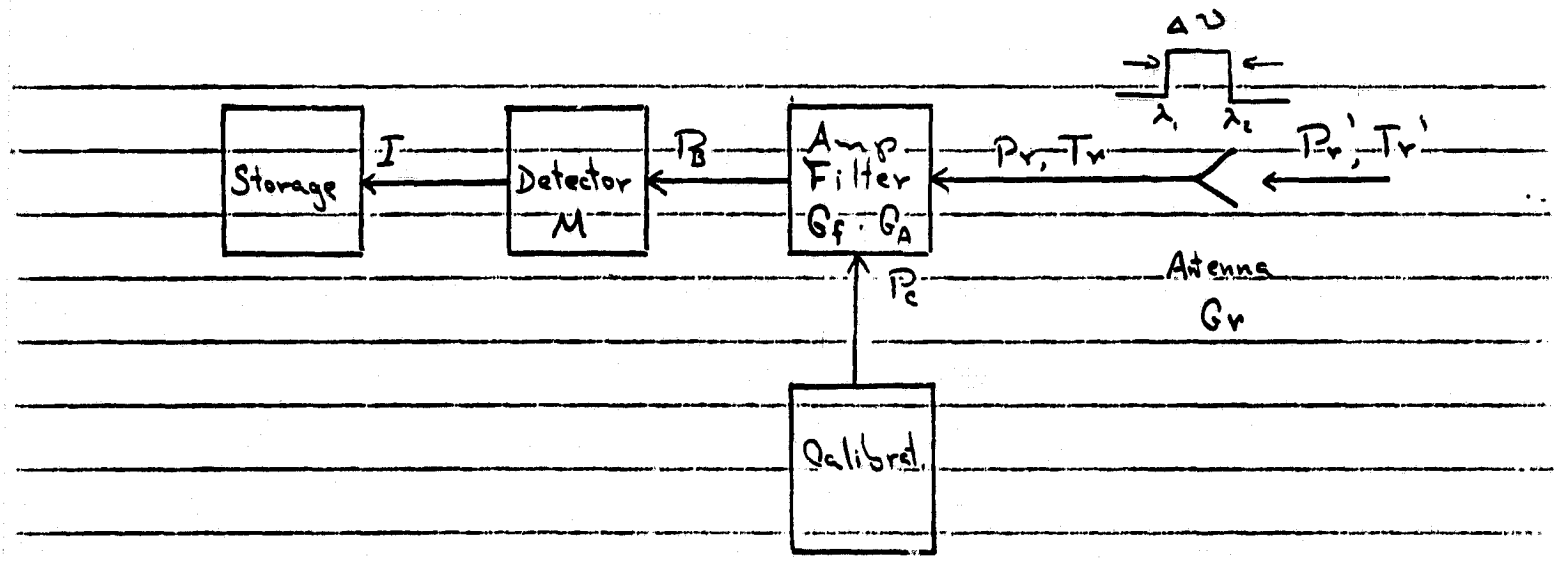

Fig. 14

where

T_a' = antenna brightness temperature

Pr' = total power radiated into antenna

Pr = total power passed on from the antenna to the amplifier-filter module

Gr = antenna gain

λ_1 & λ_2 = lower and upper bounds of system bandwidth (i.e., the part of the electromagnetic spectrum to which the radiometer is sensitive)

G_A = amplifier gain

G_f = filter gain

P_c = power received from calibration module

P_β = power entering detector

I = intensity of light being stored on film (if film storage is the case) - a function of P_β

M = proportionality constant between P_β and I.

Each one of these parameters will be defined entirely by any proposed radiometer system, be it a Dicke receiver, a Correlation receiver, a Total Power receiver or any other configuration likely to be produced.

The total power passed on to the amplifier-filter module from the antenna is the product of the antenna gain with the total power radiated into the antenna. For the first order simulation the antenna gain was assumed to be unity and uniform throughout the beamwidth of the main lobe. The effect of side lobes was neglected. The foot print covered by the antenna was assumed to be a square, with an area equal to the area of the radiometer resolution cell. The total power reaching the detector is

then the product of the power entering the amplifier-filter module, the amplifier gain G_A, and the filter gain G_f. The power entering this module comes either from the antenna or from the calibration module. For the assumption of a perfectly calibrated system, the calibration power P_c has been ignored. Therefore,

$$P_\beta = Pr'GrG_AG_f \tag{3-37}$$

where P_β, Pr', Gr, G_A and G_f are defined as noted earlier, and

$$P_\beta = Pr' \tag{3-38}$$

for the hypothetical system of our first order approximation. From equations (3.6), (3.5) and (3.4) we can see that

$$P_\beta = K\Delta\nu \left\{(1 - 1/L)T_{sky} + \frac{\varepsilon Te}{L} + \frac{(1 - \varepsilon)Tr}{L}\right\} GrG_AG_f \tag{3-39}$$

For an imaging radiometer, the output of the detector will be in the form of an image intensity I, directly proportional to the power P_β entering the detector, according to the equation

$$I = MP_\beta \tag{3-40}$$

where

I = image intensity

P_β = power entering detector

M = detector proportionality constant (= 1.0 for the first order simulation)

This value for intensity is then transformed into an image greytone value via a greytone equation developed in a following section.

3.3.2. Simulation Programs

Two computor programs have been developed for simulating radiometer images. The first program, named POWER, computes the energy being emitted

from each picture element (pixel) of the data base, on a line by line basis. The second program, SIMULATE, assumes a flight path, determines which data base cells comprise each pixel of the simulated image, sums the power coming from all those cells and converts the total power return into a greytone for visual display. The greytone equation is derived analogously to the one derived by Holtzman, et.al. (10) for the Point Scattering Model of Radar Simulation as follows:

Equation 3-40 showed the light intensity I coming from the detector module to be

$$I = MP_{\beta} \tag{3-40}$$

where

I = light intensity

P_{β} = power coming out of the radiometer

M = proportionality constant (= 1.0 for this first order simulation)

This light intensity is used to expose a photographic film. The amount of exposure is measured in terms of film density D, and it has been well documented that this film density is defined as

$$D = \gamma \log_{10} I + \log_{10} K \tag{3-41}$$

where

γ = gamma of the film

K = a positive constant which depends upon the exposure time and on the film processing and development techniques,

D = photographic density

Substituting equation (3-40) into equation (3-41) we have

$$D = \gamma \log_{10} P_{\beta} + \log_{10} K + \gamma \log_{10} M \tag{3-42}$$

The greytone 'G_r' for an 8-bit image is obtained by scalling down the optical density D. We assume the range of optical density values is from ϕ (zero) to some value 'χ'. If 256 greyrone levels are being used (for an 8-bit image) where black is equal to zero and white is 255, then

$$G_r = \frac{255D}{\chi} \tag{3-43}$$

defines the greytone value for an optical density D. Suppose then, two emitters C_1 and C_2 in a data base. Furthermore suppose emitters C_1 produces a known greytone. The optical density values for each would be defined as

$$D_1 = \gamma \log_{10} Pr_1 + \log_{10} K_1 + \gamma \log_{10} M_1 \tag{3-44a}$$

and

$$D_2 = \gamma \log_{10} Pr_2 + \log_{10} K_2 + \gamma \log_{10} M_2 \tag{3-44b}$$

Substracting D_1 from D_2 we get

$$D_2 - D_1 = \gamma \log_{10} \frac{Pr_2}{Pr_1} + \log_{10} \frac{K_2}{K_1} + \gamma \log_{10} \frac{M_2}{M_1}$$

or

$$D_2 = D_1 + \gamma \log_{10} \frac{Pr_2}{Pr_1} + \log_{10} \frac{K_2}{K_1} + \gamma \log_{10} \frac{M_2}{M_1} \tag{3-45}$$

Substituting equation (3-43) into equation (3-45) we get

$$G_{r2} = G_{r1} + \frac{255}{\chi} \left\{ \gamma \log_{10} \frac{Pr_2}{Pr_1} + \log_{10} \frac{K_2}{K_1} + \gamma \log_{10} \frac{M_2}{M_1} \right\} \tag{3-46}$$

Since for this case the film used to store the information from emitter C_1 is the same as for C_2, equation (3-46) reduces to

$$G_{r2} = G_{r1} + \frac{255}{\chi} \gamma \log_{10} \frac{Pr_2}{Pr_1} \tag{3-47}$$

In this first order simulation, for a non-varying radiometer, the ratio $\frac{P_{r2}}{P_{r1}}$ reduces by substitution of equation (3-36) and the knowledge that

$$P_r = G_r P_r' \tag{3-48}$$

where

P_r = power entering emplifier and filter module, coming from the antenna

G_r = antenna gain

P_r' = power entering antenna

and we obtain

$$\frac{P_{r2}}{P_{r1}} = \frac{Ta'_2}{Ta'_1} \tag{3-49}$$

Finally, substituting (3-49) into (3-47), and then (3-47) into (3-39), we get

$$G_{r2} = G_{r1} + \frac{255}{\chi}\ \gamma \log_{10} \left\{ \frac{(1 - 1/L_2)T_{sky_2} + \varepsilon_2 Te_2/L_2 + (1 - \varepsilon_2)Tr_2/L_2}{(1 - 1/L_1)T_{sky_1} + \varepsilon_1 Te_1/L_1 + (1 - \varepsilon_1)Tr_1/L_1} \right\} \tag{3-50}$$

where G_{r1}, T_{sky_1}, Te_1, Tr_1, L_1 and ε_1 are all known for a specific emitter C_1. This then is the greytone equation for the radiometer simulation if a density representation is used as the final image product.

3.3.3. Ground Truth, Data Base and Flight Geometry

The same data base used for radar simulation can be used for radiometer simulations if emissivity data are substituted for radar reflectivity data (σ^o). Appendix G presents the graphs of emissivity vs. nadir look angles for the different categories of the data base. These values are summerized in

TABLE 3

CATEGORY	EMISSIVITY								
	0°	10°	20°	30°	40°	50°	60°	70°	80°
Swamp	.70	.69	.68	.67	.65	.62	.59	.58	.55
Bareground	.85	.84	.82	.81	.78	.71	.68	.65	.60
Gravel	.85	.84	.84	.83	.81	.77	.73	.64	.46
Trees	.88	.88	.88	.87	.86	.84	.82	.80	.79
Grass	.93	.93	.93	.93	.93	.93	.93	.93	.93
Scrub	.91	.91	.90	.89	.88	.86	.84	.82	.80
Hay	.93	.93	.93	.93	.93	.93	.94	.92	.93
Oats	.92	.92	.92	.92	.92	.91	.90	.88	.84
Corn	.91	.91	.90	.89	.88	.86	.84	.82	.80
Wheat	.97	.97	.96	.96	.96	.96	.97	.93	.92
Forage	.93	.93	.93	.93	.93	.93	.94	.92	.93
Vegetables	.92	.92	.92	.91	.90	.89	.88	.87	.86
Water	.41	.40	.39	.36	.31	.26	.23	.20	.18
Asphalt	.89	.87	.84	.78	.70	.62	.52	.42	.32

Table 3.

The elevation and category data are valid. Additionally, a physical temperature ranging from 300° K to 340° K as a function of time exposure to the sun was assumed for the entire simulation site.

A hypothetical aircraft flies directly over the center of the simulation site at a constant velocity and constant altitude. The sensor antenna scans the data base from its left edge to its right edge, and back again from right to left. As the position of the aircraft advances into the simulation scene, so does the antenna cover new terrain. The change in position of the aircraft is computed such that there is no overlap between adjacent ground cells at nadir look direction (i.e., directly beneath the flight path). This procedure continues throughout the entire data base.

The antenna footprint assumed for the first order simulation is a square when located directly beneath the flight path, elongating and widening as the antenna sweeps to either side of the data base (figure 15). Adjacent footprints are assumed to have no points in common even as the look angle changes, but overlap does occur on different directional scans of the antenna (figure 16),such that some data base cells are used more than once, and some are not. The power received by the antenna for each footprint is a combination of the emitted energy of the data base cells contained within it. For the sake of minimizing the program execution time, it is assumed that whenever a data base cell contributes to a footprint, the line through that point and the aircraft position is perpendicular to the flight path. This simplification is made to ease the checking needed to determine which ground cells are blocked from the antenna by a point of higher elevation between the ground cell in question and the antenna (fig. 17).

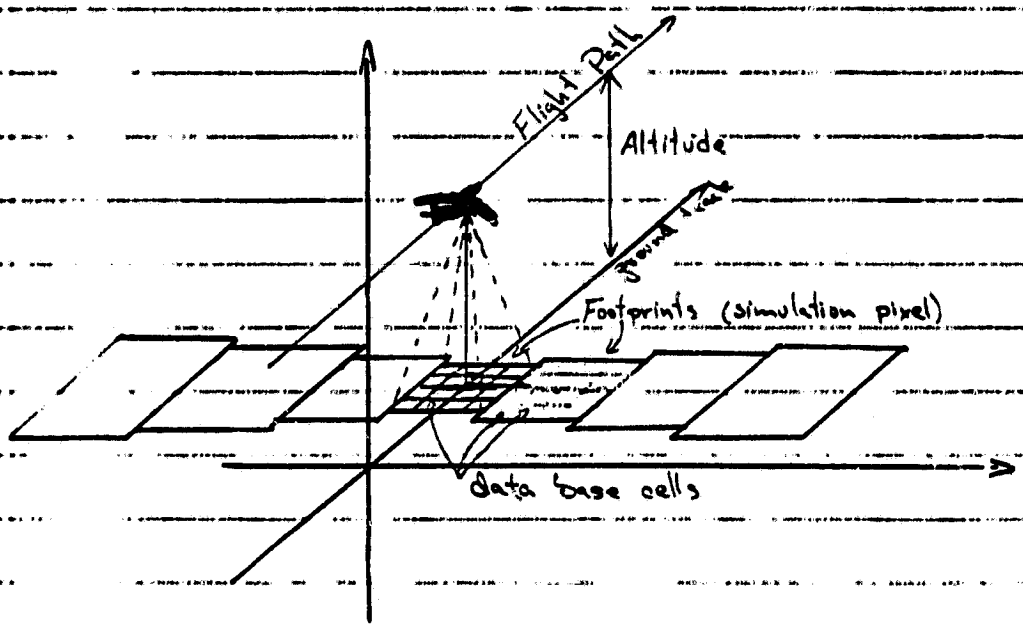

Figure 15 (Neglecting Aircraft Velocity)

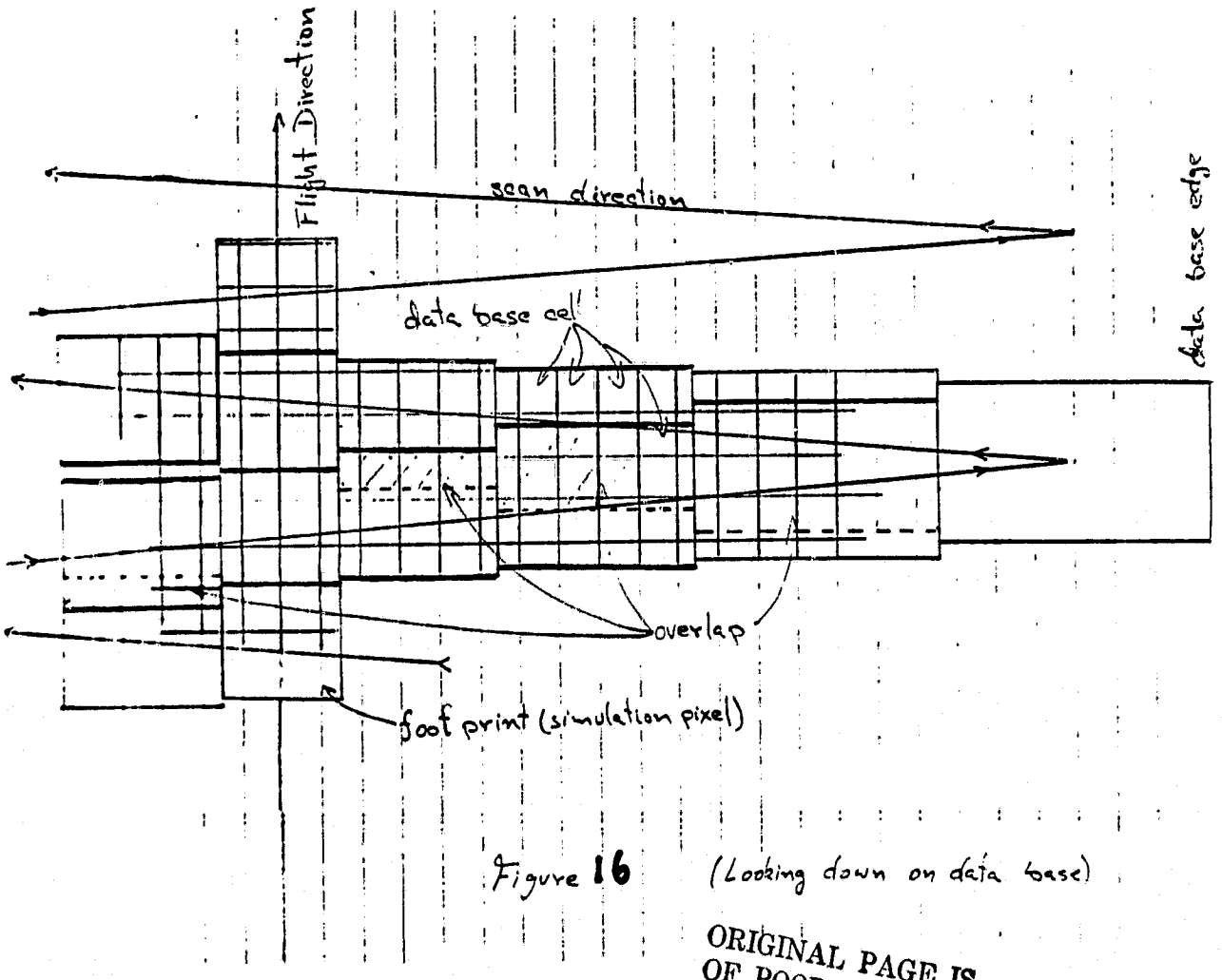

Figure 16 (Looking down on data base)

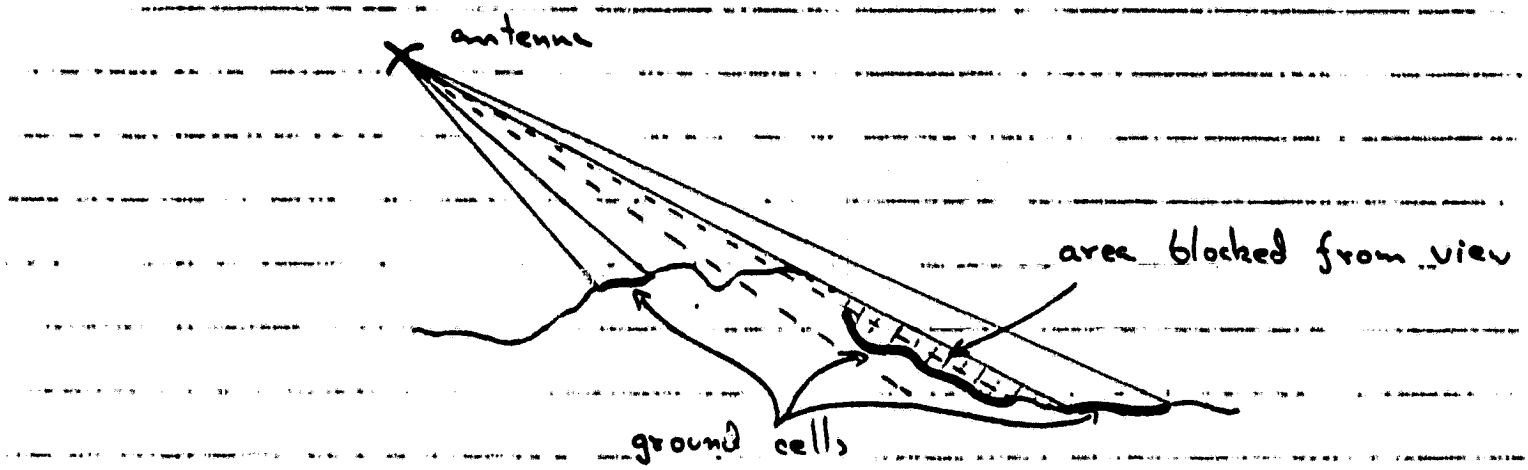

Fig. 17

This simplification allows the simulation routine to be broken into two computer programs. The first program, 'POWER', computes the amount of power returned by each resolution cell of the input cell data base. The second program, SIMULATE, simulates the flight, determining which ground truth cell makes up each footprint, summing the power of all those cells, and converting the return power into a grey tone for visual display.

3.3.4 Results of the PRM

Results have been produced via the PRM for several different geographic regions. These are included in Appendix B.

4.0 SUMMARY AND RECOMMENDATIONS

This report documents an effort which developed a technique for the selection of optimum microwave sensor parameters for specific applications. This method is an empirical exploration of the unknown function which relates sensor parameters, such as, resolution, bandwidth, or polarization, to the utility of the sensor data for specific applications, e.g. soil moisture detection, crop classification, or sea state estimation. A configuration of sensor parameters which optimize this function is selected as the best for each specific application. Because this technique is based upon empirical observation, data must be collected and the parameter/utility function estimated. The data in this case is both sensor products representing various system configurations and the utility of those products for specific applications. Unfortunately there does not exist a data base of sensor products extensive enough to supply the needed data. Therefore a large portion of this report was devoted to illustrating how image simulation for both passive and active microwave sensors can be used to provide the required data.

There are many sensor parameters which affect the utility of the output products. An efficient technique for specifying the specific combinations of sensor parameter to be evaluated is required. This report thus reviews linear statistical models and the estimation of the model parameter. A linear statistical model is used to describe the unknown parameter/utility relationship.

The combination of sensor image simulation and statistical modeling is a powerful approach for determining an optimum set of microwave sensor parameters for a wide variety of applications.

REFERENCES

1. Abbott, J.L., V.H. Kaupp, and J.C. Holtzman, 1977, "Medium Resolution Radar Image Simulation of Deciduous Forests: A Study of Candidate Techniques," Remote Sensing Laboratory Technical Report, RSL TR 319-9, University of Kansas Center for Research, Inc., Lawrence, Kansas.

2. Bates, R.E., 1976, "Winter Thermal Structure and Ice Conditions on Lake Champlain, Vermont," CRREL Report 76-13, U.S. Army Corps. of Engineers Cold Regions Research and Engineering Laboratory, Hanover, New Hampshire.

3. Batlivala, P.P. and F.T. Ulaby, 1977, "Feasibility of Monitoring Soil Moisture Using Active Microwave Remote Sensing," Remote Sensing Laboratory Technical Report, RSL TR 264-12, University of Kansas Center for Research, Inc., Lawrence, Kansas.

4. Bertram, S., March 1965, "The Universal Automatice Map Compilation Equipment," Photogrammetric Engineering and Remote Sensing, Vol. 31, No. 2.

5. Bilello, M.A. and R.E. Bates, 1966, "Ice Thickness Observations, North American Arctic and Subarctic, 1962-63, 1963-64, Pt. 3," Special Report No. 43, U.S. Army Corps. of Engineers Cold Regions Research and Engineering Laboratory, Hanover, New Hampshire.

6. Blackman, R.B. and J.W. Tukey, 1959, "The Measurement of Power Spectra from the Point of View of Communications Engineering," New York: Dover.

7. Bowman, I., 1914, Forest Physiography - Physiography of the United States and Principles of Soils in Relation to Forestry, John Wiley and Sons, New York, 759 pages.

8. Box, G.E.P. and J.S. Hunter, "Multifactor Experimental Designs for Exploring Response Surfaces," 1957, Ann. Matr. Stat. 28(1), 195.

9. Brigham, E.O., 1974, "The Fast Fourier Transform," Prentice-Hall, Inc., Englewood Cliffs, New Jersey.

10. Brown, W.M. and C.S. Palermo, 1969, "Random Processes, Communications, and Radar," McGraw-Hill, New York.

11. Bush, T.F. and F.T. Ulaby, October 1976, "Fading Characteristics of Panchromatic Radar Backscatter from Selected Agricultural Targets," IEEE Transactions on Geoscience Electronics, Vol. GE-13, pp. 149-157.

12. Bush - Ph.D. - Thesis

13. Coiner, J.C. and L.F. Dellwig, September 1972, "Similarities and Differences in the Interpretation of Air Photos and SLAR Imagery," Electro-Optical Systems Design Conference, New York, pp. 89-93.

14. Cooley, J.W. and J.W. Tukey, April 1965, "An Algorithm for Machine Calculation of Complex Fourier Series," Math. Computation, Vol. 19, pp. 297-301.

15. Cosgriff, R.L., W.H. Peake, and R.C. Taylor, May 1960, "Terrain Scattering Properties for Sensor System Design," Engineering Experiment Station Bulletin, 181, Vol. 29, Ohio State University, Columbus, Ohio.

16. Davison, E., V.H. Kaupp, and J.C. Holtzman, July 1976, "Baseline of Planimetric Data Base Construction: Pickwick Site," Remote Sensing Laboratory Technical Report, RSL TR 319-2, University of Kansas Center for Research, Inc., Lawrence, Kansas.

17. Dellwig, L.F., B.C. Hanson, N.E. Hardy, J.C. Holtzman, P.L. Hulen, J.R. McCauley, and R.K. Moore, October 1975, "A Demonstration and Evaluation of the Utilization of Side-Looking Airborne Radar for Military Terrain Analysis," Remote Sensing Laboratory Technical Report, RSL TR 288-1, University of Kansas Center for Research, Inc., Lawrence, Kansas. Supported by U.S. Army Contract DAAG02-75-C-0145.

18. Dellwig, L.F., 1976, "Remote Sensing with Exploration Applications," A seminar sponsored by the New Orleans Geological Society.

19. Dickey, F.M., October 1974, "Image Oriented Analysis of the Synthetic Aperture Radar System," Remote Sensing Laboratory Technical Report, RSL TR 234-6, (Ph.D. thesis), University of Kansas Center for Research, Inc., Lawrence, Kansas.

20. Duda, R.P. and P.E. Hart, 1973, "Pattern Classification and Scene Analysis," John Wiley and Sons, Inc., New York.

21. "Earth Resources Concepts Proposed," Aviation Week & Space Technology (AS&WT), March 26, 1979.

22. Eppes, T.A. and J.W. Rouse, February 1974, "Viewing Angle Effects in Radar Imagery," Photogrammetric Engineering, Vol. 40, No. 12.

23. Evans, G. and C.W. McLeish, R.F. Radiometer Handbook, Aiteeh House, Inc., Dedham, Mass., 1977.

24. Frost, V.S., J.L. Abbott, V.H. Kaupp, and J.C. Holtzman, November 1976, "A Mathematical Model for a Terrain-Imaging Radar and Its Potential Application to Radar Image Simulation," Remote Sensing Laboratory Technical Report, RSL TR 319-6, University of Kansas Center for Research, Inc., Lawrence, Kansas.

25. Frost, V.S., J.L. Abbott, V.H. Kaupp, and J.C. Holtzman, September 1977a, "Derivation of the Radar Image Fading Characteristics," Remote Sensing Laboratory Technical Report, RSL TR 319-29, University of Kansas Center for Research, Inc., Lawrence, Kansas.

26. Frost, V.S., J.L. Abbott, V.H. Kaupp, and J.C. Holtzman, March 1977b, "An Alternative Approach for the Simulation of Cultural Targets in the Pickwick Area," Remote Sensing Laboratory Technical Report, RSL TR 319-12, University of Kansas Center for Research, Inc., Lawrence, Kansas.

27. Frost, V.S., 1978, "Development of Statistical Models for Radar Image Analysis and Simulation," Master's Thesis, University of Kansas, Lawrence, Kansas.

28. Frost, V.S. and J.C. Holtzman, January 1979, "Sensitivity Study of Radar Parameters for Simulation (Part II)," Progress Report Number 2, Remote Sensing Laboratory Technical Report, RSL TR 342-2, University of Kansas Center for Research, Inc., Lawrence, Kansas.

29. Fung, A.K. and H.L. Chan, September 1969, "Backscattering of Waves of Composite Rough Surfaces," IEEE Transactions on Antennas and Propagation.

30. Goodman, J.W., 1968, Introduction to Fourier Optics, McGraw-Hill, New York, pp. 150-153.

31. Gordon, R.B., 1940, "The Primeval Forest Types of Southwestern New York," New York State Museum Bulletin Number 321, pp. 1-102.

32. Harger, R.O., 1970, "Synthetic Aperture Radar System - Theory and Design," Academic Press, New York.

33. Harris, D.B., "Microwave Radiometry," The Microwave Journal, Vol. 4, May 1960, p. 47.

34. Hevenor, R.A., October 1971, "Backscattering of Electromagnetic Waves from a Surface Composed of Two Types of Surface Roughness," TR ETL-TR-71-4, Engineering Topographic Laboratories, The U.S. Army, Fort Belvoir, Virginia.

35. Holtzman, J.C. et al., February 1976, "Radar Image Simulation Project: Development of a General Simulation Model and an Interactive Simulation Model and Sample Results" Remote Sensing Laboratory Technical Report, TR 234-13, The University of Kansas Center for Research, Inc., Lawrence, Kansas.

36. Holtzman, J.C., V.H. Kaupp, J.L. Abbott, V.S. Frost, E.E. Komp, and E.C. Davison, September 1977a, "Radar Image Simulation: Validation of the Point Scattering Method," Volume One, ETL-0117, Remote Sensing Laboratory Technical Report, RSL TR 319-28, University of Kansas Center for Research, Inc., Lawrence, Kansas.

37. Holtzman, J.C., V.H. Kaupp, J.L. Abbott, V.S. Frost, E.E. Komp, and E.C. Davision, September 1977b, "Radar Image Simulation: Validation of the Point Scattering Method," Volume Two, ETL-0118, Remote Sensing Laboratory Technical Report, RSL TR 319-28, University of Kansas Center for Research, Inc., Lawrence, Kansas.

38. Holtzman, J.C., J.L. Abbott, V.H. Kaupp, E.E. Komp, E.C. Davison, and V.S. Frost, June 1978a, "Radar Image Simulation: Validation of the Point Scattering Method," Addendum, ETL-0155, Remote Sensing Laboratory Technical Report, RSL TR 319-31, University of Kansas Center for Research, Inc., Lawrence, Kansas.

39. Holtzman, J.C., J.E. Bare, V.H. Kaupp, E.E. Komp, J.L. Stiles, and V.S. Frost, November 1978b, "Radar Simulations of a Winter Scene: Application of the Point Scattering Method," Remote Sensing Laboratory Technical Report, RSL TR 370-1, University of Kansas Center for Research, Inc., Lawrence, Kansas.

40. Kaupp, V.H., "Radar Image Simulation: A Project to Develop a Moody, Define its Operational Constraints, Validate its Accuracy, and to Produce Sample Results," (Doctor of Engineering Thesis), Volumes I and II, University of Kansas, Lawrence, Kansas.

41. Klass, P.J., 12 May 1975, "Guidance Device Set for Pershing Tests," Aviation Week and Space Technology.

42. Kuchler, A.W., 1964, "The Potential Natural Vegetation of the Conterminous United States," Map and Accompanying manual, American Geographical Society, New York.

43. Leith, E.N., November 1968, "Optical Processing Techniques for Simultaneous Pulse Compression and Beam Sharpening," IEEE Transactions, Vol. AES-4, No. 6.

44. MacDonald, H.C., 1969, "Geologic Evaluation of Radar Imagery from Darien Province, Panama," Modern Geology, Vol. I. No. 1, pp. 1-63.

45. McNeil, M., V.H. Kaupp, and J.C. Holtzman, July 1976, "Digital Elevation Data Base Construction: Pickwick Site," Remote Sensing Laboratory Technical Report, RSL TR 319-3, University of Kansas Center for Research, Inc., Lawrence, Kansas.

46. McNeil, M., V.H. Kaupp, and J.C. Holtzman, February 1977a, "Digitization of Pickwick Site Data Base," Remote Sensing Laboratory Technical Report, RSL TR 319-4, University of Kansas Center for Research, Inc., Lawrence, Kansas.

47. McNeil, M. J.L. Abbott, V.S Frsot, V.H. Kaupp, and J.C. Holtzman, June 1977b, "Interactive Feature Extraction System Framework," Remote Sensing Laboratory Technical Report, RSL TR 319-25, University of Kansas Center for Research, Inc., Lawrence, Kansas.

48. McNeil, M., J.L. Abbott, V.S. Frsot, V.H. Kaupp, and J.C. Holtzman, June 1977c, "Automated Techniques in Feature Extraction," Remote Sensing Laboratory Technical Report, RSL TR 319-24, University of Kansas Center for Research, Inc., Lawrence, Kansas.

49. McNeil, M., J.L. Abbott, V.S. Frost, V.H. Kaupp, and J.C. Holtzman, June 1977d, "Image Handling and Processing," Remote Sensing Laboratory Technical Report, RSL TR 319-26, University of Kansas Center for REsearch, Inc., Lawrence, Kansas.

50. Matthews, R.E., editor, 1975, "Active Microwave Workshop Report," NASA SP-376, NASA, Washington, D.C.

51. Matthews, R.E., editor, 1976, "Active Microwave Users Workshop Report," NASA Conference Publication 2030, NASA, Washington, D.C.

52. Meyers, R.H., 1971, "Response Surface Methodology," Allyn and Bacon, Inc., Boston, Massachusetts.

53. "Microwave Remote Sensing From Earth Resources Surveys," 1977, National Academy of Science Committee on Remote Sensing Programs for Earth Resources Surveys (NAS/CORSPERS).

54. Mitchell, R.L., A.B. Lucero, R.E. Harrison, and D.J. Arnold, June 1971, "Synthetis of High Resolution Radar Systems for Display Simulation and Training," Appendix B, Computation Stereophotogrammetry, Technical Report AFHRL-TR-71-11.

55. Moore, R.K., 1970, "Ground Echo," Radar Handbook, M.I. Skolnik (editor), New York: McGraw-Hill.

56. Moore, R.K., 1975, "Microwave Remote Sensors," in R.G. Reeves, Remote Sensing Manual, Falls Church, Virginia, American Society of Photogrammetry, Chapter 9.

57. Moore, R.K., November 1978, "Active Microwave Sensing of the Earth's Surface - A Mini-Review," IEEE Transactions of Ant. and Prop., Vol. AP-26, No. 6, p. 843.

58. NASA 5-Year Plan - '77-82.

59. Ohlsson, E., 1973, "Passive Microwave Radiometry and Its Potential Application to Earth Resources Surveys - Part 1 - Basic Physics and Technology," ELDO/ESRO Scientific and Technical Review, Vol. 5, No. 3-4.

60. Patrick, E.A., 1972, Fundamentals of Pattern Recognition, Prentice-Hall, Inc., Englewood Cliffs, New Jersey.

61. Parashar, S.K. and A.K. Fung, May 1974, "Simulation of Radar Image: Garden City Test Site, Kansas," Remote Sensing Laboratory Tech. Report, RSL TR 234-5, Univ. of Kansas Center for Res., Inc., Lawrence, Kansas.

62. Parashar, S.K., A.K. Fung, and R.K. Moore, Feb. 1975a, "Simulation of a Radar Image for Garden City Test Site," Remote Sensing Laboratory Tech. Report, RSL TR 234-8, Univ. of Kansas Center for Research, Inc., Lawrence, Kansas.

63. Parashar, S.K., A.K. Fung, and R.K. Moore, July 1975b, "Digital Simulation of a Radar Image of Pisgah Crater Test Site California," Remote Sensing Laboratory Tech. Report, RSL TR 234-10, Univ. of Kansas Center for Research, Inc., Lawrence, Kansas.

64. Porcello, J.L., N.G. Massey, R.B. Innes, and J.M. Marks, Nov. 1976, "Speckle Reduction in Synthetic-Aperture Radars," J. Opt. Soc. Am., Vol. 66, No. 11.

65. Rainwater, J.H., Sept. 1978, Radiometers: Electronic Eyes that "See" Noise, Microwaves, p. 58.

66. Roberts, E.A. and H.W. Reynolds, 1938, "The Role of Plant Life in the History of Dutchess County, New York," Dutchess County Planning Board, Poughkeepsie, New York, 44 pages plus map.

67. Rosenfeld, A. and J.S. Weszka, 1976, "Picture Recognition," in K.S. Fu (Editor), Digital Pattern Recognition, Springer-Verlag, New York.

68. Rydstrom, H.O., G.L. LaPrade, J.D. Greer, and L.C. Aldrich, 1966, "Textbook of Radar Interpretation," Goodyear Aerospace Corporation, GERA 124-A, pp. 24.03.

69. Schepis, E.L., 1968, "Time Lapse Remote Sensing in Agriculture - An Application of Aerial Photographs," Unpublished Master's Thesis, Cornell Univ., 116 pages.

70. Schuchardt, J.M. and J.A. Stratigos, Sept. 1978, "Detected Noise Levels Guide Radiometer Design," Microwaves, p. 64.

71. Simonett, D.S., (editor), 1976, "Applications Review for a Space Program Imaging Radar," GSRU TR 1, Geography Remote Sensing Unit, Univ. of California, Santa Barbara, Calif.

72. Skolnik, M.I., (editor), 1970, Radar Handbook, Moore, R.K., "Ground Echo," New York: McGraw-Hill.

73. Spaeth, J.N. and C.H. Diebold, 1938, "Some Interrelationships Between Soil Characteristics, Water Tables, Soil Temperature and Snow Cover in the Forest and Adjacent Open Areas in South-Central New York," New York Agricultural Experiment Station Memoirs, No. 213, Cornell Univ., Ithaca, New York, 76 pages.

74. Stiles, H. and F.T. Ulaby, June 1979, "Microwave Remote Sensing of Snow," Remote Sensing Laboratory Tech. Report, RSL TR 340-3, Univ. of Kansas Center for Research, Inc., Lawrence, Kansas.

75. Stogryn, A., Sept. 1978, "Estimates of Brightness Temperatures from Scanning Radiometer Data," IEEE Trans. of Ant. and Prop., Vol. AP-26, No. 5, p. 720.

76. Ulaby, F.T., January 1975, "Radar Response to Vegetation," IEEE Trans. on Ant. and Prop., Vol. AP-23, No. 1, pp. 36-45, and "Radar Response to Vegetation II: 8-18 GHz Band," IEEE Trans. on Ant. and Prop., Vol. AP-23, Sept. 1975, pp. 608-618.

77. Ulaby, F.T., January 1976, "Passive Microwave Remote Sensing of the Earth's Surface," IEEE Trans. on Ant. and Prop., p. 112.

78. U.S. Army Terrain Analysis Laboratory, October 1977, "Fort Drum, New York, Terrain Analysis," U.S. Army ETL, Fort Belvoir, Virginia, 45 pages.

79. U.S. Department of Commerce National Oceanic and Atmospheric Administration, 1974-1976, "Climatological Data: New York, Volumes 86-88," Environmental Data Service, National Oceanic and Atmospheric Administration, U.S. Department of Commerce.

80. Williges, R.C. and C.W. Simon, 1971, "Applying Response Surface Methodology to Problems of Target Acquisition," Human Factors, Vol. 13, No. 6, pp. 511-519.

81. Wing, R.S., 1971, "Structural Analysis from Radar Imager, Eastern Panamanian Isthmus," Part I, Modern Geology, Vol. 2, No. 1, pp. 2-21, and Part II, Modern Geology, Vol. 2, No. 2, pp. 75-127.

82. Zelenka, J.S., November 1976, "Comparison of Continuous and Discrete Mixed-Integrator Processors," J. Opt. Soc. Am., Vol. 66, No. 11.

APPENDIX A

LITERATURE SEARCH

Introduction

An automated literature search was performed yielding an extensive list of publications (See Appendix A). Five data bases were investigated. The first four were NTIS (Copr. N.T.I.S.) containing articles from 1964 through 1978, COMPENDEX (Copr. Engineering Index) containing publications ranging from 1970 through May 1978, INSPEC (Copr. I.E.E.) containing articles published from 1964 through December 1977, and INSPEC (Copr. I.E.E.) with publications from 1978 to present. These are all available from Lockheed's Dialog Information Retrieval Service. The fifth data base to be investigated belongs to NASA and is available from the NASA Scientific and Technical Information Facility. The listings obtained from this search were used to determine different types of present and potential civilian applications of microwave remote sensors of both active (radar) and passive (radiometer) types. Different sensor parameters required for the different applications envisioned or in use were investigated as well. Additional pertinent listings were also furnished in the Active Microwave Workshop Report ( ) and in the Active Microwave Users Workshop Report ( ). Finally, in order to obtain a clear picture of the feasibility of satellite based sensors, supplementary literature obtained through personal contacts as well as the sources mentioned previously were studied.

The results of the literature search are presented in the following sections on Applications and Satellite Configurations.

Applications

The Active Microwave Workshop Report ( ) and the Active Microwave Users Workshop Report ( ) contain the bulk of the findings of the literature

search for active microwave sensor applications. The listings of civilian applications found in these reports, through automated literature search and several papers acquired through personal contacts were summarized in tabulated form. These tables present applications both as a function of required resolution and as a function of required sensor operating frequencies. User areas are divided into seven main categories. They are:

Mineral Resources

Water Resources

Land Use Resources and Geographic Applications

Natural Vegetation

Cultivated Vegetation

Damage Assessment and Hazard Surveys

Oceanography

These categories are further divided into specific applications that vary with the different resolutions and frequencies which are tabulated as follows:

Table A.1	Active Systems	less than 10m resolution
Table A.2	Active Systems	10m to 25m resolution
Table A.3	Active Systems	25m to 30m resolution
Table A.4	Active Systems	50m to 100m resolution
Table A.5	Active Systems	100m to 250m resolution
Table A.6	Active Systems	250m to 500m resolution
Table A.7	Active Systems	greater than 500m resolution
	Passive Systems	15km X 25km resolution
Table A.8	Active Systems	P-Band Frequency
		L-Band Frequency
Table A.9	Active Systems	S-Band Frequency

Table A.10	Active Systems	C-Band Frequency
Table A.11	Active Systems	X-Band Frequency
Table A.12	Active Systems	K-Band and High Frequencies
Table A.13	Passive Systems	P-Band Frequency L-Band Frequency
Table A.14	Passive Systems	S-Band Frequency C-Band Frequency X-Band Frequency
Table A.15	Passive Systems	K-Band Frequency Q-Band Frequency U-Band Frequency W-Band Frequency

A summary of the most important required radar parameters as a function of the different user needs was also compiled. These parameters are wavelength, interpretation resolution, polarization and nadir angle and are presented in Table A.16 through A.20 as follows:

Table A.16	Vegetation Resources System Requirement
Table A.17	Water Resources System Requirements
Table A.18	Mineral Resources and Geologic Application System Requirements
Table A.19	Oceanographic Applications System Requirements
Table A.20	Cartography and Land Use System Requirement

Table A.1

Resolution - less than 10m

Active Systems

I. Mineral Resources and Geologic Applications

- Detailed Geologic Analysis

II. Water Resources

- Ground Water Analysis
- Areal Extent of Water Resources
- Surface Water Composition Changes and Water Pollution
- Drainage Patterns
- Soil Moisture Differences

III. Land Use Resources and Geographic Applications

- Habitat Inventory
- Surface Soil Boundaries

IV. Natural Vegetation

- Dominant Rain Forest Trees
- Density of Woody Vegetation
- Individual Tree Counts
- Species of Dominant Trees

V. Cultivated Vegetation

- Mature Orchard Trees
- Mapping of Planimetric Details in Agriculture Areas
- Crop Stress for 150 ft Diameter Areas
- Species of Continuous Cover Crops Including Weed Patches
- Soil Moisture Differences

Table A.1 (continued)

VI. Damage Assessment and Hazard Surveys

None

VII. Oceanography

Ocean and Sea State Monitoring

Fishing Intensity

Sea State and Surface Winds

Wave Measurements

Table A.2

Resolution 10m to 25m

Active System

I. Mineral Resources and Geologic Applications

- 'General' Applications
- Mineral Exploration
- Offshore Geologic Surveys
- Coastal Processes
- Hazard Surveys
- Surface Mining
- Civil Works Applications

II. Water Resources

- Streamflow Forecast
- Watershed Characteristics
- Surface Water Identification
- Lake Ice

III. Land Use Resources and Geographic Applications

- Habitat Inventory
- Farmsteads

IV Natural Vegetation

- Forest/Non-Forest Discrimination

V. Cultivated Vegetation

- Crop Stress
- Crop Species in Fields 1 Acre or More in Size
- Farmsteads
- Areas Greater than 150 ft Diameter in Agriculture Crops for Stress

Table A.2 (continued)

VI. Damage Assessment and Hazard Surveys

- Hurricane Damage Assessment
- Tornado Damage Assessment
- Earthquake Prediction and Damage Assessment
- Landslide/Earth Slippage

VII. Oceanography

- Ocean Engineering Hazard
- Sea Ice Monitoring
- Oil Pollution Monitoring

Table A.3

Resolution 25m to 50m

Active Systems

I. Mineral Resources and Geologic Applications

- Mineral Exploration
- Geologic Mapping
- Surface Mapping
- Civil Works Applications
- Ground Water Exploration

II. Water Resources

- Frozen-Lake Mapping
- Watershed Characteristics
- Surface Water Identification
- Snow Cover and Glacier Monitoring
- Roughness and Hydrologic System Classification
- Snowfield Mapping (Moisture and Liquid Water Content)
- Water Line
- Snow Line
- Desert Line

III. Land Use Resources and Geographic Applications

- Nonvegetation Land Use
- Surface Slope
- Habitat Inventory
- Major Roads, Railroads and Waterways

Table A.3 (continued)

IV. Natural Vegetation

- Range Improvement
- Forest Assessment
- Tropical Forest Inventory
- Forest Moisture and Health
- Timberline
- Grassland-Brushland Interface
- Brushland-Timberland Interface
- Grassland-Timberland Interface

V. Cultivated Vegetation

- Yield Prediction
- Crop Stress
- Crop Identification
- Vegetation Discrimination
- Plant Moisture (Maturation)
- Bare Soil vs. Vegetated Areas and Crop Species in 10 Acre Fields
- Areas Greater Than 300 ft. in Diameter for Stress (Damage Due to Disease, Insects, Fire, etc.)

VI. Damage Assessment and Hazard Surveys

- Flood Mapping
- Tornado Damage Assessment
- Forest and Range Fire Damage Assessment
- Landslide/Earth Slippage

Table A.3 (continued)

VII. Oceanography

Pollution Monitoring

Ocean Engineering Hazard

Sea Ice Monitoring

Table A.4

Resolution 50m to 100m

Active Systems

I. Mineral Resources and Geologic Applications

- Landform Identification and Terrain Analysis
- Mineral Deposit Location
- Geothermal Site Location
- Surface Mining
- Oil/Gas Development
- Ground Water Exploration

II. Water Resources

- Streamflow Forecast
- Snow Cover and Glacier Monitoring
- Thickness of Great Ice Sheets
- Wetland Hydrology and Delineation
- Drainage Basin Roughness and Hydrologic System Classification
- Water Pollution/Quality
- Snowfield Mapping
- Freeze/Thaw Line Monitoring

III. Land Use Resources and Geographic Applications

- Civil Works
- Wetlands Mapping
- Soil Types and Properties Mapping
- Transportation Networks
- Location of Eng. Materials
- Environmental Impact Monitoring and Prediction
- Habitat Inventory
- Resource Management

Table A.4 (continued)

IV. Natural Vegetation

- Range Biomass Productivity
- Range Inventory
- Forest Assessment
- Tropical Forest Inventory
- Forest Moisture and Health
- Forest/Range Trend

V. Cultivated Vegetation

- Soil Moisture
- Plant Moisture (Maturation)
- Saline Seep Detection
- Irrigation Drainage Investigation and Planning Trend

VI. Damage Assessment and Hazard Surveys

- Hurricane Damage Assessment
- Fault Location

VII. Oceanography

- Ship Navigation and Routing
- Navigation Hazards
- Sea Ice

Table A.5

Resolution 100m to 250m

Active System

I. Mineral Resources and Geologic Applications

None

II. Water Resources

Snow Cover and Glacier Monitoring

Wetland Hydrology and Delineation

Freeze/Thaw Line Monitoring

III. Land Use Resources and Geographic Applications

Habitat Inventory

IV. Natural Vegetation

Range Biomass Productivity

Forest Assessment

V. Cultivated Vegetation

Soil Moisture

Saline Seep Detection

VI. Damage Assessment and Hazard Surveys

None

VII. Oceanography

None

Table A.6

Resolution 250m to 500m

Active Systems

I. Mineral Resources and Geologic Applications

None

II. Water Resources

Snow Cover and Glacier Monitoring

Thickness of Great Ice Sheets

Wetland Hydrology and Delineation

III. Land Use Resources and Geographic Applications

Habitat Inventory

IV. Natural Vegetation

None

V. Cultivated Vegetation

None

VI. Damage Assessment and Hazard Surveys

None

VII. Oceanography

None

Table A.7

Resolution greater than 500m

Active Systems

I. Water Resources

Wetland Hydrology and Delineation

Resolution 15km X 23km

Passive System

The only reference found in literature refers to the resolution of the radiometer on board the Seasat-A for measuring:

Sea Surface Temperature

Wind Stress Over Oceans

with a resolution cell of 15km X 23 km.

Table A.8

Frequencies - P-Band

225-400 MHz

1.33-0.75 m

Active Systems

None

Frequencies - L-Band

0.4-1.5 GHz

75-20 cm

Active Systems

I. Mineral Resources and Geologic Applications

- Mineral Exploration
- Geologic Mapping
- Detailed Geologic Observations
- Civil Works Applications
- Ground Water Exploration
- Structure
- Lithology (unknown but the lower the better)
- Construction Materials

II. Water Resources

- Frozen-Lake Mapping
- Watershed Characteristics
- Surface Water Identification (any frequency is good for this application)
- Drainage Basin Roughness and Hydrologic System Classification
- Snowfield Mapping
- Freeze/Thaw Line Monitoring

Table A.8 (continued)

III. Natural Vegetation

- Forest Assessment
- Yield Prediction
- Crop Stress
- Saline Seep Detection

IV. Damage Assessment and Hazard Surveys

- Flood Mapping

V. Oceanography

- Ocean and Sea State Monitoring
- Sea Ice Monitoring
- Iceberg and Ship Monitoring
- Oil Pollution Monitoring
- Hurricanes

Table A.9

Frequencies - S-Band

1.5-5.0 GHz

20cm - 6.0 cm

Active Systems

I. Mineral Resources and Geologic Applications

- Mineral Exploration
- Geologic Mapping
- Detailed Geologic Observations
- Civil Works Applications
- Ground Water Explorations

II. Water Resources

- Watershed Characteristics
- Surface Water Identification
- Drainage Basin Roughness and Hydrologic System Classification
- Snowfield Mapping
- Freeze/Thaw Line Monitoring
- Soil Moisture Condition
- Rainfall Assessment

III. Natural Vegetation

- Range Biomass Productivity
- Forest Assessment
- Soil Moisture

IV. Cultivated Vegetation

- Saline Seep Detection
- Soil Moisture
- Irrigation

Table A.9 (continued)

V. Oceanography

Ocean and Sea State Monitoring

Sea Ice Monitoring

Iceberg and Ship Monitoring

Oil Pollution Monitoring

Table A.10

Frequencies - C-Band

3.9-6.2 GHz

7.7-4.8 cm

Active System

I. Mineral Resources and Geologic Applications

- Mineral Exploration
- Geologic Mapping
- Detailed Geologic Observations
- Civil Works Applications
- Ground Water Exploration

II. Water Resources

- Watershed Characteristics
- Surface Wager Identification
- Drainage Basin Roughness and Hydrologic System Classification
- Snowfield Mapping
- Freeze/Thaw Line Monitoring
- Soil Moisture Condition
- Rainfall Assessment

III. Cultivated Vegetation

- Yield Prediction
- Crop Stress
- Soil Moisture
- Saline Seep Detection

Table A.10 (continued)

IV. Oceanography

- Ocean and Sea State Monitoring
- Sea Ice Monitoring
- Iceberg and Ship Monitoring
- Oil Pollution Monitoring

Table A.11

Frequencies - X-Band

5.0-12 GHz

5.0-2.5 cm

Active Systems

I. Mineral Resources and Geologic Applications

- Mineral Exploration
- Geologic Mapping
- Detailed Geologic Observations
- Civil Works Applications
- Ground Water Exploration

II. Water Resources

- Frozen-Lake Mapping
- Watershed Characteristics
- Surface Water Identification
- Drainage Basin Roughness and Hydrologic System Classification
- Snowfield Mapping (e.g. Moisture and lig. water)
- Freeze/Thaw Line Monitoring
- Land Use (Suburban and Rural) (greater than 8 GHz)

III. Natural Vegetation

- Forest/Non-Forest Discrimination
- Forest Moisture and Health
- Pasture State of Growth and Disease (greater than 8 GHz)
- Field Boundaries

Table A.11 (continued)

IV. Cultivated Vegetation

- Yield Prediction
- Crop Stress
- Plant Moisture (Maturation)
- Saline Seep Detection
- Crop State of Growth (greater than 8 GHz)
- Crop Stress and Disease (greater than 8 GHz)
- Field Boundaries (greater than 8 GHz)

V. Damage Assessment and Hazard Surveys

- Flood Mapping

VI. Oceanography

- Ocean and Sea State Monitoring
- Sea Ice Monitoring
- Iceberg and Ship Monitoring
- Sea Ice Navigation and Mapping
- Pollution

Table A.12

Frequencies - K-Band

12-36 GHz

2.5-0.83 cm

Active Systems

I. Mineral Resources and Geologic Applications

- Mineral Exploration
- Geologic Mapping
- Detailed Geologic Observations
- Civil Works Applications
- Ground Water Exploration
- Structure

II. Water Resources

- Surface Water Identification
- Drainage Basin Roughness and Hydrologic System Classification
- Snowfield Mapping

III. Natural Vegetation

- Tropical Forest Inventory
- Forest Moisture and Health

IV. Cultivated Vegetation

- Yield Prediction
- Crop Stress
- Crop Identification
- Plant Moisture (Maturation) (below 17 GHz)

Table A.12 (continued)

V. Oceanography

Ocean and Sea State Monitoring

Sea Ice Monitoring

Iceberg and Ship Monitoring

Oil Pollution Monitoring

Sea Ice Navigation and Mapping

No requirements above 36 GHz were found.

Table A.13

Frequencies - P-Band

225-400 MHz

1.33-0.75 m

Passive Systems

None

Frequencies - L-Band

0.4-1.5 GHz

75-20.0 cm

Passive Systems

I. Water Resources

Ice and Snow Melting

II. Land Use and Geographic

Wetlands Mapping

III. Cultivated Vegetation

Soil Moisture

IV. Oceanography

Sea Surface Salinity

Frequencies - S-Band

1.5-5.0 GHz

20-6.0 cm

Passive Systems

I. Cultivated Vegetation

Soil Moisture

II. Oceanography

Sea Surface Temperature

Table A.14

Frequencies - S-Band

1.5-5.0 GHz

20-6.0 cm

Passive Systems

I. Cultivated Vegetation

Soil Moisture

II. Oceanography

Sea Surface Temperature

Frequencies - C-Band

3.9-6.2 GHz

7.7-4.8 cm

Passive Systems

I. Sea Temperature

Frequencies - X-Band

5.0-12 GHz

6.0-2.5 cm

Passive Systems

I. Water Runoff Coefficients

II. Sea Surface Temperature

III. Sea State

IV. Wind Speeds Over Oceans

V. Wind Stress

Table A.15

Frequencies - K-Band

12-36 GHz

2.5-0.83 cm

Passive Systems

I. Sea Surface Temperatures

II. Ocean Wind Speeds

III. Detection of Stationary and Moving Cultural Targets

Frequencies - Q-Band

36-46 GHz

8.3-6.5 mm

Passive Systems

I. Precipitation Over Land

II. Sea Temperature

Frequencies - V-Band

46-56 GHz

6.5-5.4 mm

Passive Systems

I. Storms Over Land

Frequencies - W-Band

56-100 GHz

5.4-3.0 mm

Passive Systems

I. Water Ice Boundaries

II. Storms Over Land

Table A.16

Vegetation Resources System Requirements

Application	Wavelength (cm)	Interpretation Resolution (m) Desire	Interpretation Resolution (m) Accept	Polarization	Nadir Angle Range (deg)	Auxiliary Revisit Interval	
Soil Moisture for Yield Estimate	1-100 (2 channels)	30	100	Any two	0-40		*Relative Accuracy=2dB
Cultivated	6-8 and 1.7-2.2	90	200	HH and Cross	7-17	1-7 days	
Natural/Range	6-8	90	200	HH and Cross	7-17	1-7 days	
Natural/Forest	5-30 multifreq.	90	200	HH and Cross	7-17		
Vegetation Identification and Mapping							
Cultivated	.8-3 multifreq.	30	90	HH/VV/Cross	40-60	10 days	
Natural/Range	.8-3 multifreq.	30	90	HH/VV/Cross	40-60		
Natural/Forest	.8-3 multifreq.	30	90	HH/VV/Cross	40-60	Seasonally	
Vegetation Moisture Monitoring							
Cultivated	.8-5 multifreq.	30	90	HH/VV/Cross	40-60	10 days	
Natural/Range	.8-5 multifreq.	30	90	HH/VV/Cross	40-60	Seasonally	
Natural/Forest	.8-5 multifreq.	30	90	HH/VV/Cross	40-60	Seasonally	
Saline Seep Monitoring	30-30 multifreq.	30	200	HH/VV/Cross	7-17	Seasonally	
Soil Mapping	.8-30 multifreq.	90	200	not specified	not spec.	event determ.	
Crop and Pasture Condition							
State of Growth	> 8 GHz (multifreq.)			Single	30-70		
Stress Disease	> 8 GHz (multifreq.)			Single	30-70		
Field Boundaries	> 8 GHz			Like and	30-70		
Farm Practices				Cross	30-80		
Forest Community							
Identification	To be Determined			Like and Cross	20-70		
Status	To be Determined			Like and Cross	20-70		
Forest Burn and Harvest	To be Determined			Single	10-40		
Erosion	To be Determined			Single	30-80		
Irrigation	4-5 GHz				5-20		
Crop Classification (Bush and Ulaby)							
Alfalfa Corn Milo Wheat	14.2 GHz or 14.2 and 9.0 GHz	25	50	VV or VV and HH	40°-50° (best=50°)	5-10 days revisit period for total of 30 days	

*Active Microwave Workshop Report

Table A.17

Water Resources System Requirements

Application	Wavelength (cm)	Interpretation Resolution (m) Desire	Interpretation Resolution (m) Accept	Polarization	Nadir Angle Range (deg)	Auxiliary Revisit Interval	
Soil Moisture Monitoring							
Cultivated Areas	6-8 and 1.7-2.2	30	90	HH and Cross	7-17	1-7 days	
Uncultivated Areas	2-30 multifreq.	30	90	HH and Cross	7-17	1-7 days	
Snowfield (eq. moist. and liquid water)	1-30 multifreq.	30	90	Unspecified	Unspec.	3-15 days	
Mapping							
Watershed	1-100 (2 channels)	30	100	Any Two	0-40		*Relative Accuracy=2dB
Runoff Coefficient Estimate	3-30 multifreq.	30	90	Unspecified (Like and Cross)	Unspec.	Seasonal	
Drainage Pattern	3-30 multifreq.	30	90	Unspecified	Unspec.	Annual	
Land Use Mapping	3-30 multifreq.	30	90	Unspecified	Unspec.	Annual	
Surface Water, Flood, and Wetland Monitoring	3-30 multifreq.	10	30	Any	Any	Event Determined	
Freeze/Thaw Line Monitoring	3-30 multifreq.	90	200	Unspecified	Unspec. (22-50(?))	3-15 days	
Rainfall Assessment	4-50 GHz			Single	7-22		
Standing Water Ponds and Lakes	High Frequencies			HH and Cross	> 30		
Lake Ice	To be Determined			To be Determined	30-80		
Water Pollution	To be Determined			VV and Cross	25-70		
1. Oil Slick Detection and Monitoring	X-Band	10	30	Vertical	> 20	Spill Report and monthly in hazard areas.	
2. Debris Spill	P-X-L-C-Bands	0.5		HH and VV	Unknown	Spill Report	
3. Surface Effects on effluent discharge detect. and monitoring	P-X-L-C-Bands	0.5		HH and VV	Unknown	To be Determined	
4. Monitoring pollution effects, algal mats, etc	P-X-L-C-Bands	1	10	HH and VV	Unknown	Seasonally	

Table A.18

Mineral and Geologic Applications System Requirements

Application	Wavelength (cm)	Interpretation Resolution (m)		Polarization	Nadir Angle Range (deg)	Auxiliary
		Desire	Accept			Revisit Interval
Mineral and Petroleum Exploration	.8-25 multifreq.	15	30	HH or VV, Cross	Stereo	Seasonal
Regional Geologic Mapping	.8-25 multifreq.	25	50	HH or VV, Cross	40-70	Seasonal
Detailed Geologic Mapping	.8-25 multifreq.	3	15	HH or VV, Cross	40-70 (Stereo)	Seasonal
Civil Works Applications	.8-25 multifreq.	15	30	HH or VV, Cross	40-70 (Stereo)	Seasonal
Ground-Water Exploration	.8-25	25	30	HH or VV, Cross	40-70 (aspect angel dependent)	Seasonal
Structure	Ku and L-Band			Like and Cross	Grazing to 45°	
Lithology	multifreq.			Like and Cross	10-20, 20-70	
Construction Materials	multifreq.			Like and Cross	10-20, 20-70	
Route and Dam Locations	one high and one low frequency			Like and Cross	grazing and 45	

Table A.19

Oceanographic Applications System Requirements

Application	Wavelength (cm)	Interpretation Resolution (m)		Polarization	Nadir Angle Range (deg)	Auxiliary
		Desire	Accept			Revisit Interval
Ocean Waves and Sea State Monitoring	1-30 multifreq.	3	25	HH,VV	0-25	6-12(hr.)
Sea Ice Monitoring	1-30 multifreq.	25	25	HH/VV/Cross	0-25	6-12(hr.)
Icebergs and Ship Monitoring	1-30 multifreq.	10	25	HH/VV/Cross	25-60	6-12(hr.)
Oil Pollution Monitoring	1-30 multifreq.	25	25	VV,Cross	0-25	6-12(hr.)
Ships and Fishing Boats	none			Single	>50	
Pollution	>5 GHz			Multiple	25 and 70	
Coastal Changes	none (TO be Deter.)			Multiple, Linear and Circular	>5	
Kelp Monitoring	>12 GHz			Multiple	>30	
Hurricane	<3 GHz			Multiple	>10	
Currents	To be Determined			Multiple	>20	

Table A.20

Cartography and Land Use System Requirements

Application	Wavelength (cm)	Interpretation Resolution (m)		Polarization	Nadir Angle Range (deg)	Auxiliary
		Desire	Accept			Revisit Inverval
Urban Changes	Any (To be Deter.)			Like and Cross	20-70	
Transportation						
Routes	To Be Determined			Like and Cross	20-70	
Traffic	To Be Determined			Like and Cross	50-80	
Remote Area Topography	To Be Determined			Like	30-80	
Land Use						
Suburban	>8 GHz			Like and Cross	20-80	
Rural	>8 GHz			Like and Cross	20-80	

Satellite Configurations

The literature was scanned for typical orbital and payload parameters of those satellites carrying or expected to carry microwave sensors. This was in order to obtain a picture of what kind of restraints would be imposed on any hypothetical spaceborne microwave sensing systems.

It appears that generally speaking, with the advent of the shuttle era, space borne vehicles will not be a limiting factor to microwave remote sensors, except for the case of rigid antenna sizes. To that end, satellite configurations were not considered to be of primary concern. However, typical parameters were obtained from two primary sources: "The Report on Active and Planned Spacecraft and Experiments" (Vette, Vostreys and Horowitz) ( ) and the "Special Programs Office Sensor Capability Handbook and Data Sheets, Vol. I" (Nagler, Steinbacker and Montgomery) ( ). These sample configurations, as well as some of the shuttle limitations are listed in the following tables A.21 through A.39.

Table A.21

Spacecraft: General (from Special Programs Office Sensor Capability Handbook)

I. Orbital Parameters	
a) Altitude	
b) Pointing Acc.	
II. Payload Data for Microwave Sensor	
a) Size	Antenna constraints: 2m max (4 for shuttle). Higher must be folded - otherwise no problem (typically).
b) Weight	25kg - 300kg
c) Power	30W - 65W
d) Telemetry	10 bits/sec - 10k bits/sec (relatively undemanding on existing systems.
e) Data Storage	

Table A.22

Spacecraft: Shuttle Launch Maximum Configurations

I. Orbital Parameters	
a) Altitude	
b) Pointing Acc.	
II. Payload Data for	
Microwave Sensor	
a) Size	Antenna Max Diameter: 4 meters
b) Weight	Typical Max ≃ 300kg (but no problem)
	(305kg projected for NOAA)
c) Power	150W (Projected for NOSS)
d) Telemetry	100k b/sec (Projected for NOSS)
e) Data Storage	

Table A.23

Spacecraft: Rocket Launch Maximum Configurations

I.	Orbital Parameters	
	a) Altitude	1100km (Thor)
	b) Pointing Acc.	0.01 Deg (Thor)
II.	Payload Data for Microwave Sensor	
	a) Size	Antenna Max Diameter: 2 meters
	b) Weight	300kg (Typical Max)
		2300kg max total payload
	c) Power	65W (Typical Max)
	d) Telemetry	10k bits/sec (Typical Max but not too demanding on existing systems.
	e) Data Storage	400 min of tape (Thor)

Table A.24

Spacecraft: DMSP F1-F3

I.	Orbital Parameters		
	a) Altitude	Periapsis: 818km	Apoapsis: 848km
	b) Pointing Acc.	0.01 Deg	
II.	Payload Data for Microwave Sensor		
	a) Size	5.4m long (total payload)	
	b) Weight	Total Payload: 450kg	
	c) Power	100 Sq. Feet solar panels	
	d) Telemetry	Recorded or Real Time through S-Band transmission	
	e) Data Storage	400 min (three high density tape recorders)	

Table A.25

Spacecraft: DMSP-F4 and F5

Launch Vehicle-Thor

I.	Orbital Parameters	
	a) Altitude	830km sun-synchronous polar orbits
	b) Pointing Acc.	0.01 Deg
II.	Payload Data for Microwave Sensor	
	a) Size	5.4m long total, with 4 sections, only one for sensors
	b) Weight	Total payload: 450kg
	c) Power	100 sq. feet solar panels
	d) Telemetry	Recorded or Real Time through S-Band transmission
	e) Data Storage	400 min (three high density tape recorders)

Reference: 'The Defense Meteorological Satellite Program' D.A. Nichols, Optical Engr., Vol. 14, No. 4, July-August 1975

Table A.26

Spacecraft: GMS

I.	Orbital Parameters	
	a) Altitude	Periap.: 35531km Apoap.: 35779km Geostationary
	b) Pointing Acc.	
II.	Payload Data for Microwave Sensor	
	a) Size	Roughly Cylindrical: Height 345cm, Dia. 216cm (total payload)
	b) Weight	647kg (total payload)
	c) Power	225W
	d) Telemetry	
	e) Data Storage	

Table A.27

Spacecraft: GOESI

I.	Orbital Parameters		
	a) Altitude	Periapsis: 34165	Apoapsis: 36458
	b) Pointing Acc.		
II.	Payload Data for Microwave Sensor		
	a) Size	190.5cm dia., 230cm length (Total payload)	
	b) Weight	631kg	
	c) Power		
	d) Telemetry	UHF-Band and S-Band frequencies	
	e) Data Storage		

Table A.28

Spacecraft: GOES-D

I.	Orbital Parameters	
	a) Altitude	35786km
	b) Pointing Acc.	
II.	Payload Data for	
	Microwave Sensor	
	a) Size	Cylindrical: 190.5cm dia., 230cm length
	b) Weight	Total payload 660kg
	c) Power	
	d) Telemetry	UHF-Band and S-Band frequencies
	e) Data Storage	

Table A.29

Spacecraft: HCMM

I. Orbital Parameters		
a) Altitude	Periapsis: 558km	Apoapsis: 646km
b) Pointing Acc.		
II. Payload Data for		
Microwave Sensor		
a) Size		
b) Weight	117kg (total payload)	
c) Power		
d) Telemetry	S-Band	
e) Data Storage		

Table A.30

Spacecraft: LANDSAT 1 (former ERTS 1)
(same basic configuration as 2 and 3)

I.	Orbital Parameters	
	a) Altitude	Periapsis: 897km Apoapsis: 917km
	b) Pointing Acc.	± .7 Deg
II.	Payload Data for Microwave Sensor	
	a) Size	
	b) Weight	891kg (total payload)
	c) Power	
	d) Telemetry	154.2 and 2106.4 MHz and PCM Narrow-band Telemetry at 2287.5 and 137.86 MHz
	e) Data Storage	Tape Recording of up to 30 min of scanner time

Table A.31

Spacecraft: LANDSAT-D

I.	Orbital Parameters	
	a) Altitude	705km
	b) Pointing Acc.	
II.	Payload Data for Microwave Sensor	
	a) Size	
	b) Weight	Total Payload: 1407kg
	c) Power	
	d) Telemetry	Data processed in TM multiplexes for transmissions via the tracking and data relay satellites and/or direct
	e) Data Storage	

Note: Six-Band, earth looking scan radiometer
30-M ground element resolution
185km ground swath

Table A.32

Spacecraft: Nimbus

I.	Orbital Parameters	
	a) Altitude	1092km - 1108km
	b) Pointing Acc.	
II.	Payload Data for	
	Microwave Sensor	
	a) Size	3.7m tall, 1.45m dia. (total payload)
	b) Weight	620kg (total payload)
	c) Power	
	d) Telemetry	
	e) Data Storage	

Table A.33

	Spacecraft: Nimbus-G
I. Orbital Parameters	
a) Altitude	955km
b) Pointing Acc.	
II. Payload Data for Microwave Sensor	
a) Size	3.7m tall, 1.5m dia. base, 3m wide with solar panels (total payload)
b) Weight	832kg (total payload)
c) Power	
d) Telemetry	
e) Data Storage	

Table A.34

	Spacecraft: NOAA-A (or Tiros N)
I. Orbital Parameters	
a) Altitude	833km
b) Pointing Acc.	$\pm$ 0.1 Deg with motion rate < 0.035 deg/sec
II. Payload Data for Microwave Sensor	
a) Size	
b) Weight	588.9kg (total payload)
c) Power	
d) Telemetry	Real time or recorded modes, low resolution (4km) and high resolution (1km) picture transmission
e) Data Storage	

Table A.35

Spacecraft: NOAA-B

I.	Orbital Parameters	
	a) Altitude	833km
	b) Pointing Acc.	± 0.1 deg
II.	Payload Data for Microwave Sensor	
	a) Size	
	b) Weight	588.9kg (total payload)
	c) Power	
	d) Telemetry	Same as NOAA-A
	e) Data Storage	

Table A.36

Spacecraft: National Oceanic Satellite System

I.	Orbital Parameters	
	a) Altitude	
	b) Pointing Acc.	
II.	Payload Data for Microwave Sensor	
	a) Size	h: 5.64m w: 4.36m l: 4.47m
	b) Weight	Antenna: 496 lb, Electronic Components and Chasis: 140 lb RF Components and Feeds: 60 lb (305kg) (Sat Total = 3816kg)
	c) Power	150W
	d) Telemetry	Raw Data: 100k b/s Calibrated and Average Data: 50k b/s
	e) Data Storage	
		Note on Radiometer Calibration: Total Power, two point calibration

Table A.37

Spacecraft: San Maneo-D/M

I.	Orbital Parameters		
	a) Altitude	Periapsis: 420km	Apoapsis: 27000km
	b) Pointing Acc.		
II.	Payload Data for Microwave Sensor		
	a) Size	Two small cylinders, 1) 70m dia, 40cm high, 2) 42cm high, 32cm dia.	
	b) Weight		
	c) Power		
	d) Telemetry		
	e) Data Storage		

Table A.38

Spacecraft: Seasat 1

I.	Orbital Parameters	
	a) Altitude	769km - 799km
	b) Pointing Acc.	
II.	Payload Data for	
	Microwave Sensor	
	a) Size	
	b) Weight	1800kg (total payload)
	c) Power	
	d) Telemetry	
	e) Data Storage	

Table A.39

Spacecraft: SMM

I.	Orbital Parameters	
	a) Altitude	575km
	b) Pointing Acc.	Oriented towards the sun
II.	Payload Data for	
	Microwave Sensor	
	a) Size	
	b) Weight	2273kg (Total payload)
	c) Power	
	d) Telemetry	
	e) Data Storage	

APPENDIX B

RADAR AND RADIOMETER PARAMETER VARIATIONS

The following pages present the results of radar and radiometer simulations as a function of seasonal, spectral and resolution variations. Table B.1 below indicates the radar simulations performed for the different parameters.

TABLE B.1

	L-Band				S-Band				X-Band				Ku-Band			
	Resolution (m)				Resolution (m)											
	25	50	100	250	25	50	100	250	25	50	100	250	25	50	100	250
Winter (15cm Snow)									X	X	X	X				
Spring/ Summer	X	X	X	X	X	X	X	X	X	X	X	X	X	X	X	X
Fall	X	X	X	X	X	X	X	X								

In addition to these, radiometer simulations were performed for antenna beamwidths of 0.01 degrees and 0.0175 degrees, for the cases of varying target temperatures and nonvarying target temperatures.

These images demonstrate the versatility of radar and radiometer simulation for evaluation of desired system parameters, as well as for image interpretation applications. Radar seasonal variations are clearly seen in the L- and S-Band example sets, while spectral differences are demonstrated in the Spring/Summer set. Resolution effects are shown for all cases. The radar images are presented as follows:

Figure #	Label
B.1a	Watertown, N.Y. L-Band, Spring/Summer 25m resolution
B.1b	Watertown, N.Y. L-Band, Fall 25m resolution
B.2a	Watertown, N.Y. L-Band, Spring/Summer 50m resolution
B.2b	Watertown, N.Y. L-Band, Fall 50m resolution
B.3a	Watertown, N.Y. L-Band, Spring/Summer 100m resolution
B.3b	Watertown, N.Y. L-Band, Fall 100m resolution
B.4a	Watertown, N.Y. L-Band, Spring/Summer 250m resolution
B.4b	Watertown, N.Y. L-Band, Fall 250m Resolution

Figure #	Label
B.5a	Watertown, N.Y. S-Band, Spring/Summer 25m Resolution
B.5b	Watertown, N.Y. S-Band, Fall 25m Resolution
B.6a	Watertown, N.Y. S-Band, Spring/Summer 50m resolution
B.6b	Watertown, N.Y. S-Band, Fall 50m resolution
B.7a	Watertown, N.Y. S-Band, Spring/Summer 100m resolution
B.7b	Watertown, N.Y. S-Band, Fall 100m resolution
B.8a	Watertown, N.Y. S-Band, Spring/Summer 250m resolution
B.8b	Watertown, N.Y. S-Band, Fall 250m resolution

Figure #	Label
B.9a	Watertown, N.Y. X-Band, 15cm of Snow 25m resolution
B.9b	Watertown, N.Y. X-Band, Spring/Summer 25m resolution
B.10a	Watertown, N.Y. X-Band, 15cm of Snow 50m resolution
B.10b	Watertown, N.Y. X-Band, Spring/Summer 50m resolution
B.11a	Watertown, N.Y. X-Band, 15cm of Snow 100m resolution
B.11b	Watertown, N.Y. X-Band, Spring/Summer 100m resolution
B.12a	Watertown, N.Y. X-Band, 15cm of Snow 250m resolution
B.12b	Watertown, N.Y. X-Band, Spring/Summer 250m resolution

Figure #	Label
B.13a	Watertown, N.Y. Ku-Band, Spring/Summer 25m resolution
B.13b	Watertown, N.Y. Ku-Band, Spring/Summer 50m resolution
B.14a	Watertown, N.Y. Ku-Band, Spring/Summer 100m resolution
B.14b	Watertown, N.Y. Ku-Band, Spring/Summer 250m resolution

Following these, the radiometer simulations are presented as follows.

Figure #	Label
B.15a	Watertown, N.Y. (Site II) 0.01 Beamwidth Varying temperature
B.15b	Watertown, N.Y. (Site II) 0.0175 Beamwidth Varying temperature
B.16a	Watertown, N.Y. (Site II) 0.0175 Beamwidth Constant temperature

Figure #	Label
B.16b	Watertown, N.Y. (Site II) 0.0175 Beamwidth Varying temperature
B.17a	Watertown, N.Y. (Site II) 0.01 Beamwidth Constant temperature
B.17b	Watertown, N.Y. (Site II) 0.0175 Beamwidth Constant temperature

Figure B.1a

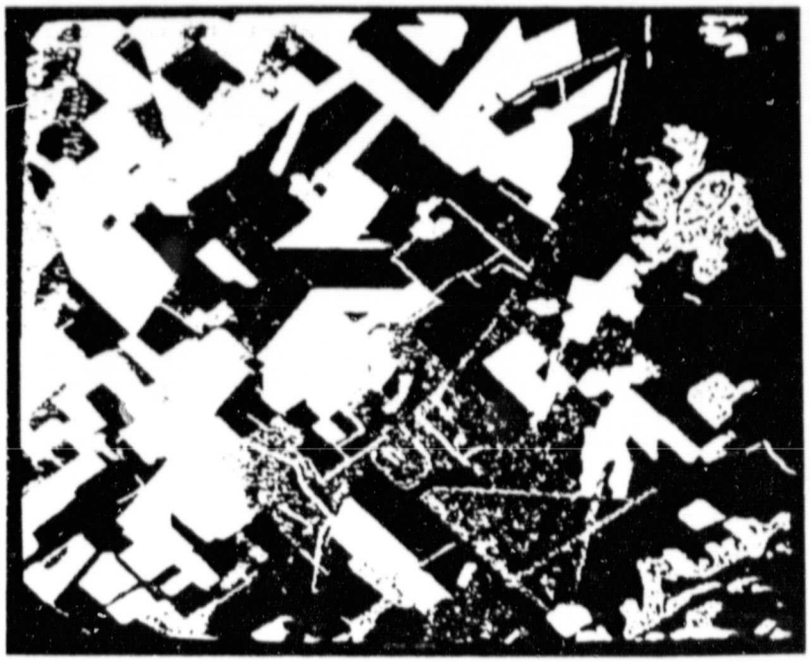

Figure B.1b

Figure B.2a

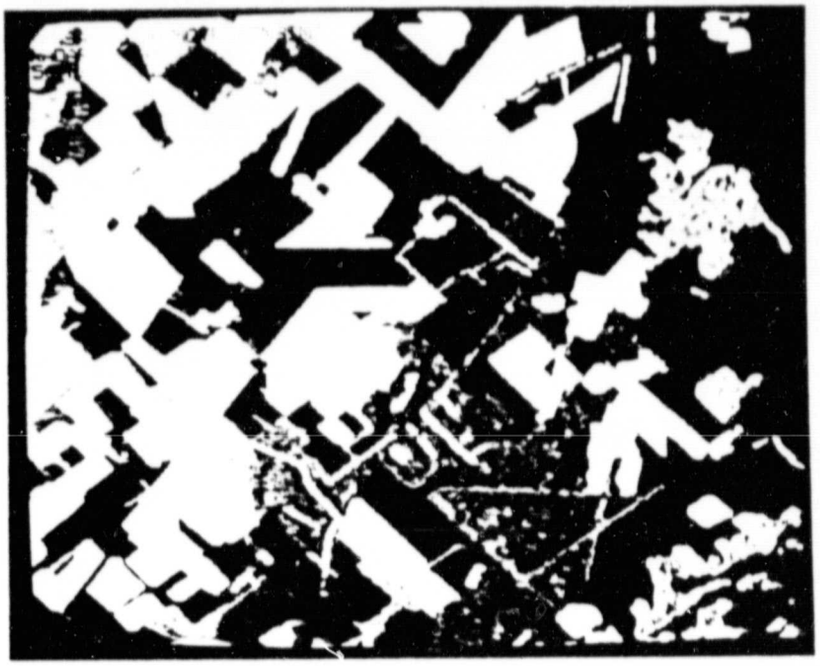

Figure B.2b

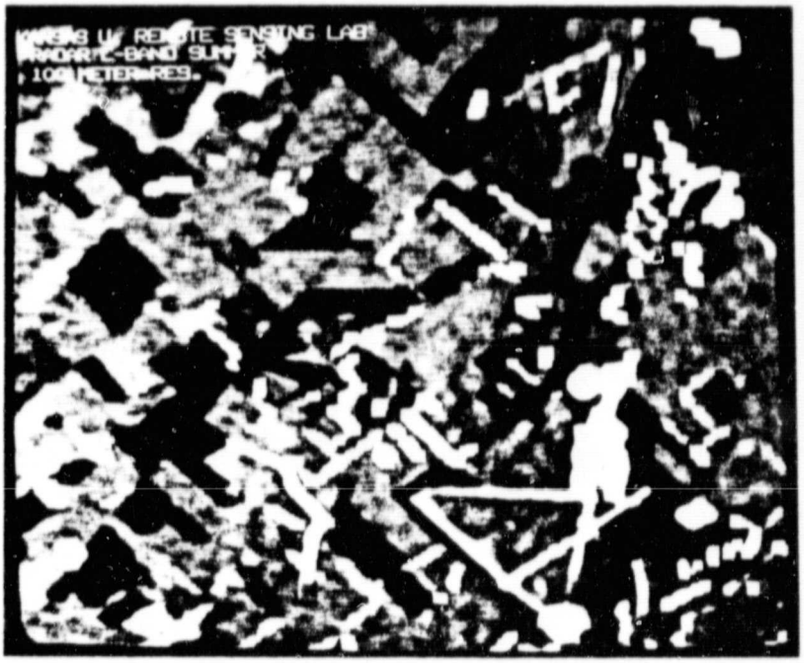

Figure B.3a

Figure B.3b

Figure B.4a

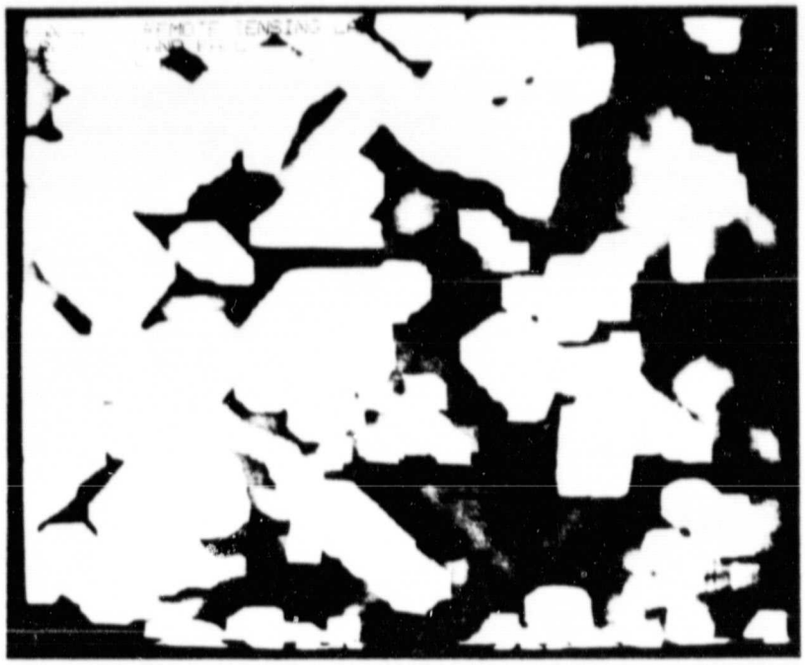

Figure B.4b

Figure B.5a

Figure B.5b

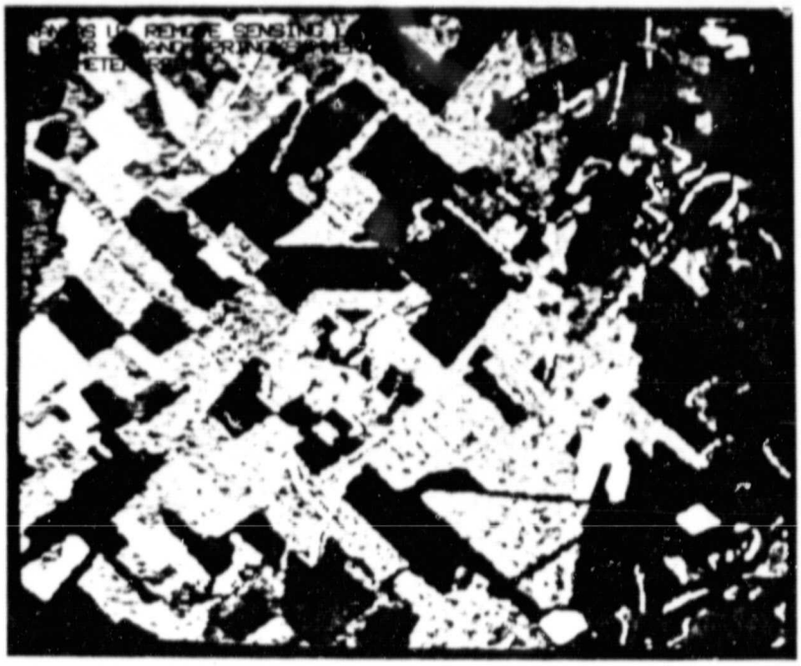

Figure B.6a

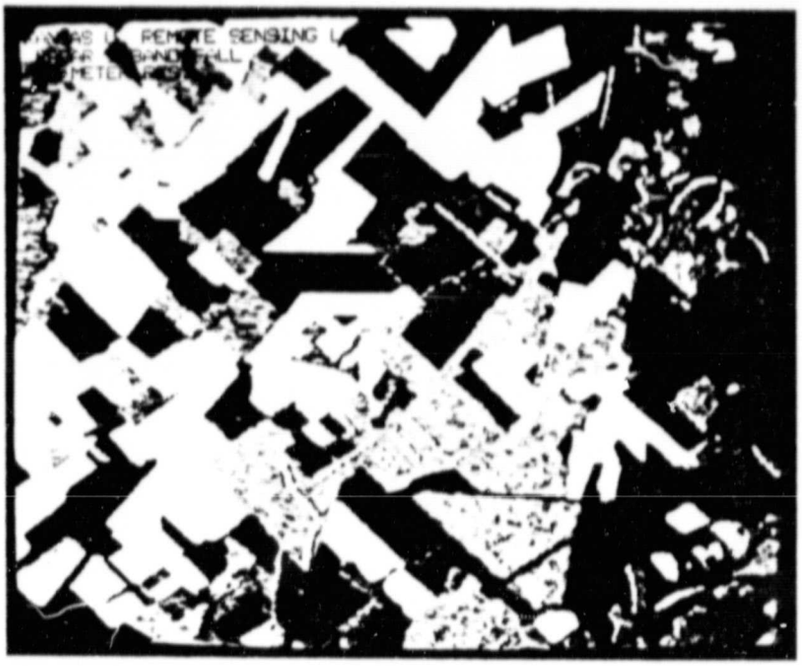

Figure B.6b

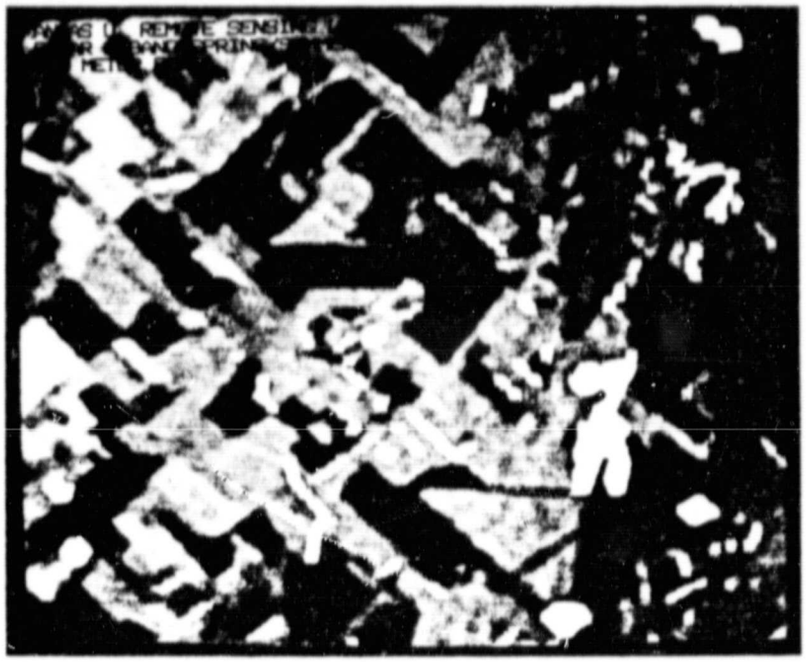

Figure B.7a

Figure B.7b

Figure B.8a

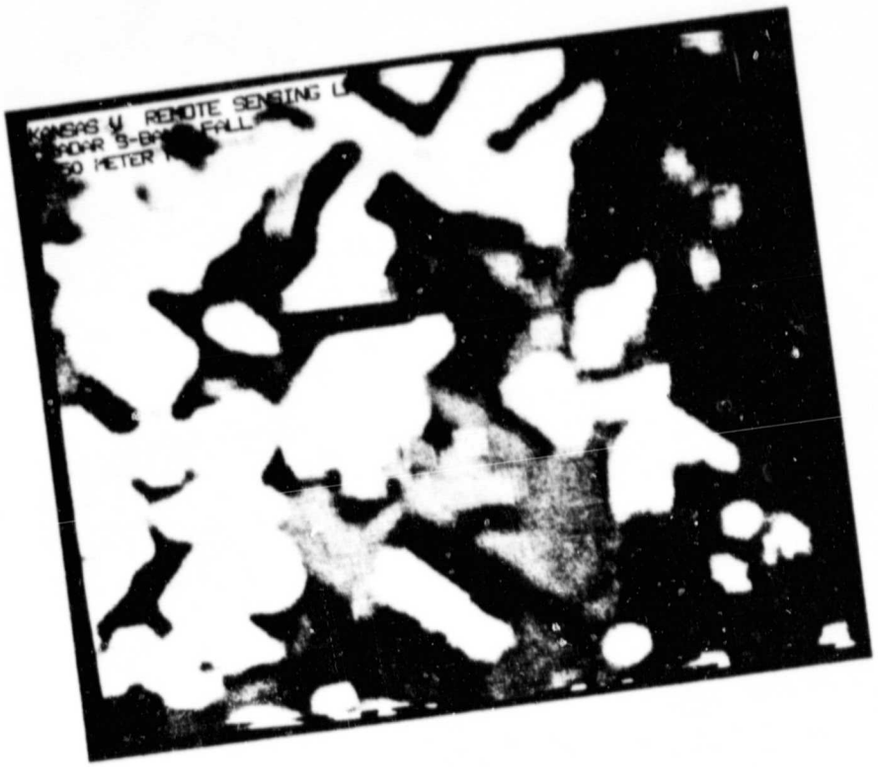

Figure B.8b

Figure B.9a

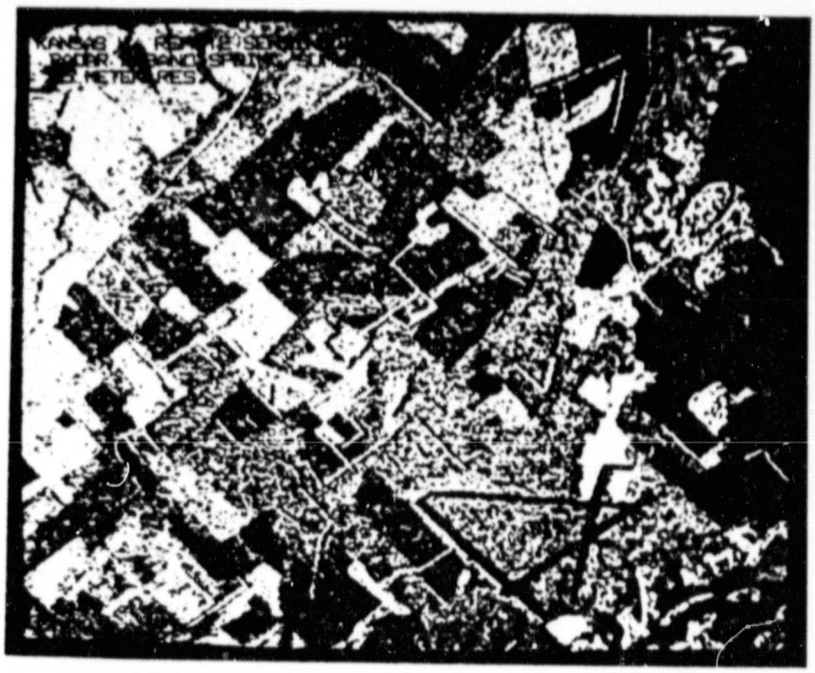

Figure B.9b

Figure B.10a

Figure B.10b

Figure B.11a

Figure B.11b

Figure B.12a

Figure B.12b

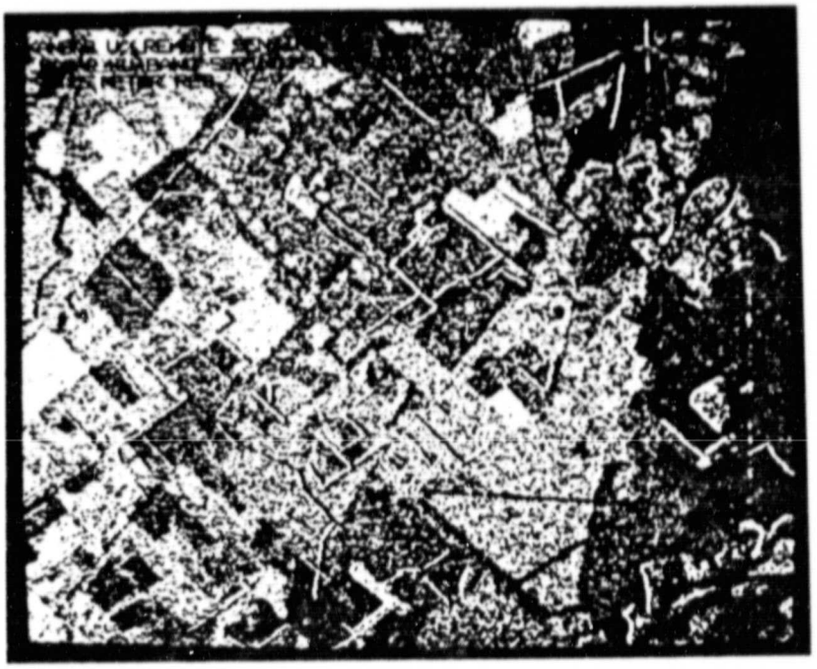

Figure B.13a

Figure B.13b

Figure B.14a

Figure B.14b

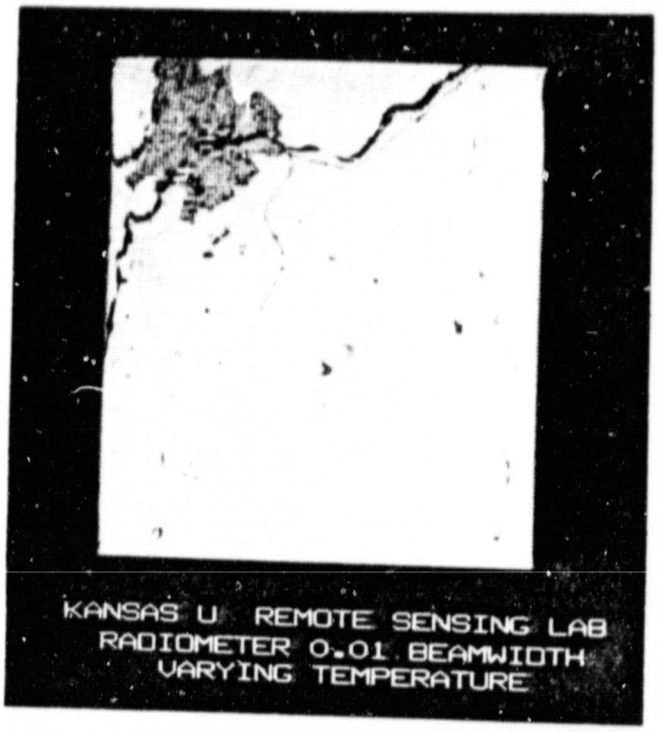

Figure B.15a

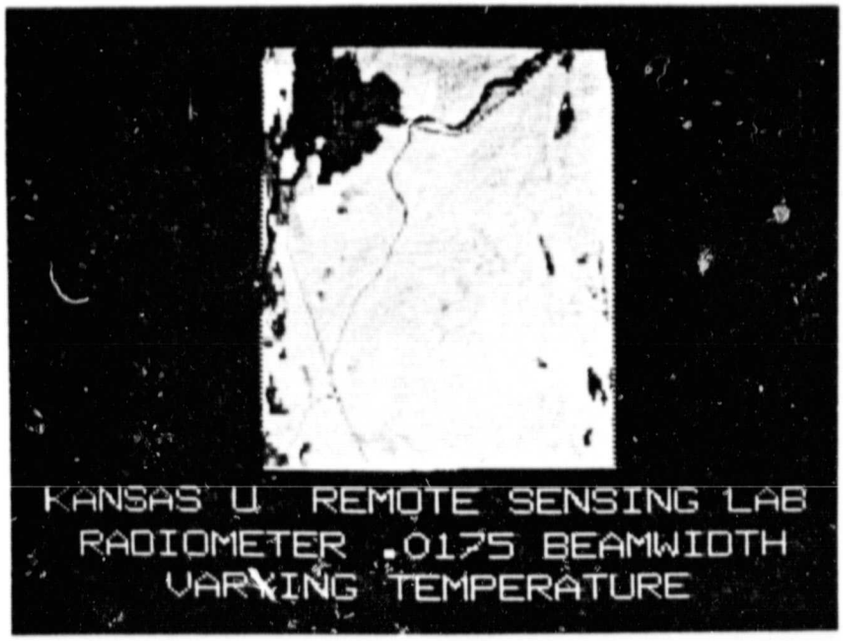
KANSAS U REMOTE SENSING LAB
RADIOMETER .0175 BEAMWIDTH
VARYING TEMPERATURE

Figure B.15b

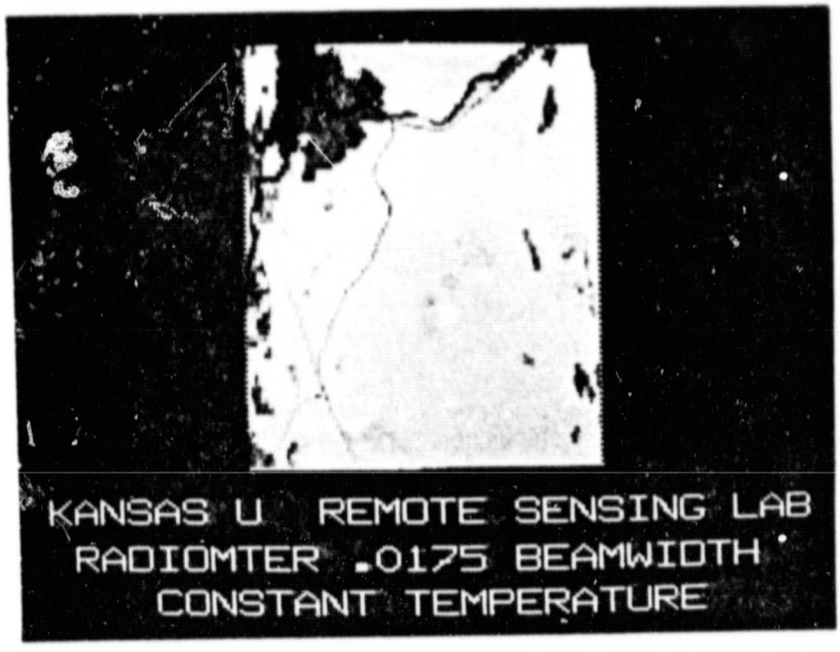
KANSAS U REMOTE SENSING LAB
RADIOMTER .0175 BEAMWIDTH
CONSTANT TEMPERATURE

Figure B.16a

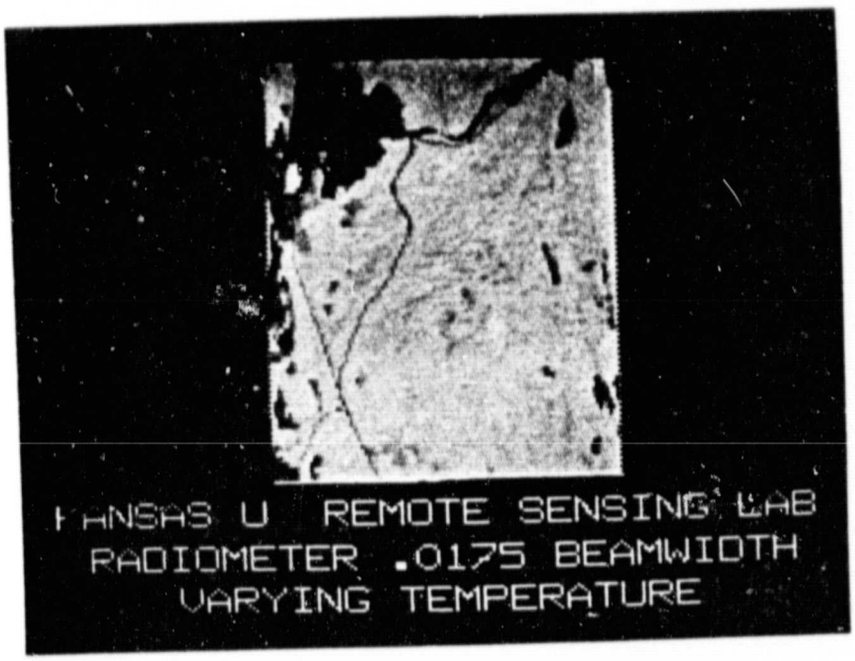

Figure B.16b

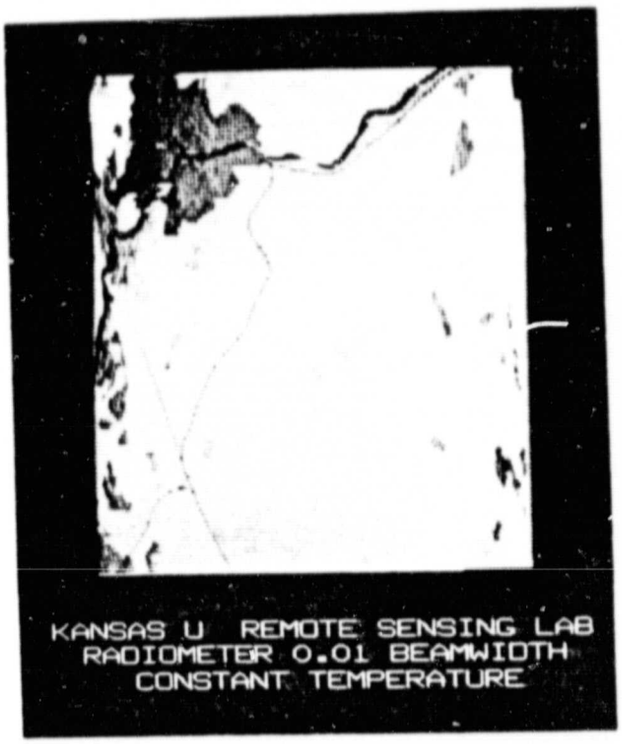
KANSAS U REMOTE SENSING LAB
RADIOMETER 0.01 BEAMWIDTH
CONSTANT TEMPERATURE

Figure B.17a

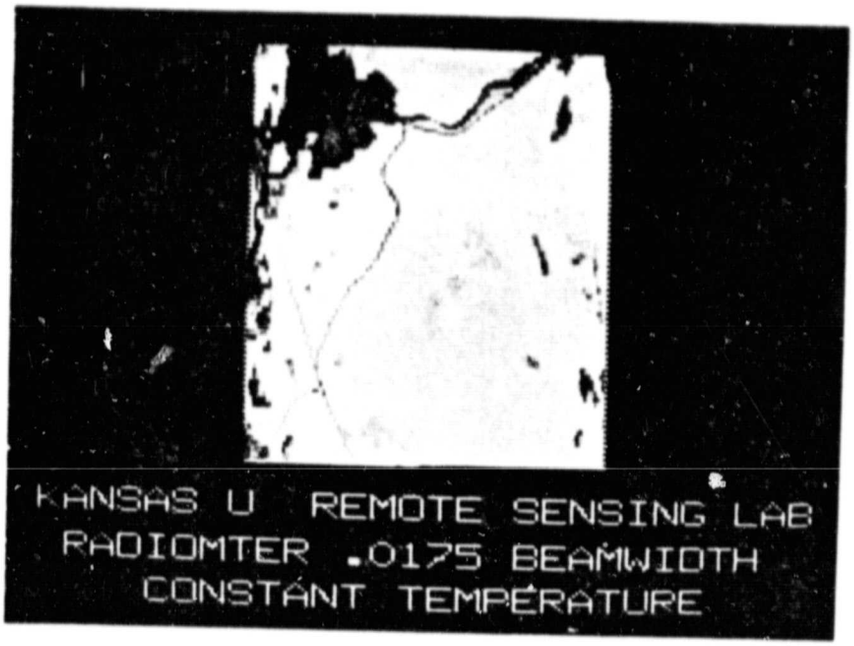

Figure B.17b